8-2018

Wnt/β-Catenin mediated cancer stem cell activation in hepatocellular carcinoma.

Harshulkumar M. Pandit
University of Louisville

WNT/β-CATENIN MEDIATED CANCER STEM CELL ACTIVATION IN HEPATOCELLULAR CARCINOMA

By

Harshulkumar M. Pandit

B.Sc., Biotechnology, Sardar Patel University, India, 2004

M.Sc., Biochemistry, M. S. University of Baroda, India, 2007

M.S. Pharmacology & Toxicology, University of Louisville, USA, 2015

A Dissertation Submitted to the Faculty of the

School of Medicine of the University of Louisville

In Partial Fulfillment of the Requirements

For the Degree of

Doctor of Philosophy in Pharmacology and Toxicology

Department of Pharmacology and Toxicology

University of Louisville, Louisville, Kentucky

August, 2018

WNT/β-CATENIN MEDIATED CANCER STEM CELL ACTIVATION IN HEPATOCELLULAR CARCINOMA

By

Harshulkumar M. Pandit

A Dissertation Approved on

July 26, 2018

By the following Dissertation Committee:

_____

Robert C.G. Martin II, MD, Ph.D., FACS

_____

David Hein, Ph.D.

_____

Aruni Bhatnagar, Ph.D.

_____

Haribabu Bodduluri, Ph.D.

_____

Yong Li, Ph.D.

DEDICATION

I dedicate this Ph.D. dissertation to my parents, Mayank Pandit and Manorama Pandit. I am eternally grateful for their love, and the sacrifices they made for me. Without their support, it would have been impossible for me to achieve this accolade.

ACKNOWLEDGEMENTS

I would like to sincerely thank my mentor, Dr. Robert C.G. Martin, for his encouragement and guidance. I am truly grateful to him for offering me this valuable and amazing opportunity to work in his lab in the field of Hepatocellular Carcinoma (HCC). During my Ph.D. journey, Dr. Martin has spent countless hours guiding me, pushing me to pursue novel and challenging scientific questions, and help navigate me through tough times. I am honored and feel very fortunate to work with such a dynamic person, a diligent and intelligent research science, and a great human being. I feel very blessed to have him as my mentor.

I would also like to express my deepest gratitude to Dr. Yan Li, who provided invaluable timely help and continuous support on every step of my Ph.D. project. Most importantly he helped me acquired *in vivo* experimental skills, the *in vivo* studies presented in this dissertation would not have been possible without his assistance and guidance.

My deepest gratitude also goes to the members of my committee, Dr. David Hein, Dr. Aruni Bhatnagar, Dr. Haribabu Bodduluri, and Dr. Yong Li for agreeing to offer their expertise, valuable time, feedback and assistance. Right from the beginning, their constructive critics helped me identify important unknown research questions, and align my research approaches in the precise

direction. Their timely advice and instrumental guidance made my Ph.D. project innovative and novel.

Special thanks to Dr. Bradly Keller for providing access to ultrasound instrument and Joe Tinney for helping me learn the skills. I would also like to thank Dr. Levi Beverly for providing help with lentivirus and reporter assay experiments, and generously sharing plasmid vectors. Also, I would like to thank Dr. Haribabu Bodduluri's Lab (Dr. Venkatakrishna Jala and Zinal Chedda) for timely support for Confocal and Flowcytometry experiments.

A special thanks to my lab-mates, past and present: Steven Agle, Salina Li, Jack Rostas III, Young Hong, Gordon, Cecilia, Joe, Wei, Yingbing Yang, Weizhong Zhang, for proving great support and making my time in the lab enjoyable. I would like to specially thank Ms. SuPing Li, our wizard lab-technician, who helped me learn and troubleshoot many techniques and experiments, and provided exceptional support. I am also appreciative to everyone at the Price Institute of Surgical Research, specially Rob and Sarah, as well as, Division of Surgical Oncology's clinical staff, specially Mary, Mellissa, and Traci, for providing timely support for acquiring patient's specimens.

Most importantly, I am truly grateful to my wife, Reema, who stand by me during this entire Ph.D. journey. Her love, encouragement and support was vital force for me to stay focused and finish my studies on time. Last but not least, I would like to thank my parents, my family, and all my friends for their love and continuous support.

ABSTRACT

WNT/β-CATENIN MEDIATED CANCER STEM CELL ACTIVATION IN HEPATOCELLULAR CARCINOMA

Harshulkumar M. Pandit

July 26, 2018

Hepatocellular carcinoma (HCC) is one of the deadliest cancers, with variable presentation, high chemotherapy resistance and early tumor recurrence. In this dissertation, we have systematically enriched, identified and characterized HCC cancer stem cells (CSCs) from 3 different HCC cell lines (Hepa1-6, HepG2, and Hep3B) using *in vitro* serum-free culture method. Enriched spheroids acquired CSC properties, primarily self-renewal capability, spheroid formation ability, and drug resistance. Heterogeneous CSCs enriched from Hepa1-6 cells demonstrated higher tumor initiation and proliferation capability *in vivo,* compared to control HCC cells in orthotopic immunocompetent mouse model.

EpCAM+ CSCs were significantly enriched within heterogeneous Hepa1-6 CSC spheroids. Consequently, we studied the fate of EpCAM+ CSCs in orthotopic immunocompetent mouse model with 3 different liver microenvironments i.e. control normal liver, steatosis (fatty liver induced), and nonalcoholic steatohepatitis (NASH). EpCAM+ CSC mediated HCC carcinogenesis was observed in NASH livers, but failed to develop in control and steatosis liver microenvironment. This is

the first study evaluating CSCs in immunocompetent mouse model and demonstrated the importance of liver microenvironment for EpCAM+ CSC mediated tumor initiation. We then performed a lineage tracking study by stably incorporating copGFP or mCherry in Hepa1-6 cells by lentivirus transduction, and examined the origin of tumors in NASH liver microenvironment using orthotopic C57L/J immunocompetent mouse model. Our findings suggest that tumor growth was dose dependent and most tumor nodules arose from copGFP expressing EpCAM+ CSCs.

The Wnt/β-catenin pathway components were also found to be overexpressed in CSCs when compared to control. Human HCC specimen analyses suggested concomitant changes in β-catenin and EpCAM levels. Gene analyses of step-wise spheroid formation process identified possible dedifferentiation mechanisms regulated by β-catenin in CSC spheroids. Loss of function analysis by siRNA mediated transient knockdown of β-catenin confirmed its role in spheroid enrichment and doxorubicin resistance. Canonical Wnt pathway study using chemical inhibitors identified β-catenin mediated CSC activation was regulated at nuclear level, and not at the cytoplasmic GSK3β destruction complex level. Analysis of human and mouse tumors suggested that constitutive activation of β-catenin transcription failed to respond to NOTUM, a feedback inhibitor of canonical Wnt/β-catenin signaling.

TABLE OF CONTENTS

PAGE

LIST OF FIGURES

PAGE

CHAPTER 1

HEPATOCELLULAR CARCINOMA

Background:

The most common primary liver cancer (80-90%) in the United States is Hepatocellular carcinoma (HCC) [1]. Also referred to as hepatoma, HCC is a type of epithelial cancer in liver, and one of the most common form of liver cancers in adults, age 50 or older. HCC is the fifth most common cancer in men and seventh in women worldwide, and accounts for the third major cause of cancer related deaths worldwide [2, 3]. Men are two to four times more likely to develop liver cancer than women. The development of HCC is closely associated with the presence of chronic liver disease, and therefore HCC remains a dynamic and challenging condition due to the dual effects from the malignancy and fragile liver function [3]. A 2013 CDC report has suggested that liver cancer related deaths in US men is increasing at the rate of 2% per year despite better success rates in other cancers [4]. HCC confers the highest death rate (~2.4%) and 2nd highest cancer incidence rate (~3.6%) amongst all cancers in United States [5] (Figure 1.1).

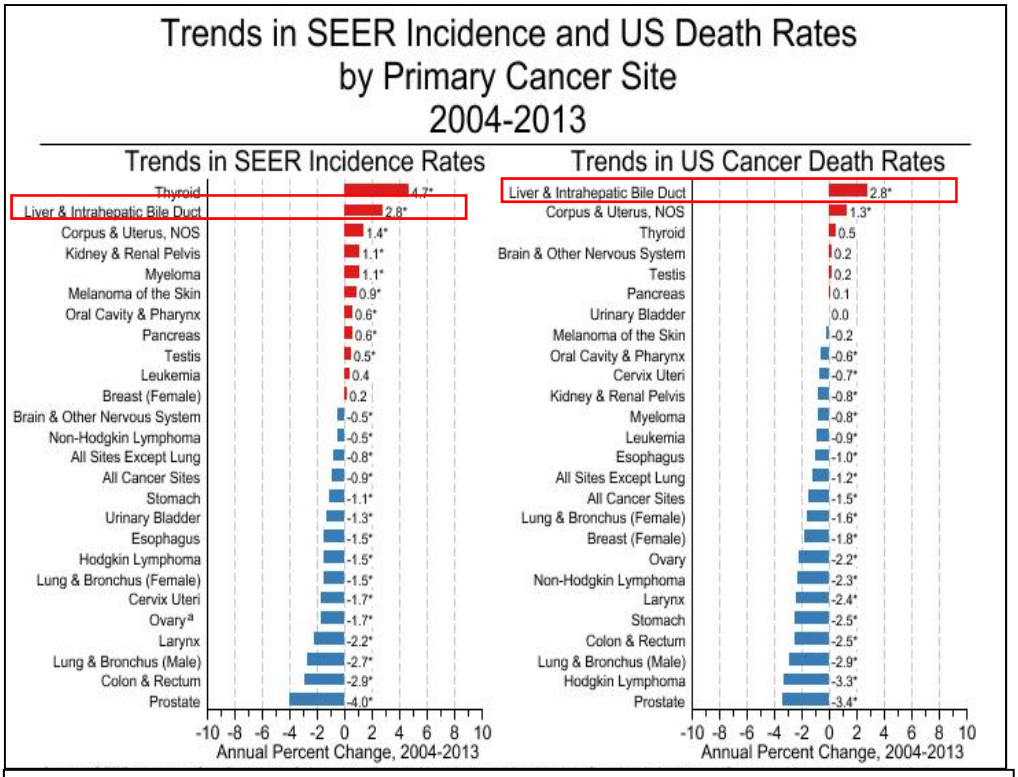

Figure 1.1: Trends in HCC incidence and mortality in the US. Surveillance, Epidemiology, and End Result program (SEER) revealed liver cancer is challenging condition in US population. (Figure is adapted from the SEER website http://seer.cancer.gov/data/)

Etiology of HCC

Major known risk factors for HCC are cirrhosis, Hepatitis B virus (HBV) or Hepatitis C virus (HCV) infection, alcoholic liver disease, and non-alcoholic fatty liver disease (NAFLD) [3]. Newly added risk factors are obesity and type-II Diabetes for development of HCC [6, 7]. In HCC patients, distribution of these risk factors are highly variable, depending on ethnic groups and geographic regions [8].

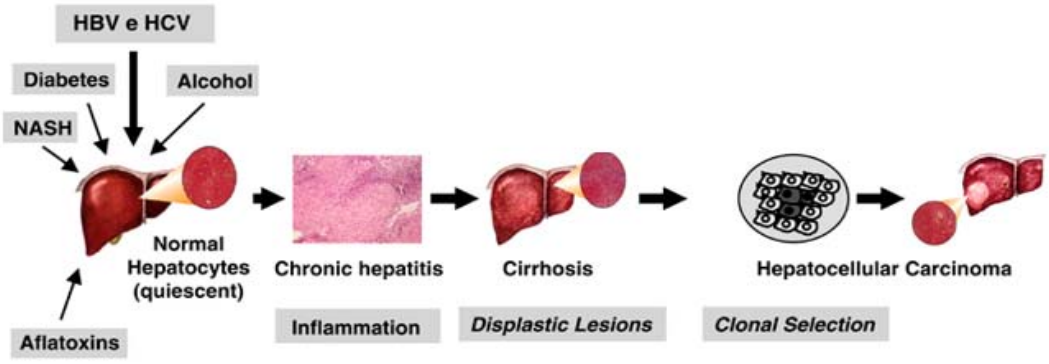

Figure 1.2: Diversity in HCC diagnosis presentation, progression and tumorigenesis. Development of HCC is heterogeneous. After primary encounter with risk factor, liver inflammatory stage develops (chronic hepatitis) if not intervened, hepatitis eventually progressed further to non-reversible liver cirrhosis stage. Apx ~80% of HCC patients have cirrhosis history. Figure is adapted from Levrero et.al. – Oncogene (2006).

Most of these risk factors lead to cirrhosis or its progression, which is present in 80-90% of HCC patients. According to a study by Fattovich et al., the 5 year cumulative risk for HCC development in cirrhosis patients ranges between 5% and 30% globally, 18% in the United States, depending on cause, ethnic group, and stage of cirrhosis [9]. As a result of the variety of causes and risk factors for HCC, patients show vast diversity in clinical presentation and disease progression, compared to any other solid malignancies (Figure 1.2).

Non-alcoholic fatty liver disease (NAFLD) and the rise in incidence of NASH-HCC

Success of new direct-acting antiretroviral (DAA) therapy for Hepatitis C Virus (HCV) infection (the largest risk factor of HCC) has shifted recent epidemiology of cirrhosis and HCCs (Figure 1.3) [10, 11]. DAA also reduced liver transplant waitlist of patients with decompensated cirrhosis secondary to HCV by

32% compared with interferon treatment era, while simultaneously increased waitlist of patients in NASH by 41% [11].

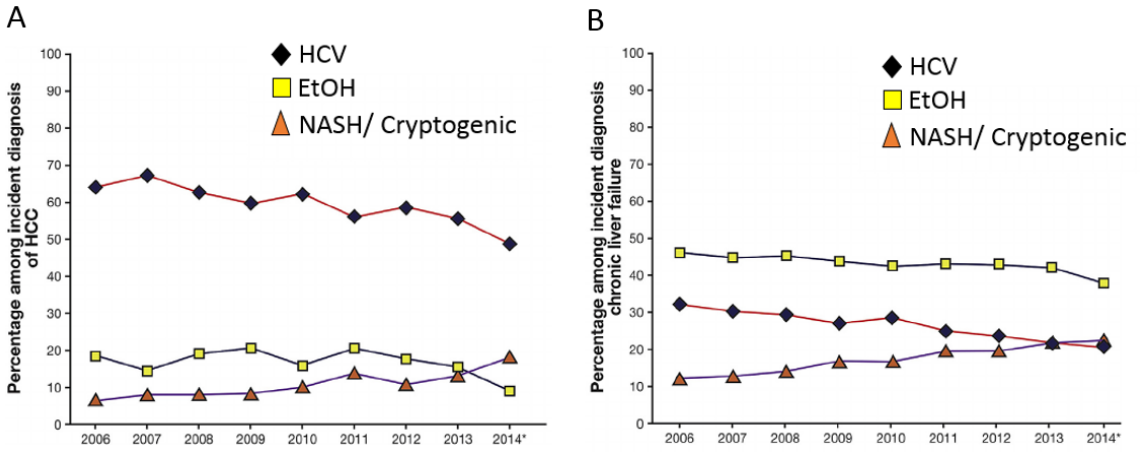

Figure 1.3: Diagnosis distribution of HCV, alcohol liver disease (EtOH), and NASH in patients with HCC and chronic liver failure. (A) Incident diagnosis of HCC (B) Incident diagnosis of chronic liver failure. Database: Healthcore 2006-2014. Figure is adapted from Goldberg et.al 2017.

SEER-Medicare database study by Welzel et.al. reported that metabolic syndrome is significant risk factor in the United States [12]. American Society of Clinical Oncology (ASCO) reported that obesity will overtake tobacco as the leading cause of cancer in near future [13]. Around 1/3 of US population [14], and 17% children and adolescents are considered obese [15]. Most comprehensive study in US population by Calle et.al. showed that liver cancer related death rates are correlated with body mass index [16]. Davila et.al. reported that Diabetes alone increases the risk of HCC by 2-3 fold, independent of presence of other risk factors of HCC [17]. A recent study by Kasmari et.al. reported that metabolic syndromes such as Diabetes and hypertension, are independent risk factors in development

of HCC in absence of Cirrhosis [18]. Most of these metabolic syndromes are also associated to NAFLD progression.

In developed countries, increased incidence of HCC has been attributed to increase in incidence of NAFLD [10]. At least 25% of the US population has NAFLD, and NAFLD is becoming an epidemic [19, 20]. NAFLD is a range of chronic liver disease from steatosis (without inflammation) to NASH (inflammatory steatosis), and NASH is the most severe form of NAFLD and present in 6% to 17% population, and a major source of cryptogenic cirrhosis [20]. It is predicted that NASH will constitute the most frequent cause of HCC and cirrhosis in developed countries in next decade [21].

NASH patients without fibrosis are at lower risk of progressing to cirrhosis compared to advanced fibrosis , while progression to cirrhosis in NASH patients was reported to be 25% over 9 years [22]. NASH mediated HCC carcinogenesis can be either cirrhosis mediated or non-cirrhotic [21, 23]. Metabolic syndrome secondary to NASH is growing epidemic with higher risk associated with HCC carcinogenesis (Figure 1.4) [24]. Indeed, around 15% to 50% cases of NASH progresses to HCC without cirrhosis, confer a new challenge to clinicians and researchers to understand NASH mediated HCC progression [25]. Significant gaps remain to understand mechanisms by which NAFLD/NASH and its metabolic risk factors promote HCC progression.

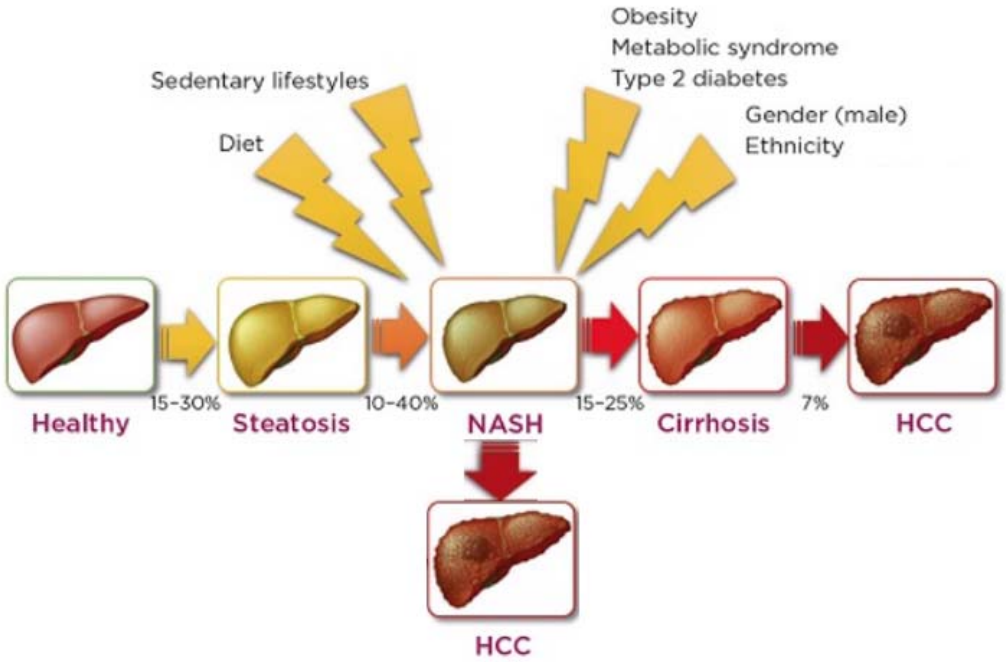

Figure 1.4: NASH is a growing HCC epidemic. Different stages and pathophysiology during progression of NASH. Figure is adapted and modified from the Allison et.al https://www.endocrinology.org/endocrinologist.

Treatment modalities, staging guidelines and prognostic assessment

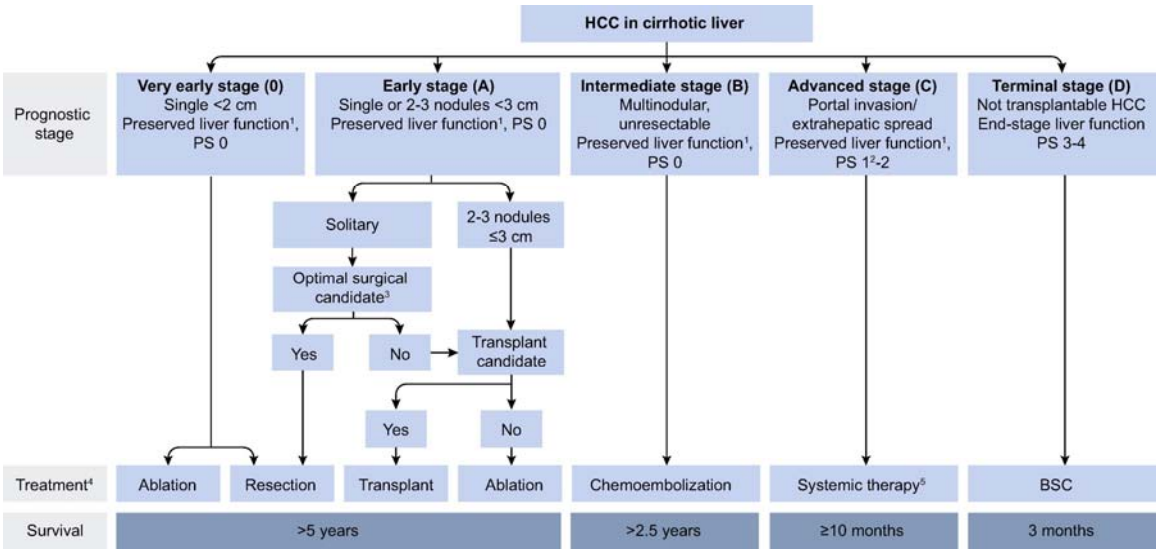

Figure 1.5: Modified BCLC staging system and treatment strategies. Figure is adapted from the most recent EASL clinical practice guidelines (2018)

HCC has primarily two different growth patterns, and the most common growth pattern seen in the United States is development of HCC secondary to cirrhosis (chronic liver damage), where HCC typically starts as several small cancer nodules at multiple sites in the liver, referred as global growth pattern (global hepatic damage). Diagnostic presentation of global HCC tumor growth in most cases considered as non-qualifying criteria for tumor resection (the best treatment modality available with the highest disease free and overall survival). The other growth pattern widely observed is single HCC tumor which grows larger and later spreading to neighboring regions in the liver. This single HCC tumor growth pattern, in most cases, qualifies for tumor resection and thus offers a better prognostic outcome.

HCC prognosis and treatment modalities are not considered solely based on HCC tumor growth pattern, but rather follow systemic guidelines. **Barcelona Clinic Liver Cancer (BCLC)** staging system [26] (Figure 1.5), and **Child-Pugh** cirrhosis classification system are the two most widely practiced HCC staging/treatment guidelines to determine HCC prognosis and primary tumor treatment options for HCC patients [27, 28]. The BCLC staging guidelines are based primarily on radiological images, and do NOT consider HCC grade or other known risk factors. After following staging criteria, if patient's tumor is categorized as "Resectable" then surgical resection (ideal treatment option with the best overall survival and outcome) or liver transplantation is considered. If staging criteria categorize HCC as "Unresectable" then palliative treatment options are considered, i.e. local thermal ablation, Local Regional Therapies (LRTs) such as trans-arterial

drug eluting beads (loaded with Doxorubicin) (TACE-DEB) and Radioembolization (Y-90 beads), targeted molecular therapy (Sorafenib – multikinase inhibitor, Regorafanib), or immunotherapy (Nivolumab).

Prognosis and disease free survival are subjective to individual patient's HCC stage, hepatic synthetic function, and implementation of treatment options. HCC treatment with systemic therapy, local regional therapies (LRTs), or surgery have been marginally successful because a substantial subpopulation of HCC cells defined as **cancer stem cells (CSCs)**, which fail to respond to treatment and contribute to **minimal residual disease (MRD)** [29] and thus a very short remission time of disease free interval.

CANCER STEM CELLS

Cancer Stem Cell (CSC) Model and HCC:

Discovery of cancer stem cells (CSC) or tumor initiating cells (TIC) has changed our view of carcinogenesis and chemoresistance [30, 31]. Understanding that tumor development and growth is not only maintained by selection of genetically mutated population of cells (stochastic model), but also by the tumor microenvironment which facilitates communication between

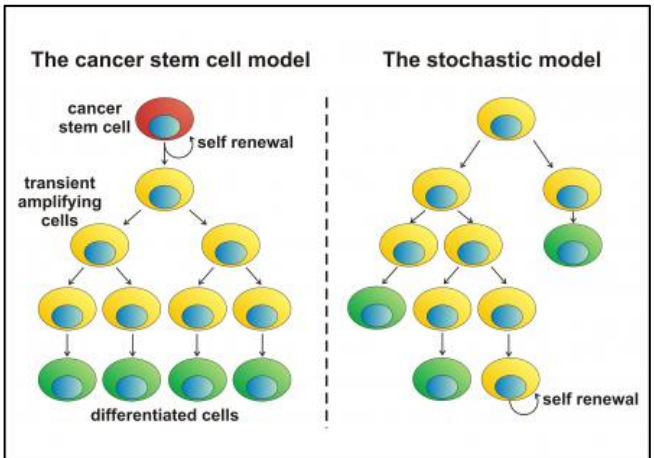

Figure 1.6: Cancer stem cell model: Cancer stem cell model can explain heterogeneity of tumor mass.

Figure source: http://www.eurostemcell.org

altered tumor cells and their unaltered neighbors like fibroblasts, endothelial cells, and inflammatory cells [32]. CSCs are a small population of less differentiated cells within the tumor microenvironment which possess stem cell like properties i.e. self-renewal capability and ability to differentiate into heterogeneous lineages of cancer cells via asymmetric division [30]. CSC model proposes hierarchical organization, where apex CSC retains self-renewal capability with the highest tumorigenic potential (Figure 1.6), while the well differentiated cancer cells lose this important stemness property and become less tumorigenic [30, 33]. Lapidot et al. proposed the CSC hypothesis for the first time in primary human acute myeloid leukemias (AMLs) in 1994 [34]. A study on breast cancer by Al-Hajj et al. was the first to report evidence of CSCs in solid tumors [35]. Since then, several studies have reported presence of CSCs in solid tumors like colon [36], pancreas [37], and liver [38-40]. The first direct evidence to support CSC theory came from lineage-tracing study by Barker et al. in 2007, where they studied tracing of lgr5+ cells in development of small intestine and colon tumors in genetically engineered mice [41]. In 2012, two more groups had published lineage-tracing studies in genetically engineered mouse models [42, 43].

Several groups have studied role of CSCs in HCC and reported their clinical significance [44, 45]. The CSC tumor model has been proven to show clinical relevance in primary HCC and HCC recurrence [45-47]. Haraguchi et al. identified a subset of stem cells, “side population” (SP) cells, in Huh-7 and Hep3B cell lines which highly express multi-drug resistant ABC-transporters [48]. Ma et.al. and colleagues have shown that sorted SP cells possess high expression of stemness

genes and higher tumorigenicity [46, 47]. Using tumorigenicity potential and stemness characteristics as CSC markers, many studies have identified CSCs from human HCC tissues and HCC cell lines expressing the following stem cell markers - EpCAM+, CD90+, CD44+, CD133+, AFP+, OV6+, and ALDH1+ [45, 47, 49, 50]. These diverse surface markers on CSCs have been thought to be a result of heterogeneity of tumor microenvironment, and no single surface marker can define HCC CSCs exclusively [51].

CSCs contribute to treatment failure

In HCC, studies have identified EpCAM+ cells in tumors of patients, and showed that these EpCAM+ cells correlate with worse prognosis and possess CSC-like properties which showed tumor initiating capabilities in as few as 200 cells in a nude mouse model [38, 50, 52-54]. Recurrence of HCC after definitive tumor treatment occurs in over 70% of patients within 14 months of initial treatment. MRD is responsible for poor prognosis and early tumor recurrence in HCC. Clinical studies have shown that recurrent HCC tumors exhibit resistance to chemotherapy treatments and attain aggressive tumor growth [47]. CSCs are resistant to chemotherapeutics and considered as the primary players for tumor relapse and metastasis in HCC [55-57]. Importantly, a multi-drug resistant transporter ABCG2, a well characterized CSC functional marker, has been implicated for doxorubicin resistance in multiple studies [48, 58-61]. Many recurrent HCC cases have a different biology than the primary index tumor. These recurrent tumors account for most therapeutic failures and eventually result in the death of patients. The

molecular mechanism underlying chemotherapy resistance and tumor recurrence in HCC is not yet clear.

Wnt/β-catenin signaling, CSCs, and HCC:

Canonical Wnt/β-catenin signaling pathway regulates several cellular events including cell proliferation, and is considered a fundamental pathway in stem cell biology [62]. It is one of the most extensively studied molecular signaling pathways in HCC and CSCs [62]. In the absence of Wnt ligand, β-catenin is bound to the complex of APC, Axin, and GSK-3β (termed degradation complex), and is phosphorylated and targeted for ubiquitin mediated degradation. β-catenin also exists in a cadherin-bound form and regulates cell–cell adhesion. When Wnt binds to frizzled receptor (Fz) and Lrp5/6 (LDL receptor family protein 5/6) on the cell membrane, the GSK-3β (non-phosphorylated, active state) is phosphorylated at the Ser-9 position (inactive state). β-catenin is uncoupled and is stabilized following inactivation of GSK-3β, and the stabilized β-catenin translocates to the nucleus, where it activates target genes by binding to TCF/LET transcription factors.

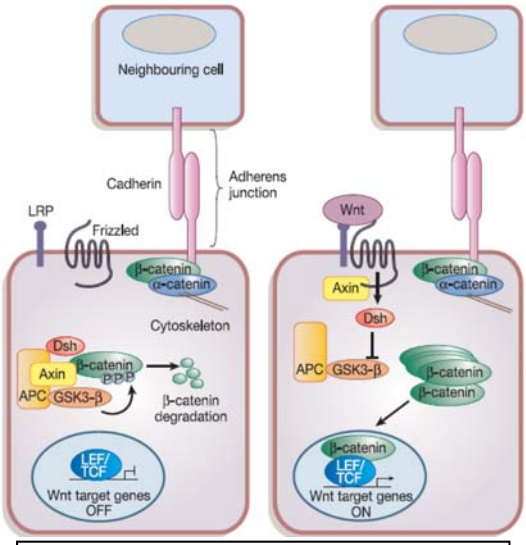

Figure 1.7: Canonical Wnt/β-catenin pathway: Canonical Wnt pathway required Wnt ligand binding on receptor, for stabilizing β-catenin and its translocation into nucleus. Figure source: Nature. 2005 Apr 14; 434 (7035):843-50.

Many reports have demonstrated the role of the Wnt/β-catenin signaling in

tumorigenic CSCs [62]. EpCAM is one of the important CSC markers, and is a target of Wnt/β-catenin signaling. The inhibition of the Wnt/β-catenin signaling has been shown to destroy EpCAM-positive cells [54, 56]. Studies have reported the role of Wnt/β-catenin signaling in self-renewal and maintenance of CSCs in HCC [63, 64]. Also, ABCG2, a functional CSC marker, was suggested to be regulated by β-catenin in CSCs and contributes to drug resistance [59, 60, 65].

Challenges in treatment outcome assessment for HCC

The current response criteria do not accurately assess HCC treatment response to more advanced modalities like Sorafenib (multikinase inhibitor), and Local Regional Treatments (LRTs) such as TACE-DEB beads, and Y-90 beads [66, 67]. Traditional Response Evaluation Criteria in Solid Tumors (RECIST) was designed for assessing chemotherapeutic agents, which are cytotoxic for rapidly dividing cancer cells, and measure reduction in tumor size. Therefore, standard tumor size criteria cannot accurately assess advanced treatment modalities which were developed in past two decades (LRTs and Sorafenib), locally targeted or targeting molecular pathways. Hence, tumor response to these new treatment modalities can also be assessed by analyzing tumor vascularity reduction, changes in metabolic activity, and tumor cell apoptosis and necrosis [68, 69].

Traditional response criteria (WHO and RECIST) may not accurately assess the response to LRTs and Sorafenib, because these criteria do not evaluate tumor necrosis and/or tumor vascularity reduction. After LRTs or Sorafenib, the tumor size may remain the same or sometimes increase. The increase in the size of a tumor (due to necrosis, hemorrhage, or edema) and decrease in vascularity can be explained by the responding effect of tumors [70] (usually interpreted as necrosis as shown in Figure 1.8, [71]). Because of these limitations of WHO and RESIST criteria (not designed to assess viable tumors but reduction in tumor size), a modified RESIST criteria was formally introduced in 2008 by AASLD (American Association for the Study of Liver Disease), defined as **mRESIST** [72]. The mRESIST criteria incorporated the concept of viable tumor introduced by EASL (European Association for the Study of the Liver) [73]. Two independed studies found that objective response calculated by EASL criteria were higher than traditional RESIST criteria [74, 75]. (The majority of this subsection is adapted from Singh et.al. 2014 [71]).

Figure 1.8: LRT response evaluation. Pre-treatment (2a and 2b) and 4 week follow-up (2c and 2d) scans by arterial phase CT after TACE-DEB. Treatment by TACE-DEB demonstrates an increase in tumor size (2c and 2d) but more than 80% of its volume is necrotic with the only viable tumor seen as a nodular enhancing area along its inferomedial margin. **This qualifies as a favorable response to treatment despite of the increase in tumor size**. Image source: Singh et.al. 2014.

However, most radiologists are neither familiar nor comfortable with this type of radiologic assessment. Similarly,

there remains no increase in payment for these types of radiologic reads which are both challenging and far more time consuming that standard reads. Until a "quality of CT and MRI" reads exist there will remain high variability in assessing tumor response in all unresectable therapies for HCC. Suboptimal assessment of HCC treatment outcome could miss early detection of HCC tumor recurrence, often contributed by activation of CSCs within minimal residual disease and miss the window of opportunity for early intervention.

Significance and research direction of this dissertation:

Published studies have shown increasing evidence that support the role of CSCs in HCC carcinogenesis, chemotherapy resistance and tumor recurrence. There is a compelling need to connect and better define these isolated findings for translational and clinical relevance. Importantly, well-reported CSC surface markers EpCAM, CD44, and CSC functional marker ABCG2 have been reported as targets of Wnt/β-catenin signaling, and also have been implicated in development of chemotherapy resistance and HCC prognosis [58, 76, 77]. However, origin and activation of CSCs in HCC is not yet been well defined. A mouse model overexpressing wild-type or mutant β-catenin failed to initiate HCC [62]. These data suggest that not much is known about **initial molecular events** triggering activation of Wnt/β-catenin signaling in HCC.

HCC Cells → **??** → Wnt/β-catenin trigger → CSC Activation → Chemotherapy resistance & HCC recurrence

In this dissertation, we sought to understand the role of Wnt/β-catenin pathway in HCC CSC activation and development of chemotherapy resistance. We hypothesize that “In HCC, the Wnt/β-catenin mediated CSC enrichment is responsible for acquiring chemotherapy resistance and therapeutic failure”.

We grow CSC spheroids without mechanical induction (or low adherent plates) using regular tissue culture plates. This allowed the pursuit of the goal, which is to identify and characterize CSCs enriched spontaneously in laboratory setting, and then methodically study role of Wnt/β-catenin in CSC activation (Chapter 3).

EpCAM, the most characterized and well accepted CSC marker is associated with poor prognosis in patients [53] and is a target of the Wnt/ β-catenin pathway. For the first time, we evaluated EpCAM+ CSCs from 3 different HCC cell lines in immunocompetent and immunocompromised mouse models with orthotopic implants (Chapter 4).

Following *in vivo* study, we sought to identify accountable triggering events of Wnt/β-catenin pathway responsible for aberrant CSC activation (Chapter 5).

CHAPTER 2

MATERIALS AND EXPERIMENTAL METHODS

2.1) Cell lines

Hepatoma cell lines, Hepa1-6 (CRL-1830), Hep3B (HB-8064) and HepG2 (HB-8065), were obtained from American Type Culture Collection (ATCC, Manassas, USA). All cell lines were validated every six months or obtained from a new ATCC stock every 6 months. All experiments were performed between 5th and 20th passage.

Hepa1-6 was reported as a non-immunogenic murine cell line with an ability to form tumors in normal immunocompetent C57L/J mice, both orthotopically and subcutaneously [78-80], thus provide more clinically relevant mouse model to study tumorigenesis in presence of all confounding immune system components, contrary to athymic nude or SCID mouse models (lacks confounding immune system components). HepG2 and Hep3B secrete 17 major plasma proteins [81], and also express high EpCAM levels, a well reported CSC marker [38].

2.2) Cell culture and spheroid formation:

Hepa1-6 and Hep3B cells were grown in DMEM (MediaTech, Corning, Cat # 10-013-CV) with 4.5% Glucose, supplemented with 10% FBS (Sigma, Cat #

F2442), 100 IU/mL Penicillin, 100 µg/mL Streptomycin, 0.25 µg/mL Amphotericin (Antibiotic and Antimycotic, MediaTech Corning, Cat # 30-004-CI), 10 µg/mL Tylosin (Antimycotic, Sigma, Cat # T3397). HepG2 cells were grown in Minimum Essential Media (MEM, Gibco, Cat # 11095-080), supplemented with 10% FBS (Sigma, Cat # F2442), Non Essential Amino Acids (Gibco, Cat # 11140-050), Sodium Pyruvate (Gibco, Cat # 11360-070), 100 IU/mL Penicillin, 100 ug/mL Streptomycin, 0.25 µg/mL Amphotericin (Antibiotic and Antimycotic, MediaTech Corning, Cat # 30-004-CI), 10 µg/mL Tylosin (Antimycotic, Sigma, Cat # T3397).

For *in vitro* enrichment of Cancer Stem Cells (CSCs), we employed a widely used and accepted spheroid formation assay. Hepa1-6, HepG2, and Hep3B cells were grown in a serum-free condition (SF Group) in DMEM/F12 (1:1) media (SIGMA, Cat # D6434), supplemented with 2 mM L-Glutamine (SIGMA, Cat # G7513), 20 ng/mL recombinant human Epidermal Growth Factor (EGF, Sigma, Cat # E9644), and 10 ng/mL recombinant human basic Fibroblast Growth Factor (bFGF, Sigma, Cat # F0291), 100 IU/mL Penicillin, 100 ug/mL Streptomycin, 0.25 µg/mL Amphotericin (Antibiotic and Antimycotic, MediaTech Corning, Cat # 30-004-CI), 10 µg/mL Tylosin (Antimycotic, Sigma, Cat # T3397).

2.3) <u>Self-renewal assay:</u>

Hepa1-6 cells were seeded in serum-free (SF) media at a density of 2000 cells/well in 6-well plate, and incubated for 4 days to allow the development of speroids. After confirming formation of spheroids under the microscope, these spheroid population of cells were collected in 15 mL centrifuge tube, treated with trypsin-EDTA for 4 minutes, and prepared single-cell suspension with 500 cells/mL

density with SF media. Seed single cell suspension at 2 uL/well in 96 well plate. Mark the wells with one or two cells. Add 150 uL SF media in each marked well and monitor for 20 days. Images were taken on a daily basis to track progress.

2.4) Cell proliferation assay:

Cell proliferation was measured using the MTT assay (3-(4,5-dimthyl-thiazol-2-yl)-2,5 diphenyltetrazolium bromide) in a 96 well format. Hepa1-6 cells were seeded in triplicates at a density of 3000 cells/well in complete media (control group) or serum-free media (SF group) and incubated overnight. A separate plate was prepared for each time-point (0, 24, 48, 72, and 96 hours). After appropriate incubation period, MTT was added in each well at the final concentration of 0.5 mg/mL, and plate was incubated for 3 hours at 37 °C in CO_2 incubator. After MTT incubation, media was removed from each well and 100 uL DMSO was added to dissolve formazon crystals which generate violet color. Absorbance was measured with plate reader at 540 nm with appropriate controls in each plate. For analysis, we considered the shorter incubation time MTT reading (overnight) as 0 hour and set it as control for the subsequent time points.

2.5) Doxorubicin (Adriamycin) resistance assay:

Hepatoma cells (Hepa1-6, HepG2, and Hep3B) were seeded at a density of 5000 cells/well in a 96 well plate in triplicates, with one set of control group (complete media) and two sets of spheroids group (serum-free media). Separate 96 well plates were seeded for different time points (24, 48, 72 and 96 hours) simultaneously on the day of seeding. After 24 hours, serum-free media is replaced with complete media in one of the two sets of spheroids group (termed as SFR,

reserum) and incubated for another 24 hours. On the day 3, media is replaced with complete or serum-free media containing different concentrations of Doxorubicin (0.05 μM, 0.5 μM (clinical), and 5 μM (10x clinical)) (SIGMA, Cat # D1515). MTT assay was performed at 24, 48, 72, and 96 hours after initiating DOX treatments as described in the cell proliferation assay. Each plate and group had appropriate untreated control in triplicates, and corresponding data for untreated group was considered as 1 i.e. 100 % viability. DOX treated cells were normalized to their corresponding untreated controls on the same plate, compared and analyzed.

2.6) Flow cytometry analysis:

Hepa1-6 control or 7 day spheroid cells grown in 100 mm discs were collected by gentle cell scraping. Collected cells were passed through 50 micron strainer 5 times to remove cell clumps, followed by repeat pipetting for 10-20 times to obtain single cell suspension. Use of trypsin was avoided to preserve integrity of surface receptors. Cell numbers were counted and single cell suspension was verified using a Hemocytometer. Each sample was transferred to a 15 mL tube and centrifuged for 5 minutes at 300 RCF to obtain cell pellet. Cell pellets were washed 2 times with 2% BSA/PBS. Pellets were resuspended in 100 uL 2% BSA/PBS and transferred into 1.5 mL microfuge tubes. Corresponding unstained and single stained controls were seperated for each sample, 10^6 cells/100 uL. FITC, APC or PE conjugated primary antibodies were added in 100 uL of cell suspension as per manufacturer recommendations or in-house optimized dilution (1:100 for most experiments and antibodies). Samples are gently vortexed and incuabted in the dark at 4 °C for 1 hour. After incubation, cells were washed once

with 1 mL 2%BSA/PBS, resuspended in 500 uL 2% BSA/PBS, transferred into labeled flow-tubes, and stored in the dark on ice until analysis were performed. Data were recorded on BD FACSCanto or BD FACSCalibur (BD Biosciences). For analysis, live cells were gated to exclude dead cells and cell debris. Required compensations were performed for dual FITC and PE staining experiments. In majority of our experiments, we chose FITC and APC. Data analysis was performed either by FACS Diva or FlowJo software suites.

2.7) Immunocytochemistry (ICC) staining:

Hepa1-6 control or spheroid cells were grown in 8 well Nunc™ Lab-Tek-II chamber slide (Thermo scientific, Cat # 154534) for 7 days (seeded at 100 cells/well to avoid overgrowth at the end of 7 days). Media was changed on the 4th day to ensure viability. Cells were fixed with 4% PFA for 30 minutes (or 70% ethanol overnight). Fixed cells were washed 2 times for 15 minutes with PBS-T, and blocked with 10% BSA in PBS for 20 minutes. Blocked cells were washed again for 2 times for 15 minutes with PBS-T and incubated with 100 uL primary FITC conjugated antibodies at room temprature for 2 hours (EpCAM, CD90, CD133, 1:100 dilution in 10% FBS in PBS-T). Following antibody incubation, cells were given 3 time 10 minute PBS-T washes and stained for nuclear staining with DAPI (1:1000 dilution). After DAPI staining, cells were given 2 time 10 minute PBS-T washes. Plastic chambers were removed from each Lab-Tek slides as per manufacterur's instructions, using the tools provided. The exposed glassslide surface with cells were sealed with coverslip using 5-10% glycerin. The slides were then examined using Olympus 1×51 microscope at 20x magnification using the

Olympus DP72 digital camera via the cellSens Dimention imaging system (Olympus, Pittsburgh, PA) with FITC, DAPI and brightfield settings. Digital images were taken, and analyzed using Cellsense software (Olympus, Pittsburgh, PA).

2.8) Aldefluor assay for ALDH activity:

Aldefluor activity was assayed in Hepa1-6 control and spheroid cells using Aldefluor kit according to the manufacturer's instructions (Stemcell technologies, Canada). Briefly, 3 mL of cell suspension was prepared in DMEM without serum at 10^6 cells/mL final dilution. These cells were centrifuged at 250 RCF for 5 minutes, and pelleted cells were resuspended in 3 mL of Aldefluor buffer on ice. To get the fluorescence product, we added 45 uL of Aldefluore substrate into 3 mL of the each of the cell suspension samples on ice. Immediately after mixing, 1 mL was transferred into a new tube containing 30 uL ALDH1 inhibitor diethylaminobenzaldehyde (DEAB), and later used as an inhibitor control (negative control). Test samples and negative controls were incubated at 37 °C for 45 minutes, mixed every 10 minutes. Then, cells were cenrifuged at 250 RCF for 5 minutes, resuspended in Aldefluore buffer and incubated on ice for 1 hour. Data were recorded on BD FACSCanto at FITC channel with 488 excitation laser.

2.9) Hoechst 33342 efflux assay:

After 7 days in culture, Hepa1-6 Control and spheroid cells were harvested in 15 mL centrifuge tubes. 5 mL cell suspension with 10^6 cells/mL was prepared for each sample, centrifuged at 250 RCF for 5 minutes, washed two times and resuspended in 2%FBS in PBS. Hoechst 33342 (Life technologeis, Cat # H1399) dye was added to 5 mg/mL final concentration in 2% FBS in PBS and cells were

incubated for 90 minutes at 37 °C. Cells were then incubated on ice for 10 minutes, followed by ice cold 1X PBS wash. These cells were immediately mounted on glass slides and analyzed within 1 hour on a fluorescence microscope with UV excitation settings. It is imperative that cells were viable during the steps of the assay. Hoechst 33342 dye stains the nuclear compartment and is visible at 355 nm excitation (blue color) using the common DAPI filter. Cells with dye exclusion property were identified by comparing/overlaping the images obtained under brightfield settings.

2.10) Lentivirus transduction and generation of stable HCC cell lines:

We used commercially available fourth generation lentivirus packing system (Lenti-X, Takara-Clontech), for generating stable cell lines. Briefly, puromycin resistant – copGFP (pLenti-CMV-GFP-Puro) and Blasticidin resistant mCherry (pLV-Bsd-CMV-mCherry) vectors were obtained and amplified in Stable competent EColi (New England Biolabs) by employing standard molecular biology protocol with 100 µg/mL Ampicillin selection, purified for lentivirus packing using commercial plasmid prep kit (Takara-Clontech). For generating lentivirus, lenti-X reagent was mixed with 6 µg of lentivirus plasmid and transfected in 293T cell line (Takara-Clontech) for packing. Harvested lentivirus were used to transduce target cell lines using polybrene with established protocol. Hepa1-6, HepG2, and Hep3B cell lines were transduced with copGFP lentivirus, and cell lines were selected with 3 µg/mL puromycin (Sigma-Aldrich) and expanded after confirmation by fluorescence microscope for copGFP expression. Hepa1-6 cell line was

transduced with mCherry lentivirus, and selected with 10 μg/mL Blasticidine (Sigma-Aldrich).

2.11) B-Mode ultrasound imaging

Linear-mode ultrasound data was generated and recorded using a VisualSonics 2100 high-frequency ultrasound system with MS-400 probe (30 MHz center frequency) and the VisualSonics 3D acquisition imaging hardware and software. To exclude noise caused by movement from respiratory and cardiac function, we acquired data using software-based respiratory and cardiac gating. Cardiac and respiration gating can synchronize data acquisition at defined time within the cardiac cycle and/or only acquire data when the animal is not actively breathing, thus allowing limiting movement artifact and high quality images. The entire liver was scanned in B-mode image using the 3D motor and Vevo2100 software. To stay consistent with animals and images, we have stored our settings on the instrument. Stored setting parameters: Frame rate = 16, depth = 12.00 mm, dynamic range = 65 dB, width = 15.36 mm. The optimal ROI plane was selected following B mode analysis of 3D liver data to allow us maximum liver plane coverage, as well as to learn organ orientation avoiding vessels/organs in that ROI plane.

2.12) Preparation of animals for imaging and contrast agent preparation

After 10 weeks on special diets, animals were evaluated by high-frequency ultrasound (VisualSonics model 2100, Toronto, Canada). The animal was

positioned on a heated platform under 1.5% isoflurane anesthesia. Abdominal fur corresponding to the liver was removed by a depilatory cream. The animal's body temperature, heart rate, and breathing were continuously monitored during the entire imaging procedure.

Shortly before each experiment, lyophilized Vevo MicroMarker non-targeted contrast agent (VS-11913, VisualSonics, Canada) was prepared to generate an injection-ready contrast agent. Briefly, we resuspended sterile 700-µL saline in each VS-11913 vial using a 1-mL syringe and 21G 5/8" needle. This stock solution (2 x 109 microbubbles/mL) was further diluted to 1:10 in saline for each animal 5 minutes before injection (2 x 108 microbubbles/mL). 100 µL of this diluted contrast-agent (2 x 107 microbubbles) was administered as a bolus injection via tail-vein method for data acquisition.

2.13) Contrast-enhanced ultrasound (CEUS) imaging

Contrast-enhanced imaging was performed using the MS-250 (22 MHz) probe. We used non-linear mode ultrasound for this application. We used a tail-vein for contrast injection using a standard technique. Briefly, the tail was submerged in warm water (35 – 45°C) for 1 minute to dilate lateral veins and then cleaned with 70% ethanol. We attached a syringe containing 100 µL contrast-agent (VS-11912 cannulation kit, VisualSonics, Canada) to PU tubing and a 27G butterfly needle and confirmed the absence of air bubbles. We then confirmed ultrasound site location, probe orientation, and instrument settings. The optimal ROI plane was selected following B mode analysis of 3D liver data to allow us

optimal liver plane coverage by avoiding vessels/organs in that ROI plane. ROI was defined manually using measurement tools of VevoCQ software. After confirming all experimental settings, we recorded pre-bolus perfusion data and then injected 100 µL of prepared contrast agent while continuing contrast-ultrasound data acquisition. To stay consistent between animals and images, we have stored our acquisition settings on the same instrument. Stored setting parameters: Frame rate = 25, depth = 12.00 mm, dynamic range = 65 dB, width = 23.04 mm.

2.14) Ultrasound data analysis

Acquired data was stored without editing and one copy was transferred to an analysis workstation. B mode quantification was carried out by calculating mean gray-scale intensity of three hepatic ROIs for each animal using pixels v/s intensity histogram, and averaged within a group. B-mode renal cortex mean gray-scale intensity was calculated for each animal, and averaged within a group. Hepatic/renal ratio was calculated as “mean gray-scale intensity of the liver/mean gray-scale intensity of the renal cortex” for each group.

Perfusion-quantification data analysis was carried out using the Vevo CQ software module (VisualSonics, Toronto, Canada). Briefly, for each animal data time point, captured contrast-enhanced ultrasound clips were analyzed independently in three steps. In the first step, the clip-editor module was used for inclusion-exclusion of frames/images to ensure data quality. We excluded any frame(s) that were not aligned with the rest of the frames due to gross motion artifact. In the second step, additional fine motion correction was used for

additional movement compensation by spatially realigning successive images to minimize respiratory background. In the third step, the quantification module was used to perform quantitative analysis of contrast-agent perfusion in regions of interest. Linear/pre-log data were analyzed for the time intensity curve analysis using VevoCQ software module. The software module uses curve-fitting algorithms based on a mathematical model of bolus-kinetics.

2.15) Animal experiments

Sexually matured 8-week-old C57L/J mice (stock # 000668, both male and female) and Nu/J (stock # 002019, males only) were purchased from Jackson laboratory. All animal studies were carried out in strict compliance with the Institutional Animal Care and Use Committee (IACUC) guidelines at the University of Louisville. All experimental procedures were approved by the IACUC at the University of Louisville (UofL). All mice were housed in the UofL Research Resources Center (RRC) at 22°C with 12-hour light/dark cycles with free access to food and water.

In vivo experiments using the Hepa1-6 cell line (control v/s spheroids) were performed in 12-week-old male C57L/J mice (inbred at UofL). Each experimental group had n=6 animals. For orthotopic inoculation, $2x10^6$ Hepa1-6 non-spheroid control cells or 7-day spheroids were injected into left liver lobe of an animal. Post injection, mice were monitored for two weeks and then euthanized on day 14. Animal weight, liver weight, tumor weight, and tumor size were recorded for each animal.

Establishing diet induced animal models (chapter 4)

Sexually matured 8-week-old C57L/J mice were inbred to develop consistent and accurate diet-induced mouse models necessary for this study. After 1 month from the birth on normal chew diet, mice were randomly assigned to one of three groups (n=6 mice/group). Then each group was assigned to one of the three diets and mice were fed a normal control diet (10% fat, D12450B, Research Diets, Inc., New Brunswick, NJ), or high-fat diet (60% fat, D12492, Research Diets, Inc., New Brunswick, NJ), or NASH diet (choline deficient diet with 0.1% methionine and 60% fat) for next 10 weeks. For orthotopic inoculation, $2x10^6$ sorted EpCAM+ or EpCAM- Hepa1-6 cells were injected into left liver lobe of an animal. Post injection, mice were monitored for 18 days by high-frequency ultrasound to follow the tumor growth and euthanized on day 18. Animal weight, liver weight, tumor weight, and tumor size were recorded for each animal.

Establishing Nu/J orthotopic mouse models (for HepG2 and Hep3B studies in chapter 4)

8-10 week-old male Nu/J mice (purchased from Jackson laboratory) were used for both HepG2 and Hep3B *in vivo* experiments. For orthotopic inoculation, $2x10^6$ sorted EpCAM-Low or EpCAM-High cells (HepG2 or Hep3B) were injected into left liver lobe of an animal. Post injection, mice were monitored for 70 days by high frequency ultrasound for tumor growth monitoring, and then euthanized on day 70. Animal weight, liver weight, tumor weight, and tumor size were recorded for each animal.

2.16) Protein extraction and Western Blot analysis:

After treating cells with respective media and/or regulators for desired time, media was aspirated from the culture and cells were washed two times with 1X PBS. Cells were lysed by adding SDS lysis buffer (supplemented with protease and phophatase inhibitors, Thermo scientific, Cat # 78443) directly into wells (100 uL per well of 6-well plate or 500 uL per 100 mm plate). For spheroids group (non-adharent cells), cells were collected by gentle scraping and pipetted into 15 mL centrifuge tube. Culture media was removed by centrifugation for 5 mins at 150 RCF to collect cells followed by two time 1x PBS washes to remove all media traces. Lysis buffer was then added into the tube according to pelleted packed cell volume (100 uL lysis buffer for each 20 uL packed cell volume). Cells were transfered to 1.5 mL microfuge tube and sonicated for 10-15 seconds on ice. After 30 minutes incubation on ice, lysates were centrifuged for 30 minutes at 14,000 RCF at 4 °C. Supernatant containing total cellular protein was collected carefully and transfered to new labeled 1.5 mL microfuge tube. Purified protein samples were stored at -80 °C untill further use. For cytoplasmic and nuclear fractionation, we used a commercially available kit (Pierce, ThermoFisher, Cat # 78833). Fractionation was performed as per manufacturer's protocol. Extracted protein were stored at -80 °C untill further use.

Extracted protein were quantified using the Bradford assay (Biorad, Cat # 500-0006) in a 96 well plate format and readings were performed at 620 nm using the ELISA reader (MultiSKAN MCC/340, Thermo Scientific).

Equal protein (20-50 μg each) were loaded on 8% SDS-PAGE electrophoresis gel. Protein samples were seperated by SDS-PAGE and then electrotransferred onto nitrocellulose membrane (Amersham, GE) . Following electrotransfer, the membane was blocked in 5% non-fat milk for 1 hour at room temprature. The membrane were incubated in primary antibody overnight (1:1000 or 1:2000 final dilution). Next day, the membrane was washed 3 times with TBST for 7 minutes each. The membrane was then incubated for 1 hour in secondary HRP conjugated-Anti-Mouse IgG (Cell Signaling, Cat # 7076; OR Santacruz Biotech, Cat # sc-2005) or secondary HRP conjugated-Anti-Rabbit IgG (Call Signaling, Cat # 7074; OR Santacruz Biotech, Cat # sc-2004). Secondary antibodies were diluted either 1:2000 or 1:4000 as per experimental requirement. Ater secondary antibody, blot was washed 3 times by TBST, followed by 1 wash of TBS and incubated in dark for 1 minute in Westen Blot Luminol Reagent (Santacruz Biotech, Cat # sc-2048). Chemiluminescence signals were detected in the darkroom using x-ray films. Densitometry analysis were conducted using ImageJ software (NIH).

Primary antibodies: β-Catenin (SantaCruz Biotech, Cat # sc-7963), β-actin (SantaCruz Biotech, Cat # sc-81178) , GAPDH (SantaCruz Biotech, Cat # sc-365062), GSK3β (Cell Signaling, Cat # 9832), phospho-GSK3β (Ser-9) (Cell Signaling, Cat # 5558), ABCG2 (Cell Signaling, Cat # 4477), Cyclin-D1 (Cell Signalling, Cat # 2978), TCF-1 (Cell Signaling, Cat # 2203), C-MYC (Cell Signaling, Cat # 5605).

2.17) RNA interference (siRNA) and Spheroid Reversibility Assay:

For each siRNA used, we provided sense and antisense sequences in table – 2.1. Lipofectamin RNAiMAX, and validated siRNA oligos targeting β-catenin (siCtnnb1: s63417, s63418; and siCTNNB1: s436, s437) or scrambled control (Cat # 4390849) were obtained (Lifetechnologies, CA, USA) and experiment was performed as per instructions provided. Cells were seeded and allowed to grow spheroids for 3-4 days, transfected on 4th day with siRNAs, and incubated for additional 72 hours (Hepa1-6) or 48 hours (HepG2). For calculating CSCs, differentiated, and single cells, 5 random fields/well were selected and quantified. Data were normalized to untransfected control, followed by mean and S.D. calculation. Experiments were performed n=3 times independently, and transfection was carried out using combination of two siRNAs targeting different exons.

Table 2.1: siRNA sequences

siRNA used (Lifetech #)	PubChem SID	Sequence (5' -> 3')	**Length**
siCtnnb1 (s63417)	N/A	Sense: CACUUGCAAUAAUUACAAAtt Antisense: UUUGUAAUUAUUGCAAGUGag	21 21
siCtnnb1 (s63418)	N/A	Sense: GACUCAAUACCAUUCCAUUtt Antisense: AAUGGAAUGGUAUUGAGUCct	21 21
siCTNNB1 (s436)	160757058	Sense: GGACCUAUACUUACGAAAAtt Antisense: UUUUCGUAAGUAUAGGUCCtc	21 21
siCTNNB1 (s437)	160757163	Sense: GGAUGUUCACAACCGAAUUtt Antisense: AAUUCGGUUGUGAACAUCCcg	21 21

2.18) Human HCC specimens:

This study was approved by the Institutional Review Board for Human Study at University of Louisville. The study samples were retrospectively collected from 24 patients who had undergone liver resection for hepatocellular carcinoma between 2002 and 2013. 24 subjects, 13 male (54.2%) and 11 female (45.8%) with a median age of 67, ranging from 41 to 84 years old, who had a clinical diagnosis of hepatocellular carcinoma and underwent liver resection, were studied. The control samples consisted of the same 24 patients' normal adjacent tissue that were within the resected liver specimen.

2.19) Hematoxylin and Eosin (H&E) staining

After animals were euthanized, liver tissues were isolated and weighted. A piece of tissue was taken from a liver lob and fixed in 10% buffered formalin for 24 hours and transferred to 80% ethanol. The formalin-fixed liver tissue was processed (stepwise dehydrated) and embedded in paraffin. Serial 5-μm sections were mounted onto glass slides. These slides were used for Hematoxylin and Eosin (H&E) staining for each animal. HE staining was blinded and analyzed by two pathologists for experimental groups and assign total NAFLD histopathology score (0-8) based on inflammation (0-3), steatosis (0-3), and Hepatocyte ballooning (0-2) [82, 83].

2.20) Immunohistochemical assay for EpCAM in human specimens:

EpCAM protein expression were determined by using an immunohistochemical assay. Staining was carried out on the paraffin-embedded tissues using the DAKO EnVisionTM+System kit (DAKO Corporation, Carpinteria, CA) according to the manufacturer's instructions. The sections were deparaffinized and hydrated, then the slides were washed with TRIS buffer. Peroxidase blocking was performed for 5 minutes. After rewashing, the slides were incubated with EpCAM antibody (1:100) (SantaCruz Biotechnology Inc, CA) for 30 minutes at room temperature. The slides were rinsed and the specimens were incubated with the labeled polymer for 30 minutes at room temperature. Then, the chromogenic substrate diaminobenzidine was added as a visualization reagent. Finally, the slides were counterstained with methyl green for EpCAM. A negative control was included in each run.

2.21) Computer image analysis of IHC:

A computer image analysis was performed to quantify the expression of EpCAM in the 24 samples diagnosed with HCC, and in the 24 samples of adjacent normal liver (AD). The imaging fields were chosen randomly from various section levels to ensure objectivity of sampling. Five imaging fields were scanned for each specimen sample. All digital images were acquired with the Olympus i×51 microscope at 40x magnification using the Olympus DP72 digital camera via the cellSens Dimention imaging system (Olympus, Pittsburgh, PA) and stored as JPG data files with fixed resolutions of 200 pixels/inch. The acquired color images from the immunohistochemical staining were defined at a standard threshold according

to the software specification. The computer program then quantified the threshold area represented by color images. EpCAM protein expression was defined by the percentages of threshold area in acquired color images.

2.22) Statistical analysis:

Appropriate statistical methods were referenced in each dataset or experiment throughout this dissertation. Primarily, data are presented as mean±S.D. or mean±SEM ($n \geq 3$ per group). Comparison statistics were performed by two-tail student's t-test with equal variance or one way analysis of variance (ANOVA). All the statistical analysis were performed (including chart, plots etc.) using either Sigmaplot statistical software or microsoft excel 2013. Results with $p \leq 0.05$ were considered statistical significant.

CHAPTER 3

CHARACTERIZATION OF HCC CELLS WITH CANCER STEM CELL LIKE PROPERTIES

Introduction:

In this first chapter, we characterized 3 HCC cell lines to study properties of CSCs. Hepa1-6 is murine cell line, and HepG2 and Hep3B are human HCC cell lines.

Serum-free conditions plus growth factors allow cells to grow in an anchorage-independent manner, and is a well-documented standard method for maintaining undifferentiated cells [84-87]. This technique is widely adapted for CSC studies in breast cancer [88] and glioblastoma [89]. Soon after, this technique was accepted and used in many other solid tumor malignancies including hepatocellular carcinoma [47, 90]. Also known as spheroid formation (sphere formation) culture, this is not only a CSC property, but also serves as a valuable tool to enrich CSC-like cells *in vitro*. Spheroids formed in serum-free culture have been suggested to mimic not only the phenotype but also the genotype of the primary tumor [89]. In fact, serum-free culture has been accepted and used for *in vitro* enrichment of CSCs [91].

A recent study reported that generating multicellular spheres followed by reversal to the attached cell line can significantly change the cell phenotype, which can be used as *in vitro* metastatic model [85]. Therefore, spheroid cultures provide a useful approach to enrich CSCs and to study CSC-like cells present in primary tumors with the added advantage of reproducibility and validity of findings. One study previously reported that not all cell lines can enrich CSC-like cells in spheroid culture, and each cancer cell line should be evaluated carefully and subjectively [92].

Unlike the previous studies in which CSC spheroids were enriched in low-attachment plates or mechanically induced [91], we used regular tissue culture-treated plates. Using adherent environment could resemble the *in vivo* microenvironment to a certain extent (metastasis migration via EMT by detaching site of primary tumor organ) [93].

Studies have reported the role of Wnt/β-catenin signaling in self-renewal and maintenance of CSCs in HCC [63, 64], and two of the most reported CSC markers in HCC, EpCAM and CD44, have been identified as the transcription targets of the canonical Wnt/β-catenin pathway [38, 94, 95]. Therefore, we studied status of Wnt/β-catenin signaling in enriched culture of HCC CSCs. Also, for the first time, we evaluated tumorigenic property of Hepa1-6 CSCs in immunocompetent orthotopic mouse model.

Results:

3.1) Hepatoma cells could form anchorage-independent, self-renewing spheroids (spheres) in serum-free culture *in vitro*:

To enrich HCC CSCs from hepatoma cell lines *in vitro*, we employed serum-free conditions using DMEM/F-12 (1:1) media supplemented with recombinant human Epidermal Growth Factor (EGF) and basic Fibroblast Growth Factor (bFGF). We evaluated spheroids for CSC properties. We found that all three hepatoma cell lines (Hepa1-6, HepG2, Hep3B) successfully formed spheroids in serum-free conditions (Figure 3.1).

Self-renewal capability is the most fundamental property of CSCs and proposed as the primary mechanism responsible for maintaining undifferentiated cells with CSC like properties in tumors [96]. We have primarily characterized Hepa1-6 spheroids. To test if enriched Hepa1-6 spheroids possess self-renewal capability, we performed two separate experiments. In the first experiment, we tested if spheroid cells can be serially passed from one generation to the next without dying or losing spheroid forming capability. The rationale behind this experiment is to show that well differentiated cells cannot survive in serum-free stress conditions optimized for anchorage independent growth, while only cells with stem-like properties are able to maintain themselves and propagate. Hepa1-6 spheroids were serially passaged for more than 10 generations in serum-free conditions, indicating their self-renewal capability (data not shown).

In the second experiment, we confirmed self-renewal capability of CSC like cells by means of more quantitative “self-renewal assay”. Hepa1-6 spheroid cells

were seeded in 96 well plates (single cell/well) and monitored for their growth pattern daily for 20 days (Figure 3.2). In this condition, cells can have one of three fates: 1) self-renewal (spheroid formation), 2) differentiation (adherent phenotype), 3) quiescence (stays as a single cell). Approximately, 24% Hepa1-6 cells showed self-renewal capability by forming spheroids. These growing spheroids (Figure 3.2 - A & C) also expressed EpCAM (CSC marker), further supporting CSC like-properties of spheroids. Around 51% cells stayed in the quiescence state, while about 25% cells lost their stem-ness and proceeded to differentiation (Figure 3.2 - D).

We also performed an MTT assay to quantitate cell proliferation rates in Hepa1-6 control and spheroid cells. We have found that Hepa1-6 spheroids retained proliferative capability, but growth rate is significantly slower than parental control cells (Figure 3.3).

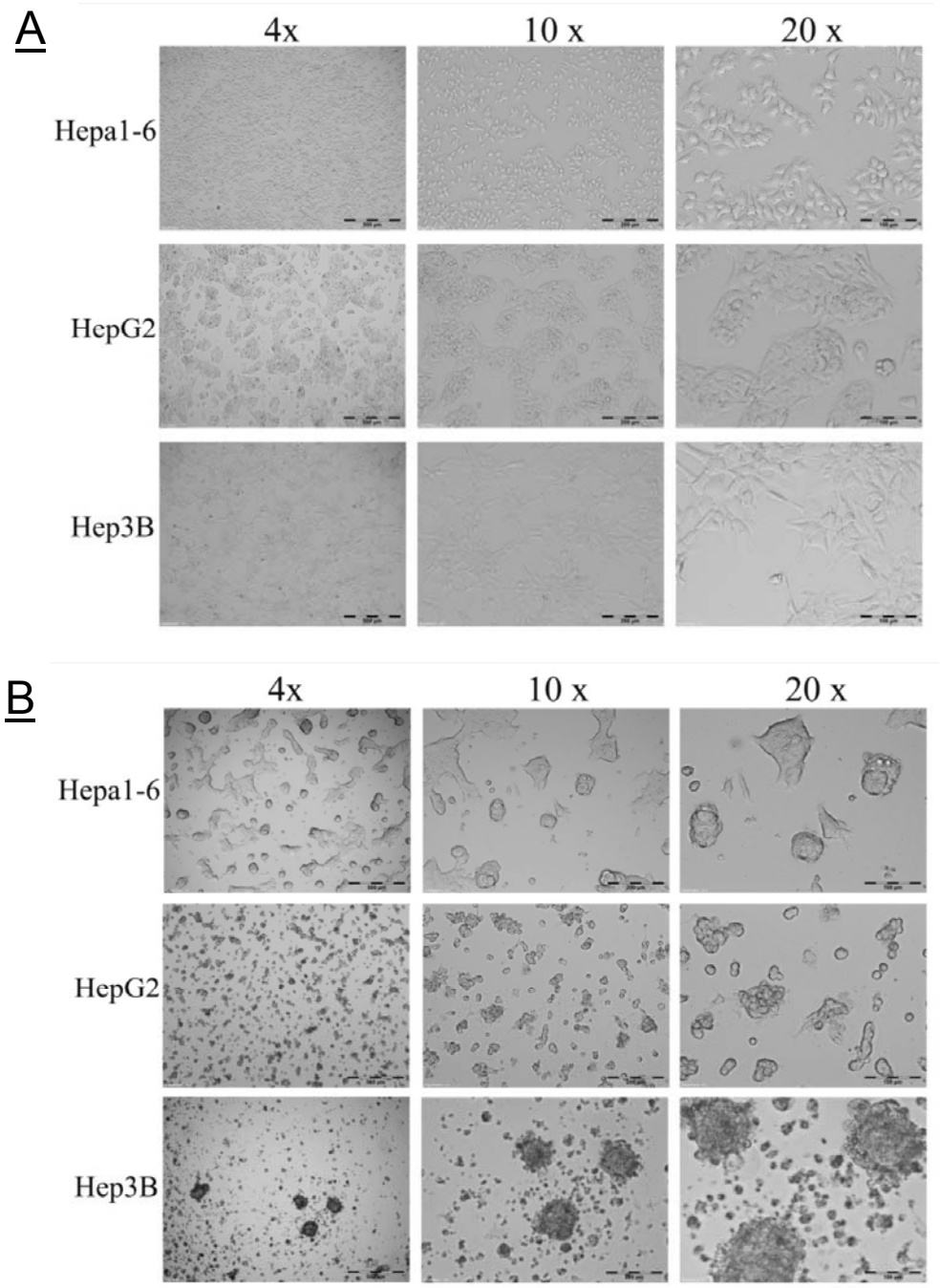

Figure 3.1: Representative images of cultured cells. Bright field microscope images. **(A)** Control hepatoma cells and **(B)** CSC Spheroids (Serum-free /SF group) in Hepa1-6, HepG2, and Hep3B cell lines. 4x (Bar = 500 μm), 10x (Bar = 200 μm), and 20x (Bar = 100 μm).

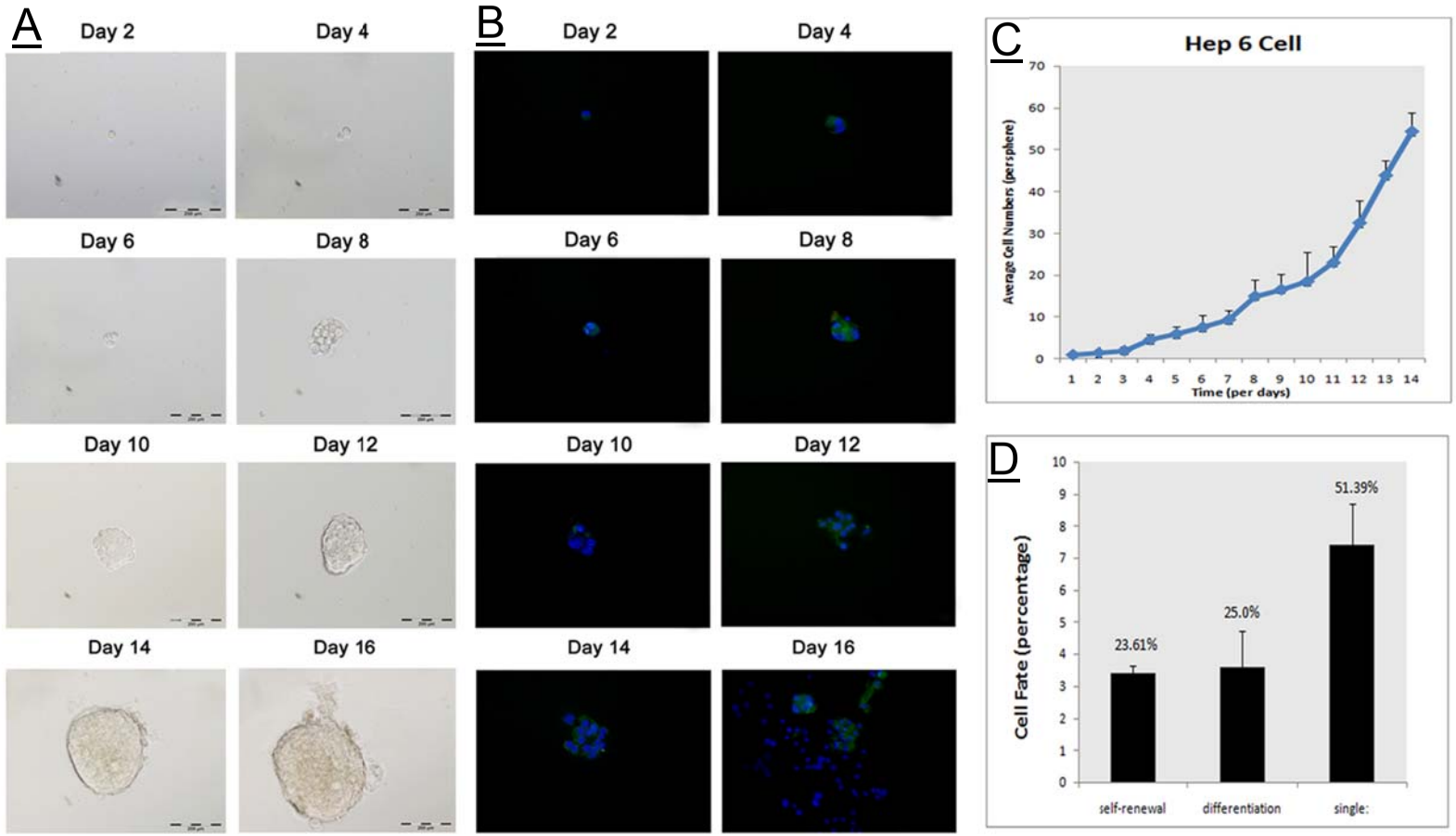

Figure 3.2: Hepa1-6 CSC Spheroids Possess Self-Renewal Capability in Serum-Free Condition. Hepa1-6 cells were seeded in 96 well plate with appropriate dilution to achieve single cell/well, and observed for two weeks. **(A)** Bright field microscope images at different time-points. **(B)** DAPI and FITC-EpCAM (CSC marker) staining, (C) Graph showing sphere growth with time, (D) Quantified cells for self-renewal (spheroid formation), differentiation (adherent growth), and single cell (Quiescent cells). 10x (Bar = 200 µm).

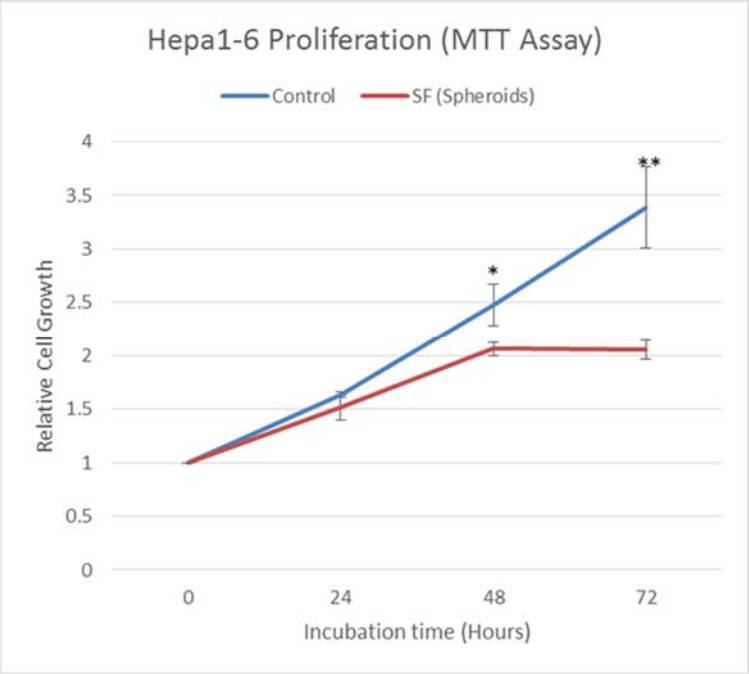

MTT Assay - Hepa1-6 proliferation				
	Incubation time (hours)			
	0	24	48	72
Control	1	1.63±0.02	2.47±0.19	3.39±0.38
SF (Spheroids)	1	1.51±0.12	2.06±0.06	2.05±0.09
P Value	NA	0.167	0.025	0.004
	NA	NS (p>0.05)	* (p<0.05)	**(p<0.005)
N=3 Experiments				
Values shown as "Mean ± S.D."				

Figure 3.3: Hepa1-6 Spheroids retained proliferative capabilities. MTT Assay was performed in 96 well plate, with seeding 3000 cells/well in triplicates. CSC spheroids retained proliferative capabilities in serum-free media, but exhibit slower growth rate compared to control group cells (complete media with serum). n= 3 independent experiments. Values shown as mean±SD.

3.2) HCC spheroids acquired doxorubicin resistance– a first line chemotherapy drug in HCC

Resistance to chemotherapeutics is another important characteristic of CSCs, and is believed to play a significant role in HCC carcinogenesis and recurrence [44]. Currently, doxorubicin (Adriamycin, DOX) is a first line drug used for HCC treatment in clinics [3].

We studied Hepa1-6 spheroids for their DOX resistance property with MTT assay as described in materials and methods. For *in vitro* experiments, we selected a clinical relevant dose (0.5 μM) as characterized in early pharmacokinetic studies in patients and widely employed by other groups for DOX studies [97]. We have also tested 1/10 (0.1x, 0.05 μM) and 10 times (10x, 5 μM) doses for characterization. Time dependent dose response curves have demonstrated that Hepa1-6 CSC spheroids were sensitive to DOX at early time points but developed resistance 48 hours post DOX treatment at both subclinical and clinical doses (Figure 3.4). We found that for the 10x dose (5 μM) there were a fraction of cells that retained higher viability after 72 hours.

When we further analyzed our data by plotting log (DOX dose) v/s viability at 96 hour time point, we found that Hepa1-6 spheroids required 2 times more DOX compared to control cells to eradicate 50% viable cells (Figure 3.5-A). Hepa1-6 spheroids were seen to have significantly increased chemotherapy resistance for doxorubicin at not only physiologically relevant dose of 0.5 μM but also to 10-fold dose increase (5 μM) ($p<0.005$) (Figure 3.5-B).

We have also investigated HepG2 and Hep3B spheroids for their DOX resistance properties. After 96 hours of treatment, both HepG2 and Hep3B CSC spheroids showed significant higher resistance for DOX compared to control cells at clinical dose of 0.5 μM ($p<0.05$) (Figure 3.6). These data support our results found in Hepa1-6 spheroids.

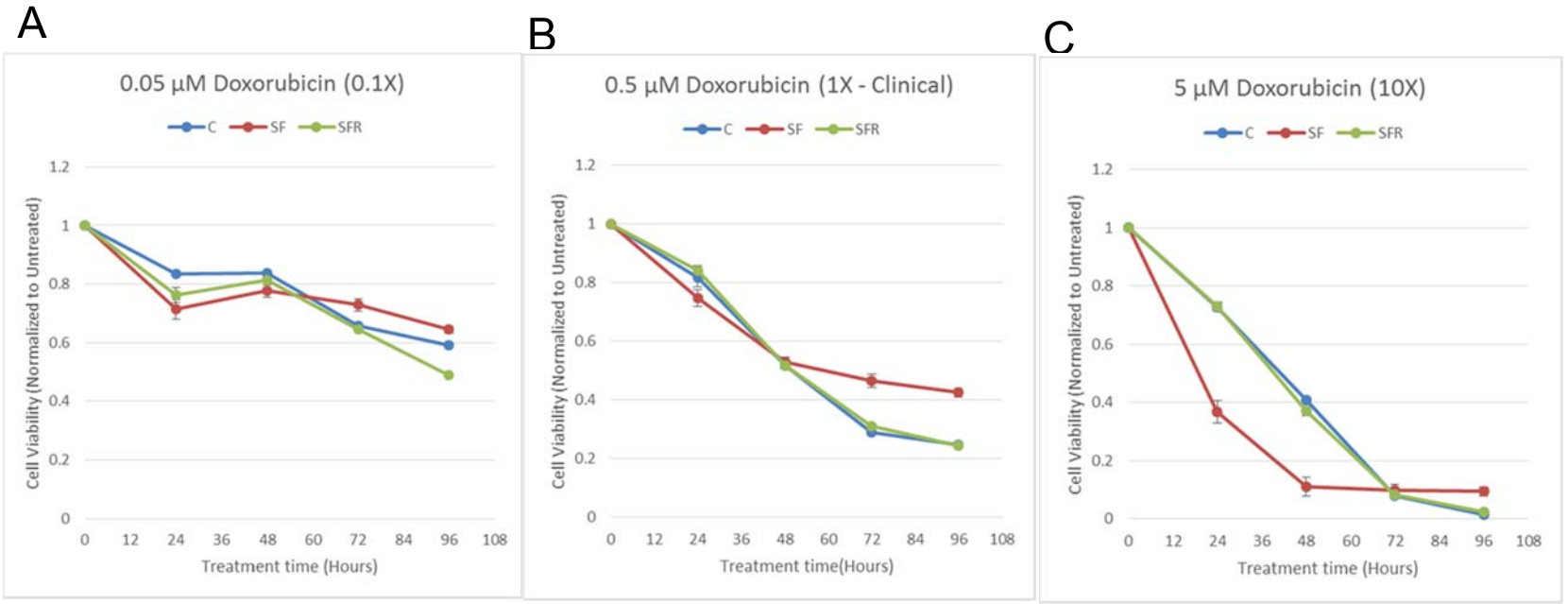

Figure 3.4: Hepa1-6 spheroids exhibit chemotherapy resistance for doxorubicin (dox) in serum-free conditions. Hepa1-6 **c**ells were seeded in triplicates in 96 well plate at 3000 cells/well, and studied for their chemotherapy resistance property by MTT assay. Media changed with DOX media (Media + Doxorubicin) after 48 hours of seeding for C and SF groups. For SFR group, 1 day serum-free treatment followed by 1 day re-serum, before changing to DOX media. Value 1 on y-axis represents 100% cell viability. **(A)** DOX treatment at 0.05 µM (subclinical dose). **(B)** DOX treatment at 0.5 µM (Clinical dose). **(C)** DOX treatment at 5 µM (10 times higher than clinical). **C** = Control Group, **SF** = Serum-free group, **SFR** = Re-serum group. Values shown in mean±SD.

A

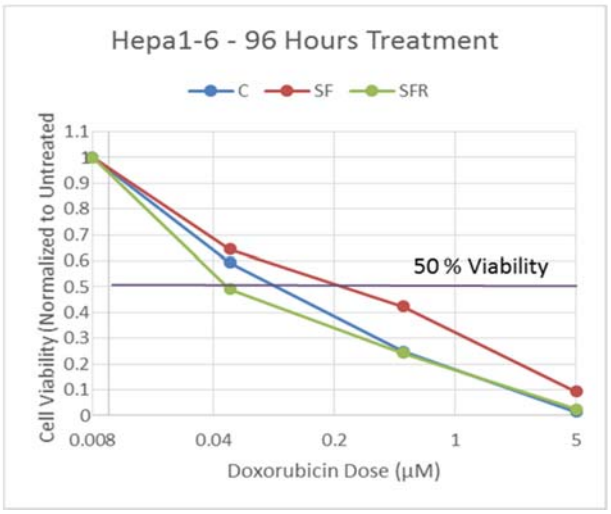

B

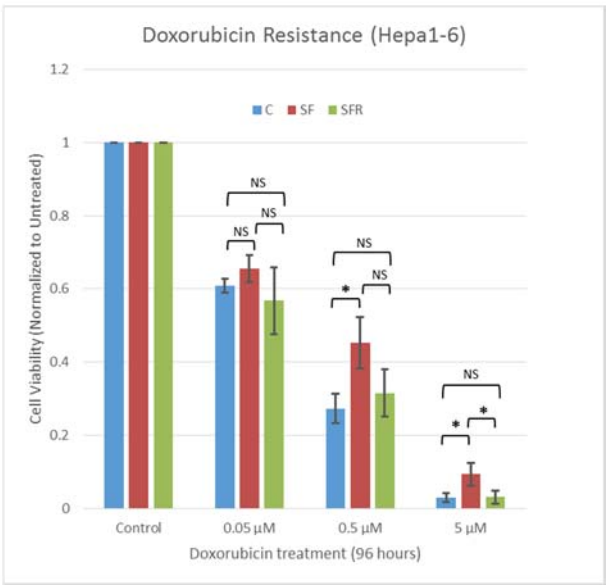

Doxorubicin (ADR) Resistance - MTT Assay (Hepa1-6 Cells)				
	Untreated	**Doxorubicin Treated (Concentrations)**		
	Control	**0.05 µM**	**0.5 µM**	**5 µM**
C	1.00 ± 0.0	0.61 ± 0.02	0.27 ± 0.04	0.03 ± 0.01
SF	1.00 ± 0.0	0.66 ± 0.04	0.45 ± 0.07	0.09 ± 0.03
SFR	1.00 ± 0.0	0.57 ± 0.09	0.32 ± 0.06	0.03 ± 0.02

Figure 3.5: Hepa1-6 spheroids exhibit doxorubicin resistance. Value 1 on y-axis represents 100% cell viability. **(A)** Dose dependent response curve (Log [Dox] v/s Cell viability) after 96 hours of Doxorubicin treatment. Hepa1-6 spheroids required increased Doxorubicin dose (2 times higher than C, and 4 times higher than SFR) to eradicate 50% cells. **(B)** Hepa1-6 spheroids (SF) are more resistant to Doxorubicin compared to control(C). n=3 independent experiments, values shown in "Mean ± S.D", *****($p<0.05$), **NS**=No significance ($p>0.05$). **C**= Control group, **SF**= Serum-free group, **SFR**= Re-serum group.

A

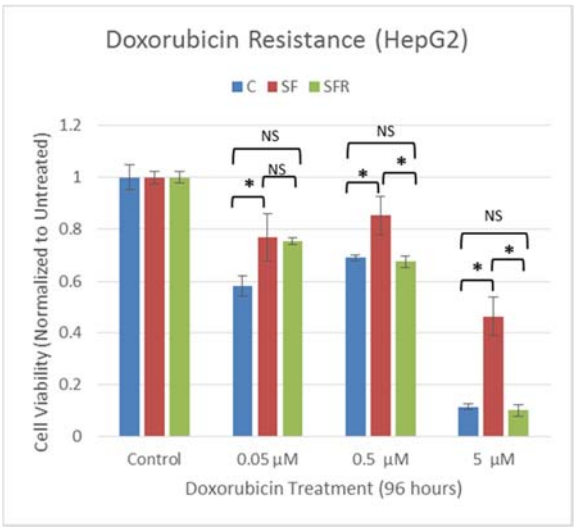

B

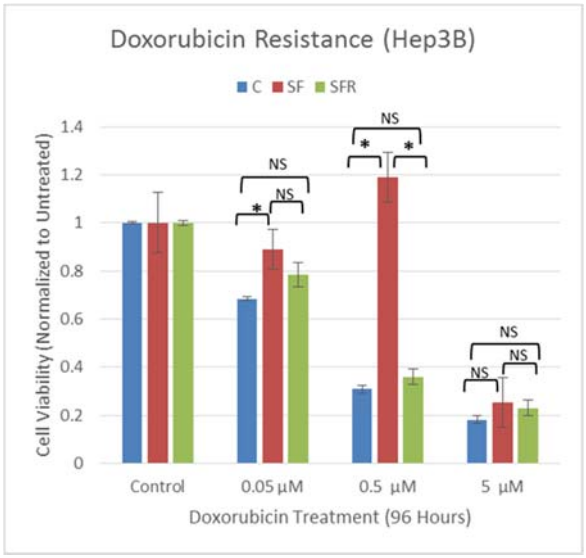

Figure 3.6. Human HepG2 and Hep3B spheroids showed doxorubicin resistance property, supporting findings in mouse Hepa1-6 cells. HepG2 or Hep3B cells were seeded in 96 well plate in triplicates at 3000 cells/well and studied for their chemotherapy resistance properties by MTT assay. Value 1 on Y-axis represents 100% cell viability. **(A)** doxorubicin resistance in HepG2 cells. **(B)** Doxorubicin resistance in Hep3B cells. For both human cell lines, HepG2 and Hep3B, spheroids showed higher resistance to doxorubicin compared to corresponding controls. Values represent mean±S.D, *****($p<0.05$), **NS**=No significance ($p>0.05$). **C**= Control group, **SF**= Serum-free group, **SFR**= Re-serum group.

3.3) Enriched HCC spheroids showed higher expressions of cancer stem cells (CSCs) surface markers and functional markers:

Surface and functional markers are currently the best available tools to define the origin and lineage of cells in animal tissues, and therefore, these tools are extensively employed to characterize CSCs in solid malignancies including HCC [31, 51, 98]. Most extensively characterized and reported surface markers for HCC CSCs are EpCAM, CD90, CD44, AFP, OV6, and CD133 [47, 51, 99]. It is noteworthy that EpCAM+ and CD90+ cells are physiologically different in terms of their tumorigenic potential and differentiation stage [54], and so is true for other markers. Because of a high degree of heterogeneity, no single maker could confidently and exclusively define HCC CSCs. Extensive research is being done globally in this pursuit.

In order to confirm CSC-like properties in HCC spheroids, we selected extensively reported and studied surface markers i.e. EpCAM, CD90, CD44, and CD133, and tested HCC spheroids for their expression by flow-cytometry and ICC. Our findings suggest that HCC spheroids showed upregulation in EpCAM levels compared to control, and EpCAM+ cells are enriched in spheroid culture (Figure 3.7-A). We confirmed our findings with ICC using anti-EpCAM antibodies (Figure 3.7-B). We also confirmed upregulation of CD90, CD44, and CD133 in spheroid culture with enrichment of CD90+, CD44+, CD90+/CD44+, and CD133+ cells (Figure 3.8). Each of these subpopulations bears different physiological properties and differentiation states e.g. CD44+/CD90+ cells were suggested as more tumorigenic and less differentiated compared to CD44+/CD90- or CD44-/CD90+

cells alone [51]. Our findings confirmed that *in vitro* Hepa1-6 spheroids can enrich all important CSC subpopulations reported so far.

As it is defined by its asymmetric cell division property and hierarchical importance, the CSC theory is a functional concept. Two extensively reported functional markers to define CSCs, ALDH activity and Hoechst 33342 efflux assays [48, 100], were also tested in Hepa1-6 CSC spheroids. Hepa1-6 spheroids showed 1.3% increase in ALDH+ cells (Figure 3.9-A). Spheroid cells also showed property of dye exclusion (Figure 3.9-B), which was confirmed by Western Blot analysis of ABCG2, multi-drug resistant transporter responsible for dye exclusion (Figure 3.9-C). Dye efflux depends on expression and activity of ABCG2, and clinically correlates with drug resistance including towards doxorubicin [48].

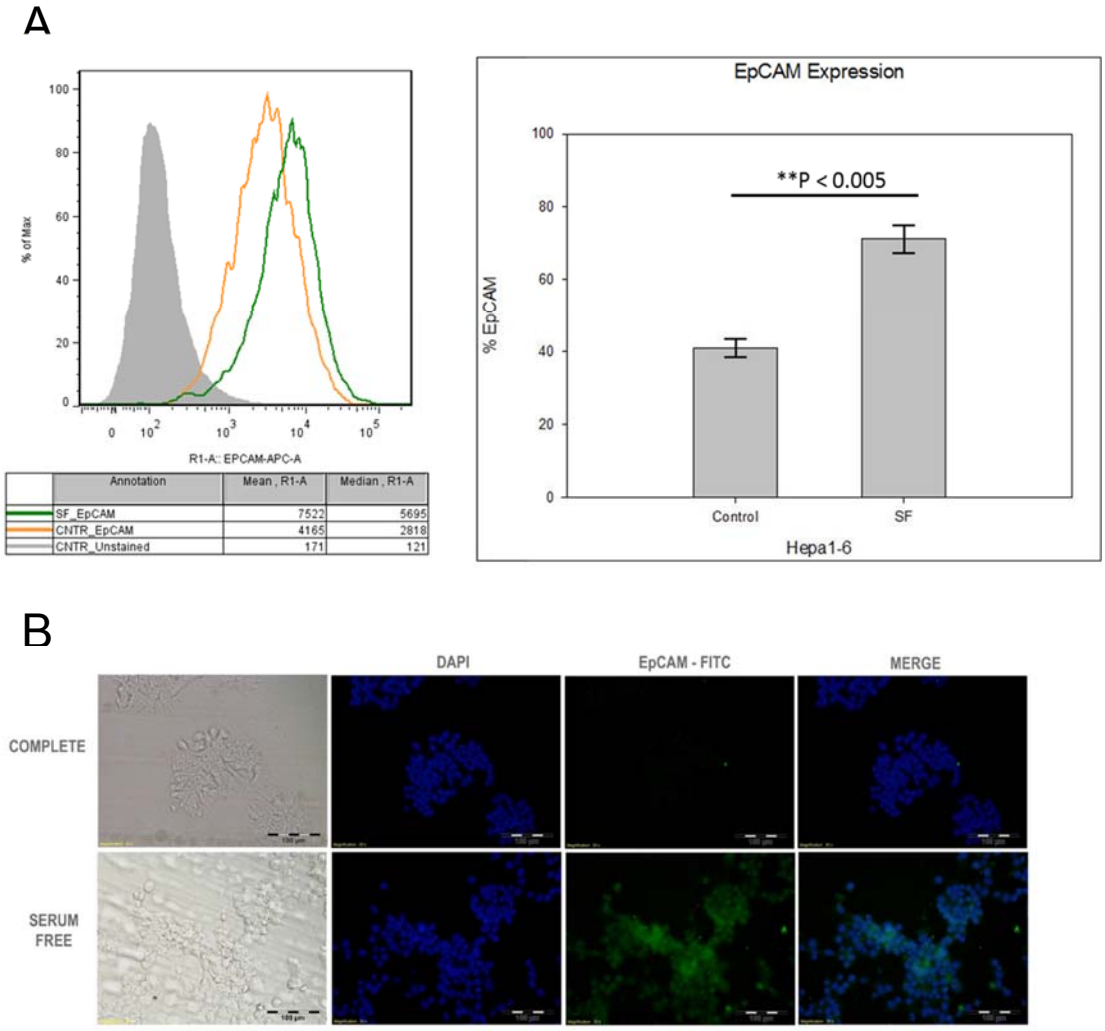

Figure 3.7: Hepa1-6 spheroids showed increased EpCAM expression. Hepa1-6 cells were grown in serum-free media (spheroids) or control media for 7 days. After 7 day treatment, cells were harvested and analyzed for EpCAM expression. **(A)** EpCAM expression analysis by flow-cytometry using APC conjugated Anti-EpCAM antibodies, **(p<0.005), n=4 independent experiments, **(B)** EpCAM expression analysis by ICC using FITC conjugated Anti-EpCAM antibodies. 7 Day SF treatment. Cells were fixed, stained and analyzed by fluorescence microscopy at 20x magnification (Bar = 100 µm). DAPI stains nuclei.

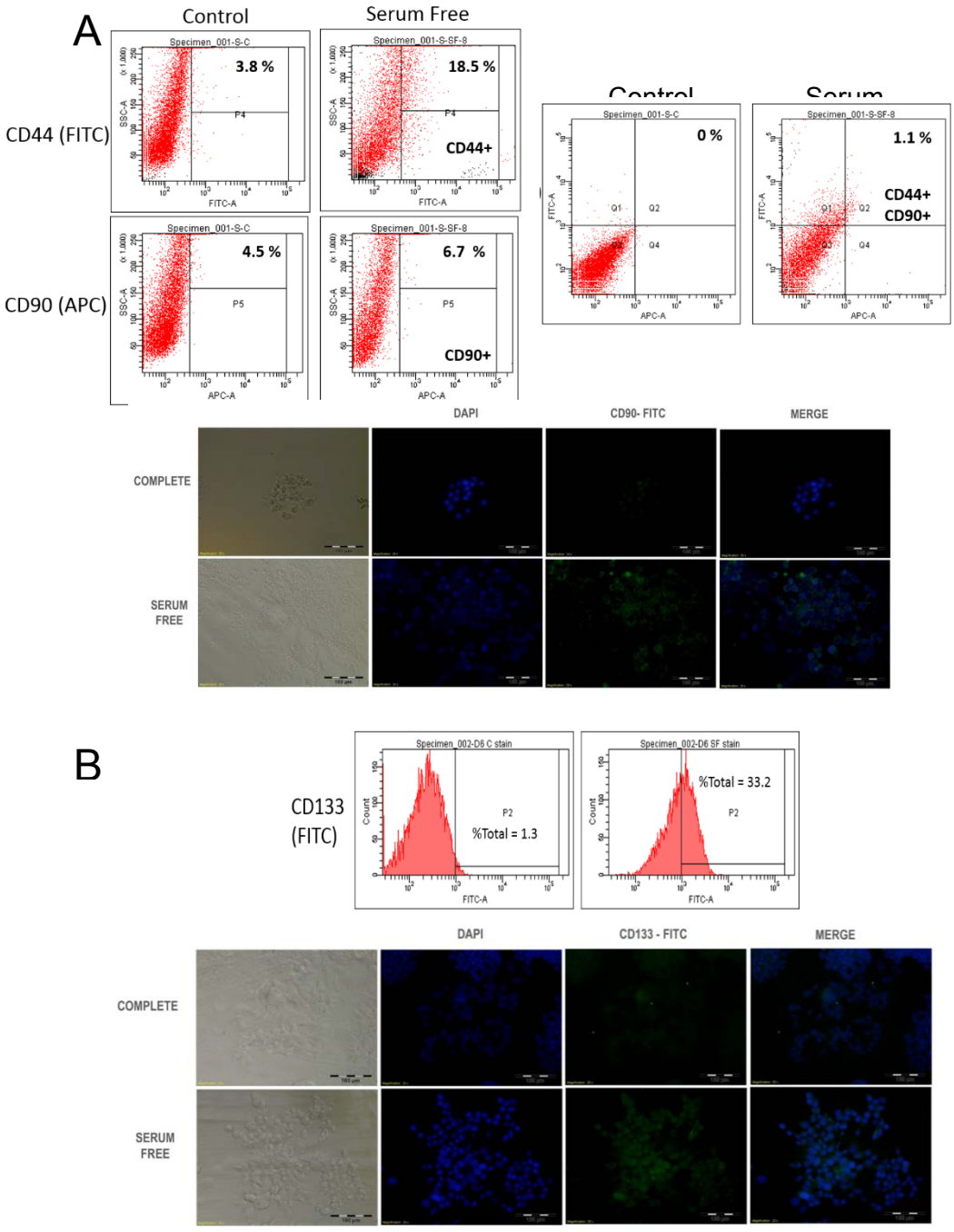

Figure 3.8: Hepa1-6 spheroids also showed increased CD44, CD90 and CD133 expression, well reported CSC surface markers. Hepa1-6 cells were grown in serum-free media (spheroids) or control media for 7 days. After 7 day treatment, cells were harvested and analyzed for corresponding markers. **(A)** CD44 and CD90 expression analysis by flow-cytometry, and CD90 analysis by ICC. **(B)** CD133 expression analysis by flow cytometry and ICC. Cells were fixed, stained and analyzed by fluorescence microscopy at 20x magnification (Bar = 100 µm). DAPI stains nucleus.

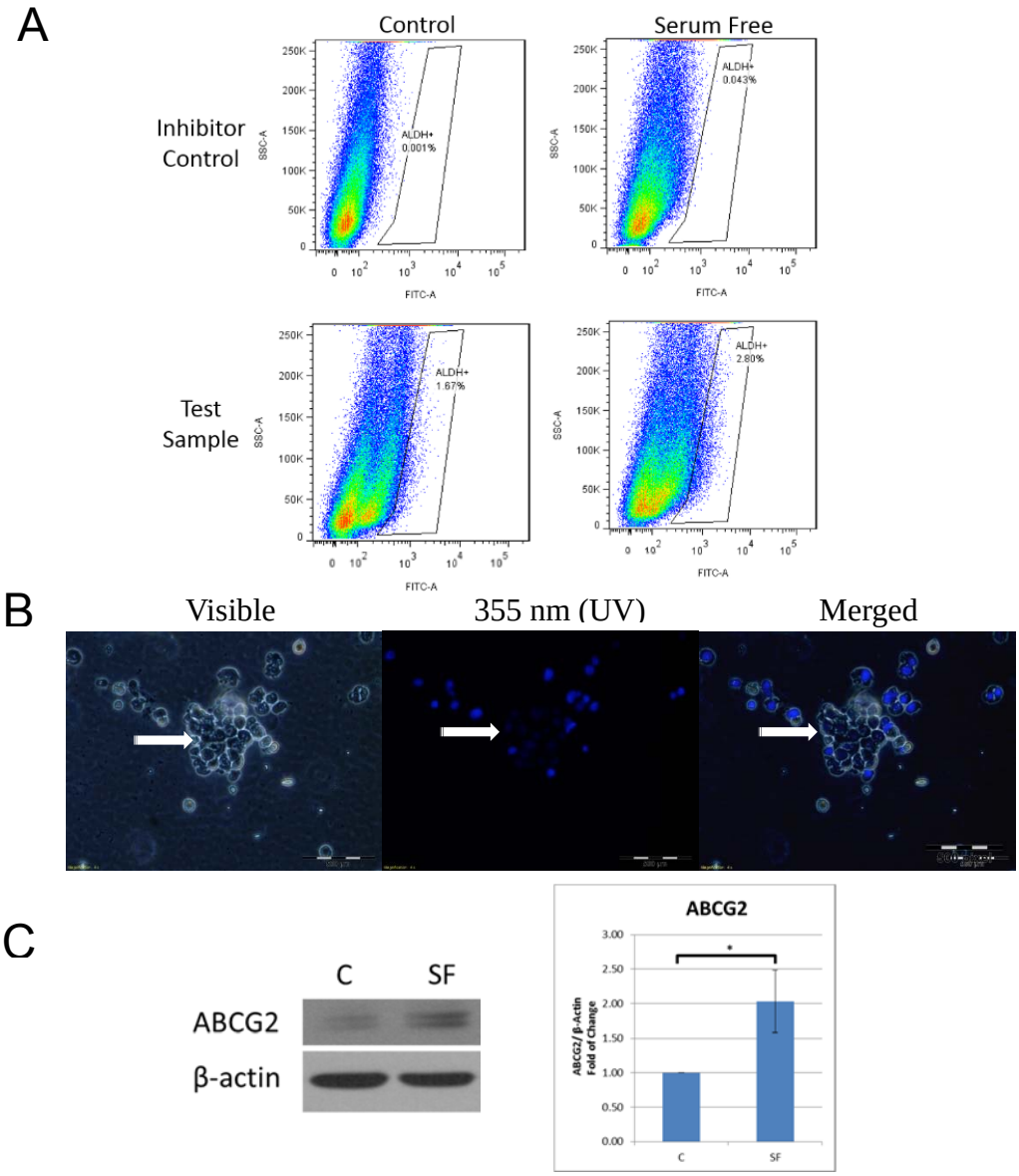

Figure 3.9: Hepa1-6 spheroids showed increased CSC functional markers. Hepa1-6 cells were grown in serum-free media (spheroids) or control media for 7 days. After 7-day treatment, cells were harvested and analyzed. **(A)** Aldefluore assay showing higher ALDH enzyme activity in CSC spheroids compared to control. **(B)** Hoechst 33342 efflux assay - ICC representative images of spheroids showing dye efflux, contributed by ABCG2 activity. Stem-like cells with high ABCG2 activity show less staining compared to normal cells (low ABCG2 activity). ICC at 10x magnification (Bar = 200 μm). Hoechst 33342 stains nuclei. **(C)** Representative Western Blot and densitometry analysis of ABCG2 expression. Increased ABCG2 expression in spheroids compared to control. *(p≤0.05), n=3 independent experiments. **C**=Control; **SF**=Serum-free.

3.4) Upregulation of β-catenin in hepatocellular carcinoma CSC spheroids:

Many signaling pathways are implicated and studied in CSCs [101]. Wnt/β-catenin pathway is the cardinal pathway in normal stem cell maintenance and highly implicated in HCC and CSCs [62, 102].

Enriched Hepa1-6 CSCs showed increased β-catenin protein levels both in the cytoplasm (1.53±0.21 fold, $p<0.05$) as well as in nucleus (1.54±0.15 fold, $p<0.001$) compared to control cells (Figure 3.10-A). We also tested β-catenin levels in HepG2 cells and found it to be consistent with our findings in Hepa1-6 cells (data not shown). Total RNA analysis by qRT-PCR further confirmed the increased β-catenin and stemness in Hepa1-6 spheroids viz. significant increase in both EpCAM and Lin28B mRNA expression (figure 3.10-B).

To further confirm functional consequences of higher β-catenin levels in Hepa1-6 CSC spheroids, β-catenin downstream targets (C-MYC, Cyclin-D1, LEF1) were analyzed by Western Blot analysis. All three downstream targets we tested were proportionately increased with increased β-catenin levels (Figure 3.11), suggesting that higher β-catenin levels in CSC spheroids have functional consequences. More importantly, C-MYC and Cyclin-D1 are strongly implicated in carcinogenesis [32].

To further investigate the increase in β-catenin levels, we tested GSK-3β phosphorylation status. Active GSK-3β (no Ser9 phosphorylation) directs cytoplasmic β-catenin to ubiquitin mediated proteasomal degradation by phosphorylating β-catenin at S33/S37/T41 positions. However, when GSK-3β itself is phosphorylated at Ser9 position, it loses its substrate specificity for β-

catenin and cytoplasmic β-catenin gets stabilized, translocates to the nucleus and regulates transcription at the gene level. Hepa1-6 CSC spheroids showed increase in inactive GSK-3β levels (phosphorylated at Ser9) compared to control cells (Figure 3.12). This finding suggests that GSK-3β activity at least partially contributed to increased β-catenin levels in Hepa1-6 spheroids and needs to be investigated further.

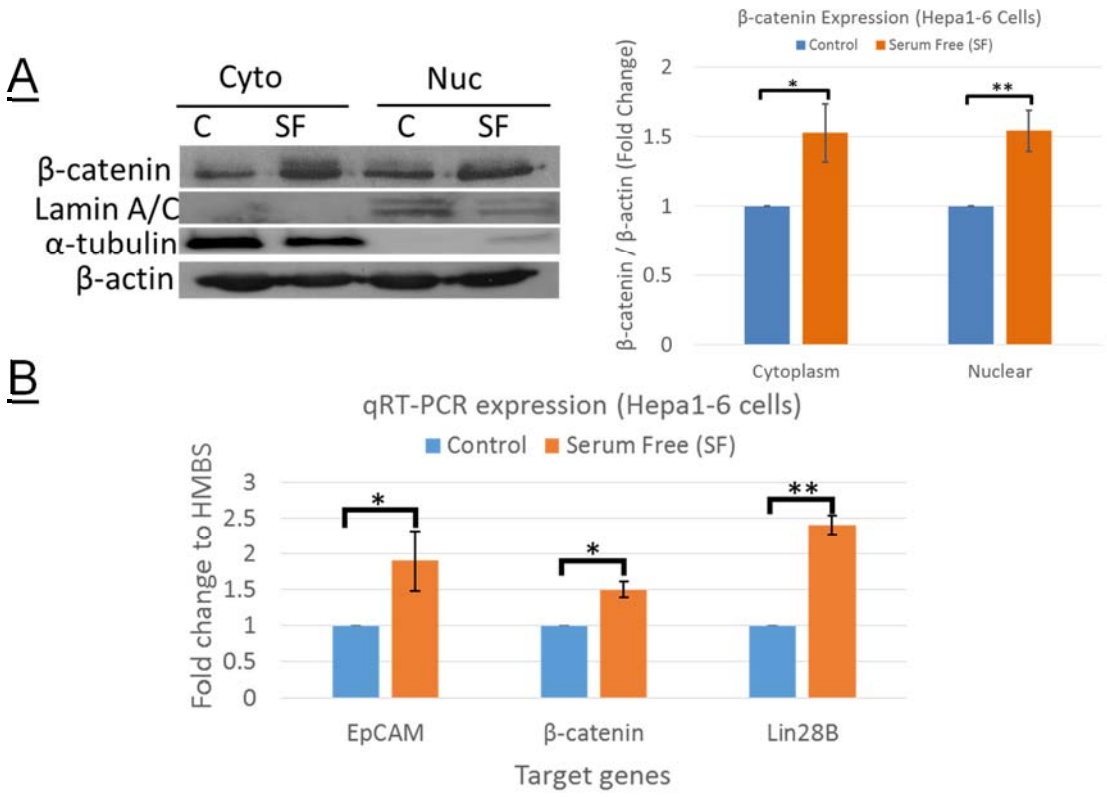

Figure 3.10: Hepa1-6 spheroids showed increased β-catenin levels. Hepa1-6 cells were grown for 7 days in serum-free media (SF) or complete media (control). Cells were harvested after 7-day treatment, and cytoplasmic and nuclear proteins were extracted. **(A)** Representative Western Blot (left), and densitometry image analysis (right). * (p≤0.05), **(p≤0.005), n=3 independent experiments. Lamin A/C and α-tubulin were used for fractionation control for nuclear and cytoplasmic fractions respectively. β-actin used as loading control and for normalization. **Cyto** = Cytoplasm; **Nuc** = Nuclear; **C**=Control; **SF**=Serum-free. **(B)** qRT-PCR analysis of total RNA for EpCAM, β-catenin and Lin28B expressions. HMBS was used as endogenous control. *(p≤0.05), **(p≤0.005), n=3 independent experiments.

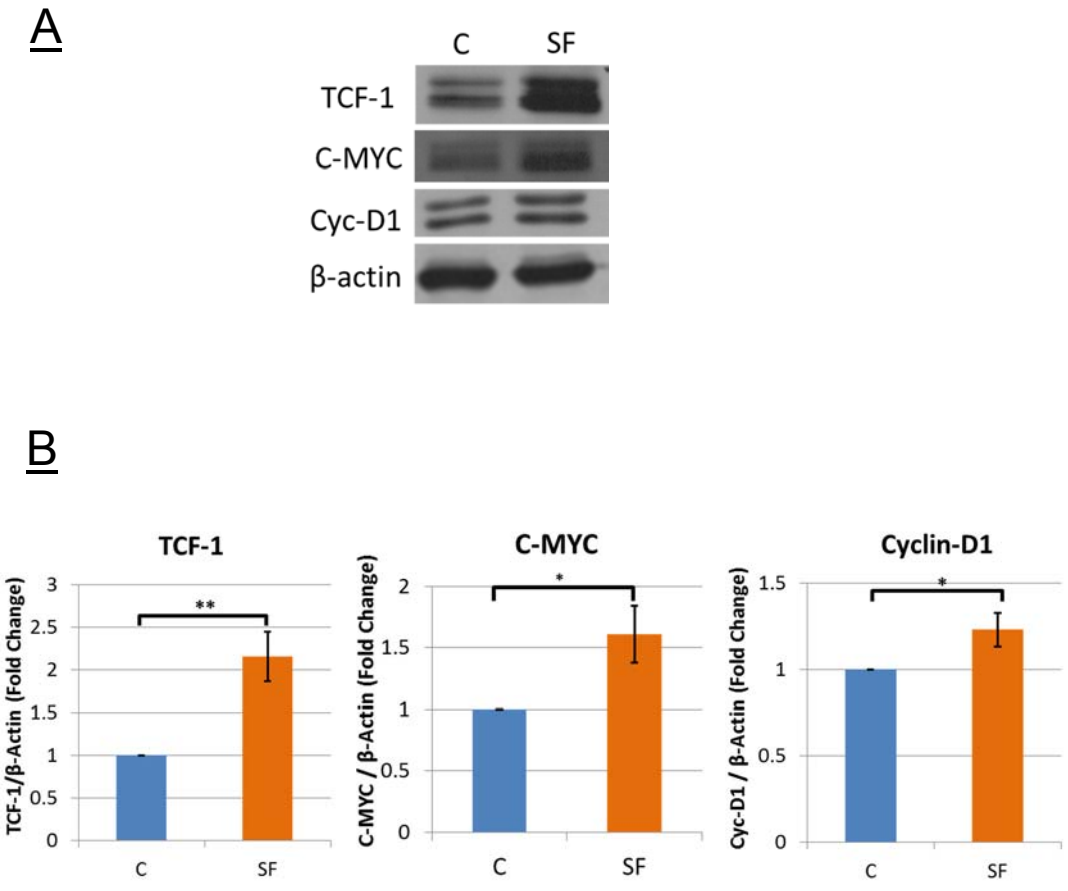

Figure 3.11: Hepa1-6 spheroids showed increased expression of β-catenin downstream targets. Hepa1-6 cells were grown for 7 days in serum-free media (SF) or complete media (control). Cells were harvested after 7-day treatment, and total proteins were extracted using SDS buffer. All three β-catenin downstream targets i.e. TCF-1, C-MYC, and Cyclin-D1, were found to be increased in CSC spheroids compared to control. **(A)** Representative Western Blot, **(B)** Densitometry image analysis. β-actin used as loading control. * ($p \leq 0.05$), ** ($p \leq 0.005$), n=3 independent experiments. **C**=Control; **SF**=Serum-free.

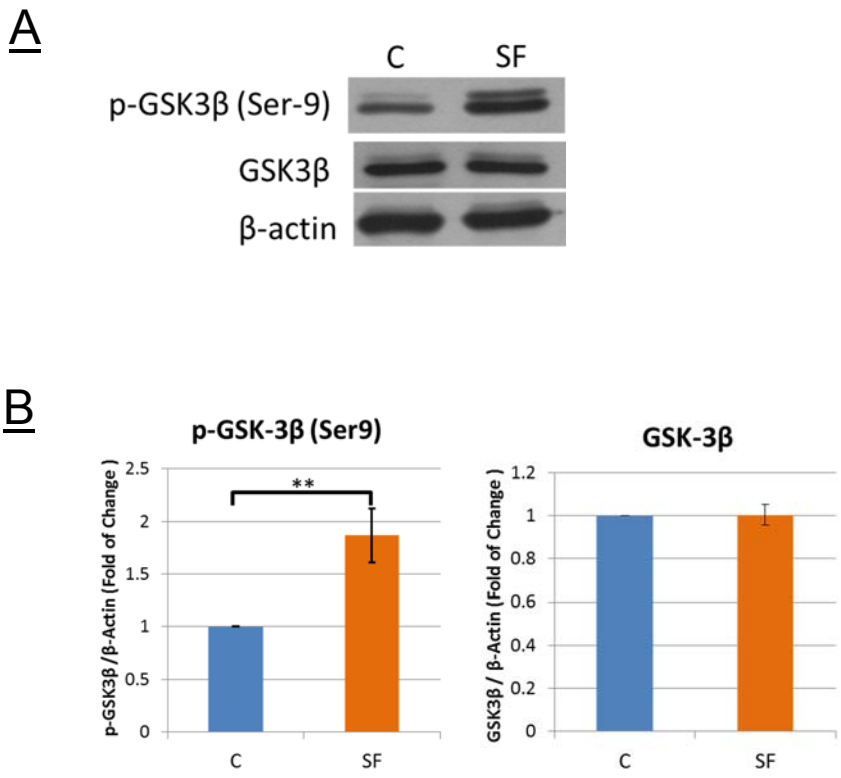

Figure 3.12: Higher β-catenin levels in Hepa1-6 spheroids may be contributed via GSK-3β activity. Hepa1-6 cells were grown for 7 days in serum-free media (SF) or complete media (control). Cells were harvested after 7 day treatment, and total proteins were extracted using SDS buffer. No change was observed in total GSK-3β levels, but phosphorylated GSK-3β (Ser9) levels were increased in CSC spheroids compared to control. **(A)** Representative Western Blot, **(B)** Densitometry image analysis. **(p≤0.005), n=3 independent experiments. β-actin used as loading control. **C**=Control; **SF**=Serum-free.

3.5) HCC CSC spheroids are more tumorigenic *in vivo*:

We used an orthotopic C57L/J mouse model to further test tumorigenic potential of Hepa1-6 spheroids where CSCs were being enriched [80]. Hepa1-6 cell line possess tumorigenic property in immunocompetent C57L/J mice [78, 79]. Seven-day cultured $2x10^6$ cells from Hepa1-6 spheroids as well as non-spheroid control cells were inoculated into upper left lobe of livers of 12-week-old immunocompetent C57L/J mice (n=6 mice/group) and monitored for two weeks. Mice injected with Hepa1-6 spheroids developed more aggressive tumors with overall higher tumor volume (6593±2615 mm^3) compared with mice injected with control cells (1388±968 mm^3; $p \leq 0.05$, n=6) (figure 3.13-C). Also, Hepa1-6 spheroids developed more aggressive tumors with significant higher tumor weight (3.1±1 g) compared with mice injected with control cells (1.1±0.5 g; $p \leq 0.05$, n=6) (figure 3.13-C). The aggressive growth pattern of CSC tumors was also witnessed by multiple HCC nodules found at different lobe sites within the liver compared to control, suggesting that CSC spheroids possess increased tumor initiation and hepatic invasive capabilities (figure 3.13-A). These findings were confirmed by H&E staining (Figure 3.13-B). Increased liver weight was also observed in the spheroid group (3.26±1.2 g) compared with the control group (1.77±0.9 g, NS, n=6), which is likely due to aggressive growth and higher tumor mass in the spheroid injected group. This justifies the increased overall body weight by about 3g in the spheroid group (25.68±3.2 g) compared to control (22.35±2.6 g; NS, n=6) (Figure 3.13-C).

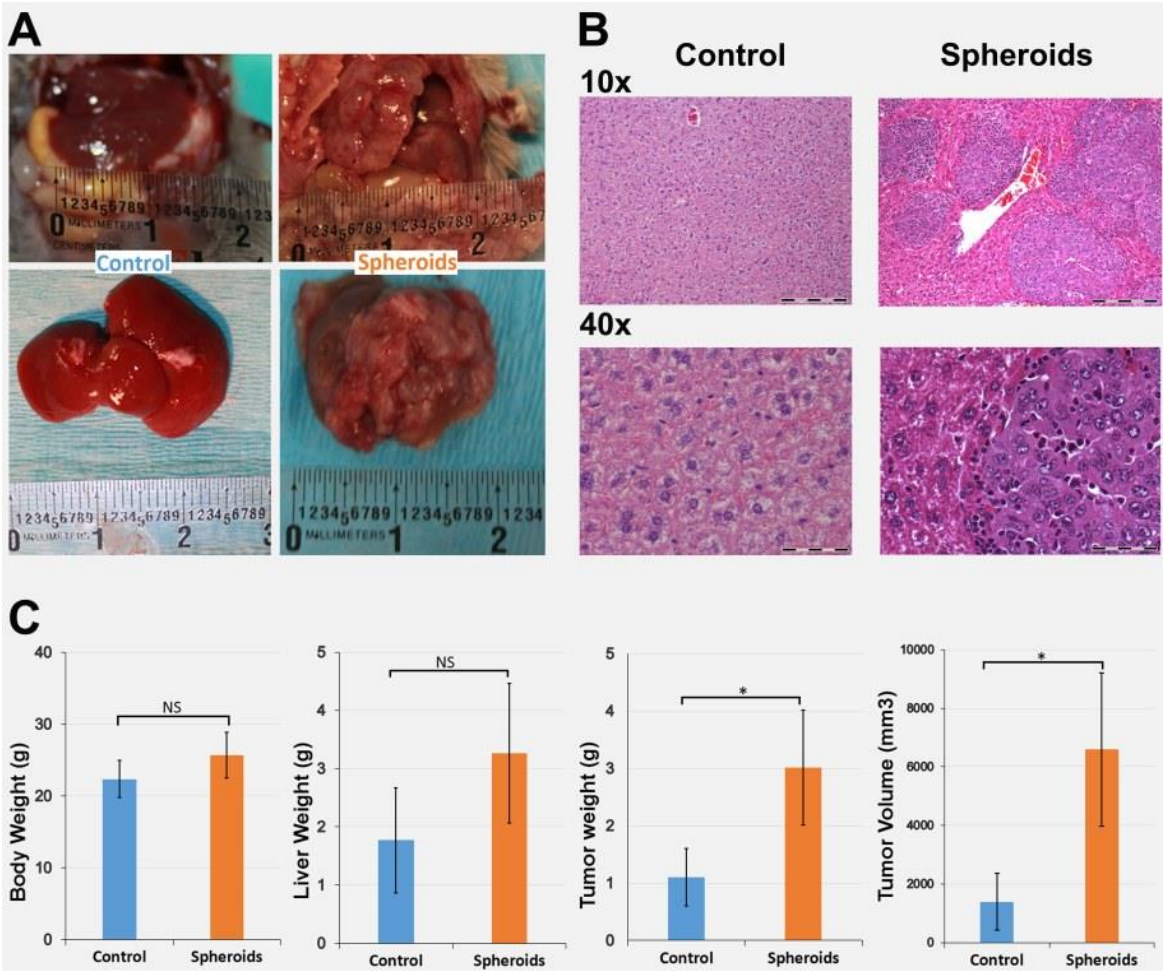

Figure 3.13: CSC spheroids demonstrated higher tumorigenic capability. 12 week old C57L/J mice were injected with $2x10^6$ control hepa1-6 cells or Hepa1-6 spheroids (n=6 mice/group) into left liver lobe. Tumors were allowed to grow for two weeks and mice were euthanized at the end of two weeks; (A) Representative liver tumors of control and spheroid group mice; (B) Representative HE staining of control group and spheroid group, bright field images with 10x magnification (upper, bar = 200 µm) and 40x magnification (lower, bar=50 µm); (C) Quantitative comparison of body weights, liver weights, tumor weights, and tumor volumes between control and spheroid group mice. *($p \leq 0.05$). NS (non-significant).

Summary

In the current work, we have successfully identified HCC cells with CSC-like properties in hepatoma cell lines using *in vitro* spheroid culture. These CSCs are poorly differentiated, and possess all defined CSC properties i.e. self-renewal, proliferation, and chemotherapy resistance. Surface markers analysis (EpCAM, CD90, CD44, and CD133) and functional marker analysis (ALDH and Hoechst efflux assays) further confirmed enrichment of CSCs, especially EpCAM+ CSC cells. Analyzing Wnt/β-catenin pathway components in CSCs showed up-regulation of β-catenin expression, which is most likely a result of changes in GSK-3β phosphorylation. Preliminary *in vivo* data in the mouse models support that spheroid forming CSCs show significant higher tumor proliferation rate compared to untreated (non-spheroid forming) HCC cells.

CHAPTER 4

EFFECT OF LIVER MICROENVIRONMENT ON FATE OF EPCAM+ CSCS IN ORTHOTOPIC ANIMAL MODELS

Introduction:

EpCAM possess prognostic value in HCC patients and is correlated with worse prognosis [53]. EpCAM is also a proposed target of the canonical Wnt/β-catenin pathway [95, 103]. As identified in the Chapter 3, EpCAM expression is significantly increased in the CSC spheroids compared to adherent control Hepa1-6 cell line. Therefore, the aim of this chapter was to systematically evaluate EpCAM expressing CSCs in a comprehensive *in vivo* study.

In order to initiate tumor in humans, tumor initiating cells (including CSCs) must overcome destruction events coordinated by host immune defense [104]. Thus, it is inaccurate to define CSCs by merely studying *in vitro* criteria such as self-renewal, drug-resistance, heterogeneity, and tumor initiation ability with lower cell numbers in immunocompromised mouse models, because these approach often ignores rate limiting immunological factors. Limited research in CSC have been attempted to understand immunological properties of CSCs [105-107]. Recent findings in tumor immunology and check-point inhibitors confirmed

that tumor microenvironment serve as key confounding factor dictating tumor growth or response to therapeutics [32, 108].

HCC carcinogenic progression is a multistep process which follows the pathogenic sequence of repeated liver damage (Figure – 1.1). Cirrhosis and NASH are the two most reported liver microenvironment influencing HCC development [109]. Previous studies had attempted to evaluate the property of CSCs in immunocompromised mouse model with hind limb xenograft [110]. However, hind limb xenograft approaches lack the liver microenvironment and also ignore the role of immunological factors observed in HCC patients, and hence are not clinically relevant. None of the previous CSC studies have examined tumor initiation properties of CSCs in orthotropic animal models of HCC.

Here, for the first time, we have systematically evaluated the fate of three EpCAM expressing HCC cell lines (i.e. Hepa1-6, Hep3B, and HepG2) in orthotopic animal models of HCC, in different immunocompetent liver microenvironments (Hepa1-6), as well as xenograft immunocompromised models (Hep3B and HepG2).

Results:

4.1) Non-alcoholic steatohepatitis promotes EpCAM positive cancer stem cells mediated tumorigenesis in immunocompetent mouse model of HCC

Establishing orthotopic immunocompetent mouse models with 3 different liver microenvironment:

To study the carcinogenic biology of EpcAM+ and EpCAM- CSCs in immunocompetent mouse model of HCC, we established 3 diet induced animal models developing three different liver microenvironments.

As shown in figure 4.1-A, clear differences in gross liver appearance and H&E histology were observed for progressive non-alcoholic fatty liver disease (NAFLD) developed in each of the three animal models. In early steatosis (HFD group), the hepatocytes present small fat vacuoles in the vicinity of the endoplasmic reticulum (liposomes) – showing microvesicular fatty change. The size of the vacuoles increase during disease development, and push the nucleus to the periphery of the cell, showing macrovesicular fatty change. In steatohepatitis (NASH group), steatosis with inflammation and ballooning can be seen, which is the hallmark of hepatocellular damages in steatohepatitis. Ballooning is characterized by cellular swelling, extreme decrease in hepatocytic cytoplasm and clumped strands of intermediate filaments. Control group mice displayed normal healthy liver pathology. NAFLD hepatopathology scores calculated from H&E histology (Figure 4.2 - A and B), confirmed inflammatory microenvironment development in NASH group of animals (6.6±0.22, n=10), compared to control (0.625±0.183, n=8) and HFD (2.5±0.267, n=8).

We also analyzed plasma alanine transaminase activity (ALT, U/L, indicator of liver damage and liver disease progression). ALT activity in NASH group animals was significantly higher compared to control and HFD animals (Control: 105.6±15.6, HFD: 143.75±10.3, NASH: 667.6±62.4, n=4/group, ##p<0.005, n=4, error bar = SD) (Figure 4.1 -C). Liver Triglycerides (TG, mg/dL/mg liver) levels were highest in NASH group animals compared to Control and HFD animals (Control: 8.73±2.11, HFD: 20.73±4.52, NASH: 30.48±4.66, n=4/group, *p<0.05, n=4, error bar = SD) (Figure 4.1-D).

We followed all animals for 16 weeks to monitor weight gain over the time. In patients, NASH developed as a result of fatty liver progression and so overall weight gain is observed. However, animal model studies found NASH development with methionine and choline deficient diet (MCD) alone resulted in significant weight loss in the first month after switching the diets. Therefore, for our study, NASH group animals were fed with modified MCD diet containing 60% Kcal fat with 0.1% methionine. This modified MCD diet does not result into significant weight loss. Control and NASH diet animals gained similar weight as showed in figure 4.2-A. This made our NASH animal model more clinically relevant because NASH pathology developed in mostly obese patients suffering with fatty liver without weight loss. After 18 weeks, we have euthanized animals and recorded body weight, liver weight, and liver/body ratio (%) as reported in figure 4.2-B. Consistent with other studies and in patients, significant higher liver/body ratio percentage were found in NASH animals compared to control and HFD (Control:

4.47±0.48, HFD: 4.90±0.34, NASH: 7.63±0.49, n=4/group, **p<0.005 error bar = SD).

To study underlying liver vascularity changes, we employed the high-frequency contrast enhanced ultrasound (CEUS) methodology (manuscript is under communication at the time of this dissertation). CEUS demonstrated more sensitive determination of diffused liver diseases including underlying changes in vascularity, in patients with NAFLD and HCC [111, 112]. We have successfully developed a methodology to track the NAFLD progression non-invasively based on study by Cocciolillo et at. 2014 using air-filled contrast agent. Vascularity of liver parenchyma is one of the key pathological factors affected by fatty infiltration and steatohepatitis development. Non-targeted contrast agent used in CEUS to confirm tumor diagnosis provides a very sensitive tool to capture vascular differences, and can be exploited for early diagnosis of fatty infiltration and steatohepatitis. Therefore, we have subjected our 3 experimental mouse models, representing different stages of fatty liver disease progression, to CEUS imaging with an aim to investigate potential application in diagnosis. We have used bolus perfusion model to record, analyze, and compare the data. The step-by-step experimental procedure and data analysis is described under Methods section (Chapter 2).

As shown in figure 4.3-A, peak enhancement (PE, representing blood flow, a.u.) was significantly deceased in the HFD group, and lowest in the NASH group compared with the Control group (Control: 37.4±2.3, HFD: 24.7±2.7, NASH: 14.8±2.7; p<0.001, n=6/group). Wash-in rate (WiR) found to be significantly

deceased in HFD group, and lowest in NASH group compared to Control group (Control: 6.6±0.44, HFD: 5.03±0.70, NASH: 1.90±0.20; $p<0.001$, n=6/group) (Figure 4.3-B). Another vascular parameter, wash-in perfusion index (WiPI = WiAUC (Area under the curve (wash-in))/RT (Rise time), WiPI is representative of blood flow), was also found to be significantly decreased in HFD, and lowest in the NASH group compared with Control (Control: 24.58±1.3, HFD: 16.28±1.85, NASH: 9.9±1.98; $p<0.001$, n=6/group) (Figure 4.3-C). PE and WiPI independently confirmed that NASH liver parenchyma exhibited the lowest blood flow, which could be due to severe fatty infiltration. Pearson correlation analysis as showed in respective lower panels of figure 4.3-C, found that PE, WiP, and WiPI significantly correlate with hepatopathology scores (showed in figure 4.1-B).

Altogether, we have successfully established 3 different diet induced mouse models representing three distinct liver parenchyma pathology, correlating with HCC development. After 10 weeks on special diets, control diet animals developed normal liver parenchyma, HFD animals developed mild steatosis, and NASH diet animals developed steatohepatitis condition with severe steatosis and inflammation (Figure 4.1-A). After successful development of animal models, we proceeded to test tumorigenic ability of EpCAM+ and EpCAM- Hepa1-6 cells (stably expressing copGFP) in these 3 distinct liver microenvironments and established orthotopic immunocompetent mouse models.

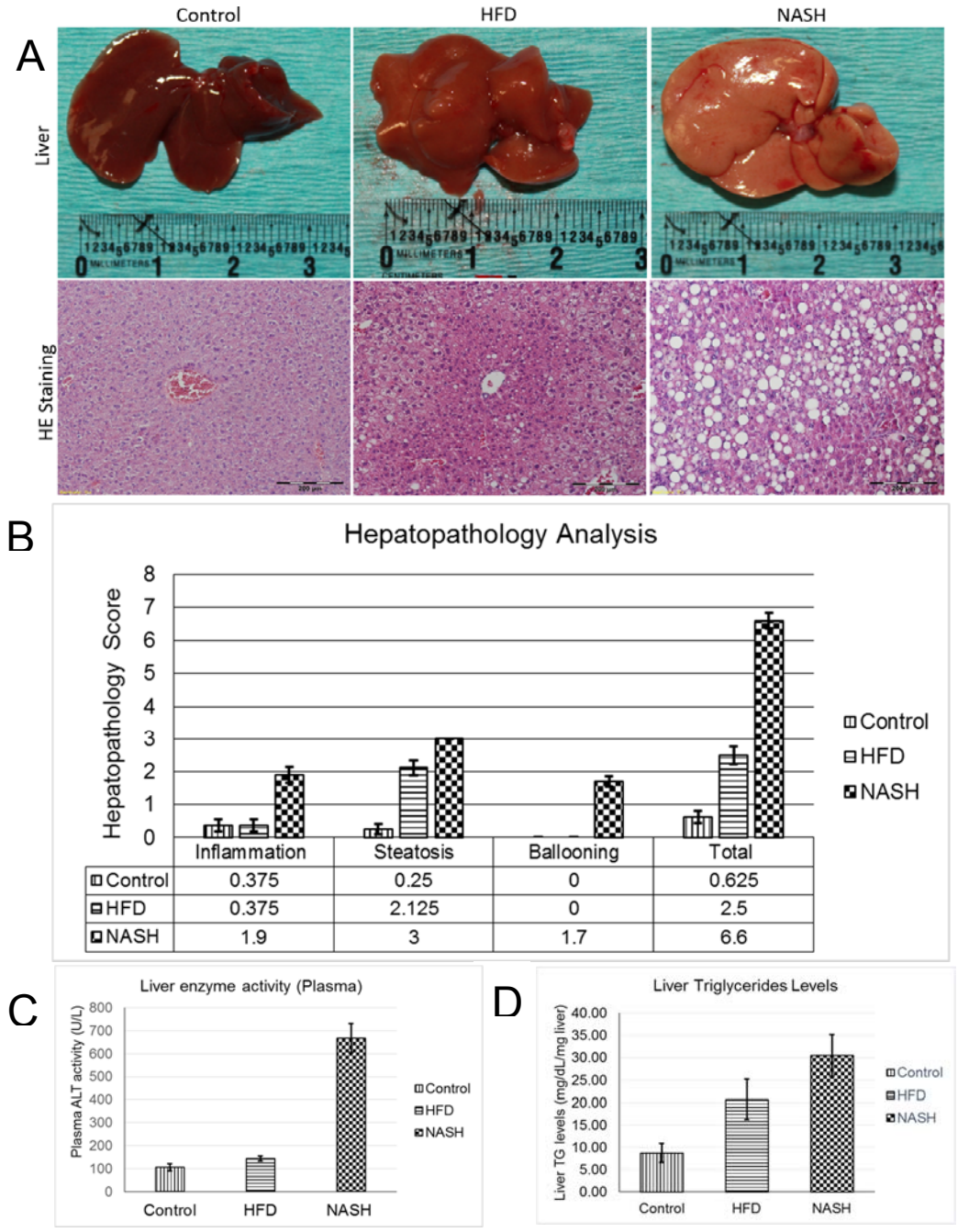

Figure 4.1: Establishing diet induced animal models – liver pathology. Animal experimental groups. **(A)** Representative images of whole liver and corresponding HE staining. 10X magnification (Bar = 200 µm); **(B)** HE staining was analyzed and assign total NAFLD hepatopathology score (0-8), based on inflammation (0-3), steatosis (0-3), and hepatocyte ballooning (0-2) features for each specimen. error bar = SEM, **Control**: control diet animals (n=8), **HFD**: high fat diet animals (n=8), **NASH**: NASH diet animals (n=10); **(C)** Plasma ALT activity (## p<0.005, n=4, error bar = SD); **(D)** Liver triglycerides levels per mg of liver tissue (*p<0.05, n=4, error bar = SD).

A

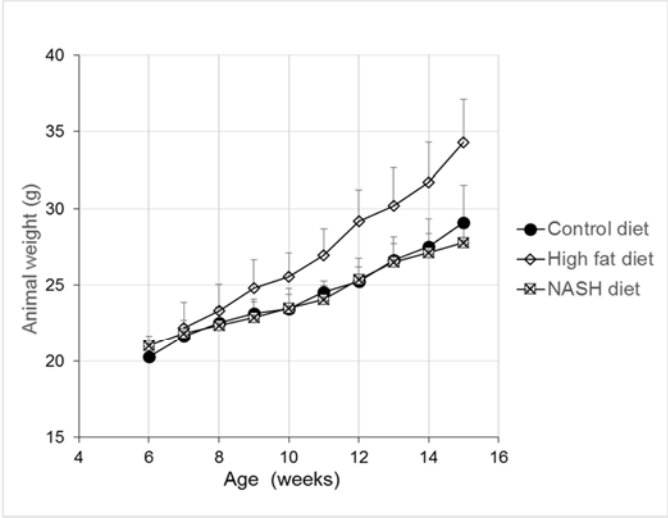

B

Age - 18 weeks	Diet		
	Control	HFD	NASH
Body weight (gm)	29.33	34.60	27.40
S.D.	2.30	1.66	1.27
Liver weight (gm)	1.31	1.84	2.08
S.D.	0.09	0.09	0.04
Liver/body weight ratio(%)	4.47	4.90	7.63
S.D.	0.48	0.34	0.49

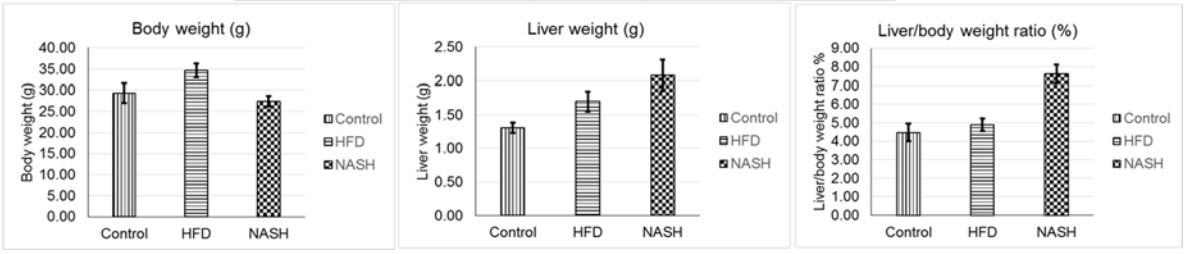

Figure 4.2: Establishing diet induced animal models. Animal were followed for 16 weeks. **(A)** Animal whole body weight changes over the time (error bars = SD); Control diet animals (n=8), High fat diet animals (n=8), NASH diet animals (n=10); **(B)** Animals euthanized at the end of 18 weeks. Comparison table for body weight and liver weight between experimental groups (n=4 in each group, **SD**=standard deviation).

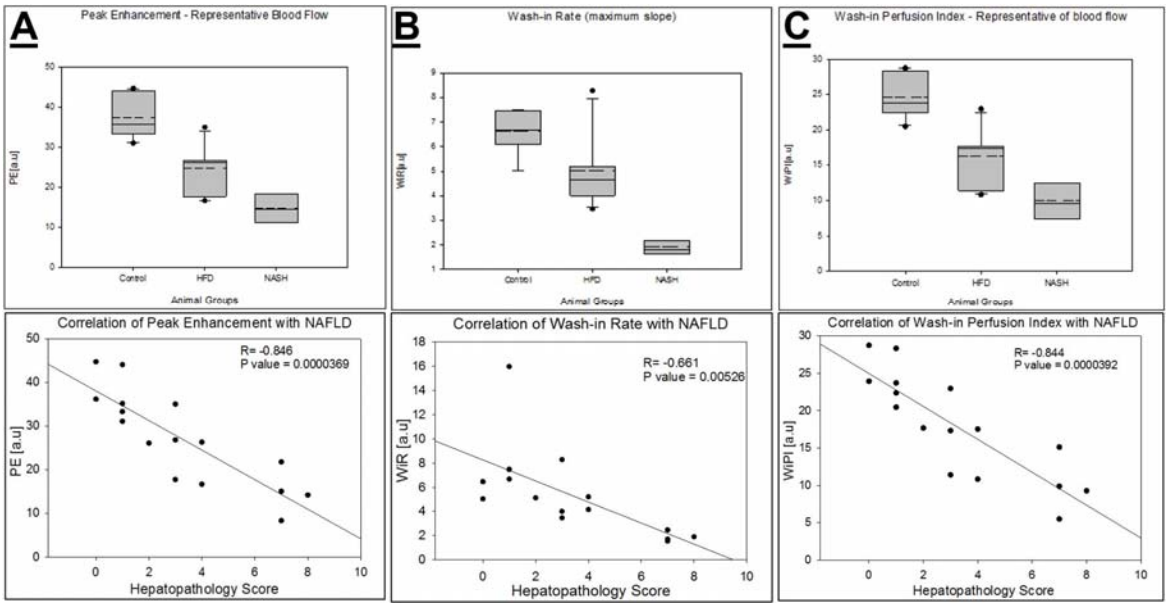

Figure 4.3: CEUS can identify loss of vascularity with fatty liver progression. CEUS was performed with tail vein intravenous injection of non-targeted contrast agent and data were captured for bolus perfusion kinetics. Data was analyzed by VevoCQ software. A: Peak enhancement (PE) found to be significantly deceased in HFD group, and lowest in NASH group compared with Control group (Control: 37.4±2.3, HFD: 24.7±2.7, NASH: 14.8±2.7; $p<0.001$, n=6/group). B: Wash-in rate (WiR) found to be significantly deceased in HFD group, and lowest in NASH group compared with Control group (Control: 6.6±0.44, HFD: 5.03±0.70, NASH: 1.90±0.20; $p<0.001$, n=6/group). C: Wash-in perfusion index (WiPI) was found to be significantly decreased in HFD, and lowest in NASH group compared with Control (Control: 24.58±1.3, HFD: 16.28±v1.85, NASH: 9.9±1.98; $p<0.001$, n=6/group). Lower panels showed Pearson correlation analysis with Hepatophatology scores and found to be significant ($p<0.05$) for all 3 contrast parameters i.e. PE, WiP, and WiPI. (showed on graphs, R=Pearson coefficient, p=significance value).

NASH microenvironment promotes EpCAM+ CSCs mediated tumorigenesis in immunocompetent microenvironment.

We hypothesize that “immunocompetent liver microenvironment affects tumorigenesis of EpCAM+ CSCs”. To test our hypothesis, we established 3 orthotopic immunocompetent HCC models and studied the oncogenic effect of EpCAM+ HCC CSCs.

Hepa1-6 is non-immunogenic murine cell line with an ability to form orthotopic and subcutaneous tumor in normal immunocompetent C57L/J mice [78-80]. Evaluating EpCAM+ CSCs derived from Hepa1-6 in above mentioned 3 different animal models exhibiting 3 distinct liver pathology (control=healthy, HFD=steatosis, and NASH=steatohepatitis respectively) allowed us to systematically evaluate the tumorigenic capability of hepatocellular carcinoma CSCs in different immunocompetent liver microenvironments. For these experiments, we generated copGFP expressing stable Hepa1-6 cell line by lentivirus transduction. Unlike hind limb flank models where tumor growth can be monitored visually and/or by using Vernier calipers, orthotopic tumor growth required sensitive non-invasive imaging modality. Therefore, to monitor orthotopic tumor growth in liver of animal non-invasively, we utilized high-frequency ultrasound imaging using Visualsonics Vevo2100 instrument.

As shown in figure 4.4-A, we first performed fluorescence assisted cell sorting (FACS) to obtain EpCAM+(positive) or EpCAM- (negative) subpopulation of Hepa1-6 cells with high copGFP expression. Animals in all 3 experimental groups (control, HFD, and NASH) were then randomly divided into 2 sub-groups

to receive orthotopic implantation of either EpCAM+ or EpCAM- cells (n=4 mice/sub-group). Baseline ultrasound data recorded day before surgery. Total 2 million (2x10^6) sorted copGFP expressing Hepa1-6 cells were then orthotopically injected into left liver lobes of animals by survival surgery (figure 4.4-B). Animals were followed up by ultrasound imaging to track tumor growth and euthanized at appropriate time. Simplified experimental workflow is shown in figure 4.4-C.

Neither control nor HFD group animals showed any tumor initiation or growth by high-frequency ultrasound imaging. Both EpCAM+ and EpCAM- Hepa1-6 cells failed to initiate tumor in healthy liver microenvironment and mild steatosis. We followed animals for total 60 days by high-frequency ultrasound and euthanized them. Gross liver analysis and dissection couldn't confirm any tumors, and pathological analysis by H&E staining of injected lobes and adjacent lobes did not detect any microscopic tumors (Table 4.1).

Table 4.1: Experimental outcomes of orthotopic implantation of EpCAM expressing CSCs in different mouse models

Animal Groups	Injection Groups	Total animals	Tumor developed
CONTROL (10% Kcal from fat)	EpCAM +/+	4	0/4
	EpCAM -/-	4	0/4
High Fat Diet (60% Kcal from fat)	EpCAM +/+	4	0/4
	EpCAM -/-	4	0/4
NASH Diet (MCD + 60% Kcal from fat) (n=3 separate experiments)	EpCAM +/+	11	10/11
	EpCAM -/-	10	2/10

NASH group of animals with EpCAM+ CSCs injection were confirmed tumor initiation as early as Day 5. On Day 13, detected tumors had grown larger while no tumors were detected in EpCAM-ve injection group of NASH animals (Figure 4.5-A). All NASH animals were euthanized on Day 18. Only EpCAM+ cells in NASH group had initiated tumors in almost all animals (10/11) (Table-4.1).

Pathological analysis of NASH animals by HE staining confirmed the tumors, detected by high-frequency ultrasound analysis, in all 10 /11 EpCAM+ animals in NASH group. IHC-P analysis confirmed significantly higher EpCAM expression compared to non-tumor EpCAM- animals (Figure 4.5-B). IHC-P analysis further confirmed expression of vimentin in EpCAM+ NASH tumors (Figure 4.5-B). Vimentin is a marker of epithelial to mesenchymal transition (EMT), suggesting that peripheral tumor cells acquired possible EMT properties which potentially helped spread of tumors and likely to be responsible for rapid growth in NASH liver microenvironment (Figure 4.5-B).

We injected copGFP expressing stable Hepa1-6 cells for the purpose of lineage tracking *in vivo*, to understand tumor growth. We performed immunofluoroscence analysis of frozen section (IHC-Fz) section of tumor tissue, and confirmed that the co-expression of EpCAM and copGFP (Figure-4.6).

To confirm tumorigenic potential of EpCAM+ CSCs in control liver microenvironment of C57L/J mouse, we repeated the experiment with only control animals but with increased number of sorted EpCAM+ or EpCAM- cells injection , 5 million instead of 2 million (data not shown). HCC tumorigenesis experiment using control-healthy liver with 5 million cells injection found tumor confirmation in

3/3 animals in EpCAM+ group and 2/3 animals in EpCAM- group, with non-significant difference in tumor size, after 18 days. These tumors were small in size (1-2 mm in diameter). This repeated experiment confirmed that significant growth in NASH animals were contributed by steatohepatic microenvironment.

In NASH group experiments, there were a few inexplicable results observed. In EpCAM+ group animals, histology analysis found a few tumors with either copGFP or EpCAM expression, but not both. This observation cannot rule out the possibility for transformation of host cells. Similarly, 2/10 animals in EpCAM-ve group had shown tumor growth, suggesting either experimental error or actual growth of EpCAM-ve cells which contributed to HCC initiation within NASH microenvironment. To answer these unanswered questions, we performed lineage tracking study in NASH group animals (Chapter 4.2).

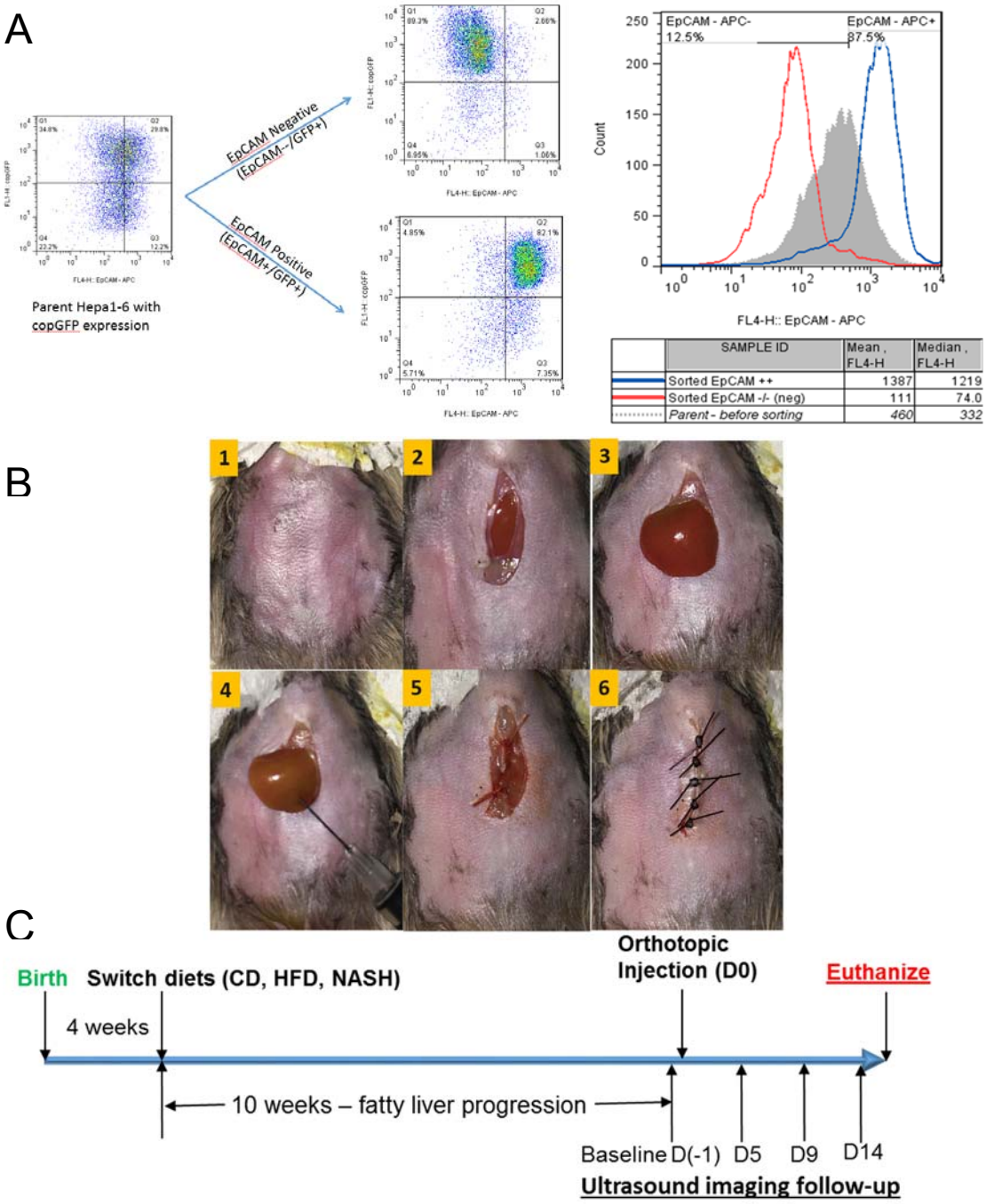

Figure 4.4: Orthotopic implantation of EpCAM expressing CSCs in mice: (A) Lentivirus transfected Hepa1-6 cells expressing copGFP were sorted by flow cytometry for EpCAM-/- and EpCAM+/+ populations; **(B)** Representative step by step surgical procedure – two million (2 x 10^6) sorted cells were injected into left liver lobe of C57L/J diet induced control, HFD, or NASH mice by survival surgery; **(C)** Simplified experimental workflow.

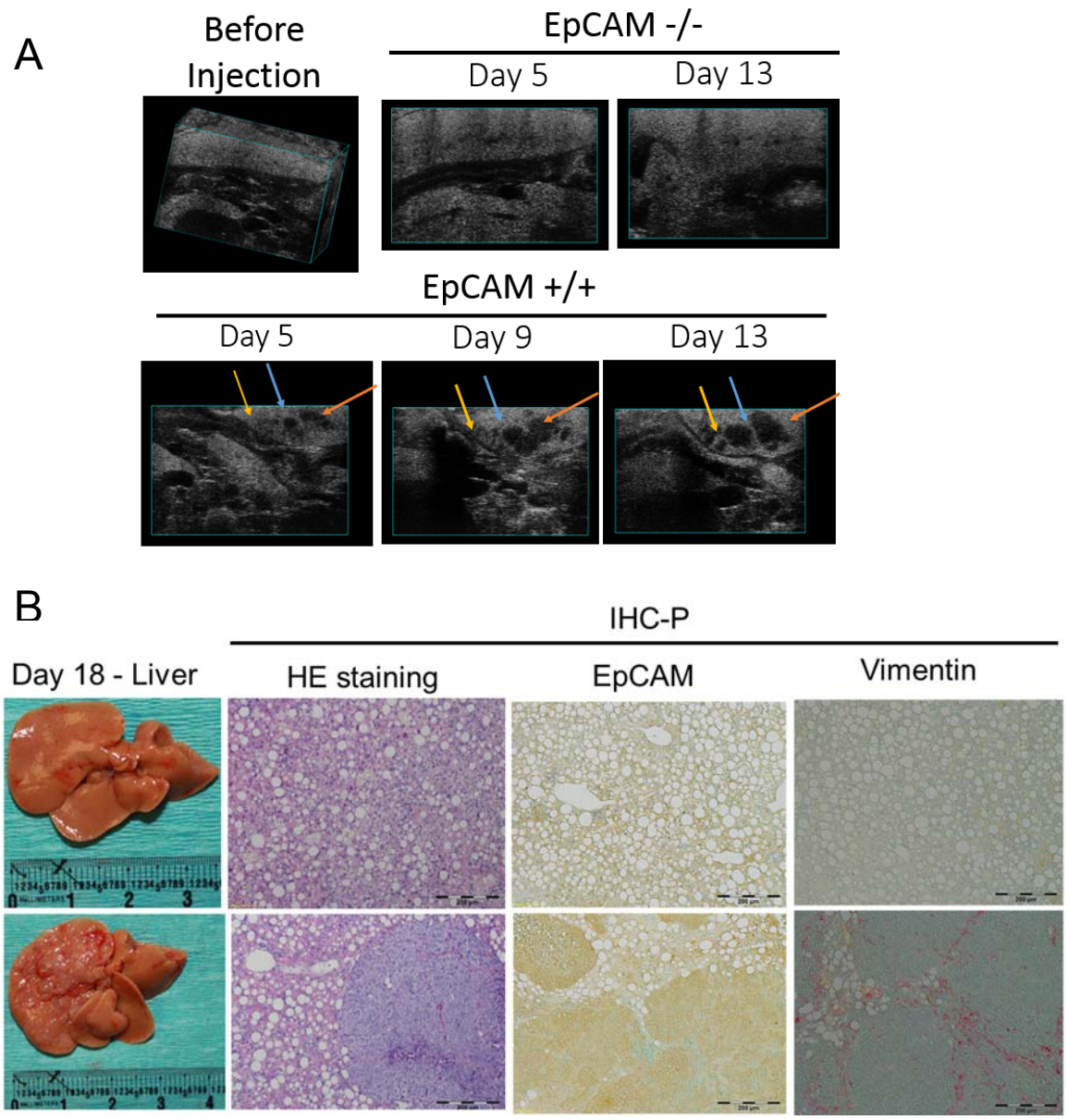

Figure 4.5: EpCAM expressing CSCs in orthotopic NASH mouse model: 2 million sorted cells were injected into left liver lobe of C57L/J diet induced NASH mice by survival surgery, and tumor growth was monitored. **(A)** Non-invasive ultrasound images recorded at different time-points to track tumor progression in EpCAM-/- and EpCAM +/+ groups. **(B)** Visual observation of livers of euthanized mice on Day 18, and representative IHC-P staining, HE stain, EpCAM, Vimentin (from left to right).

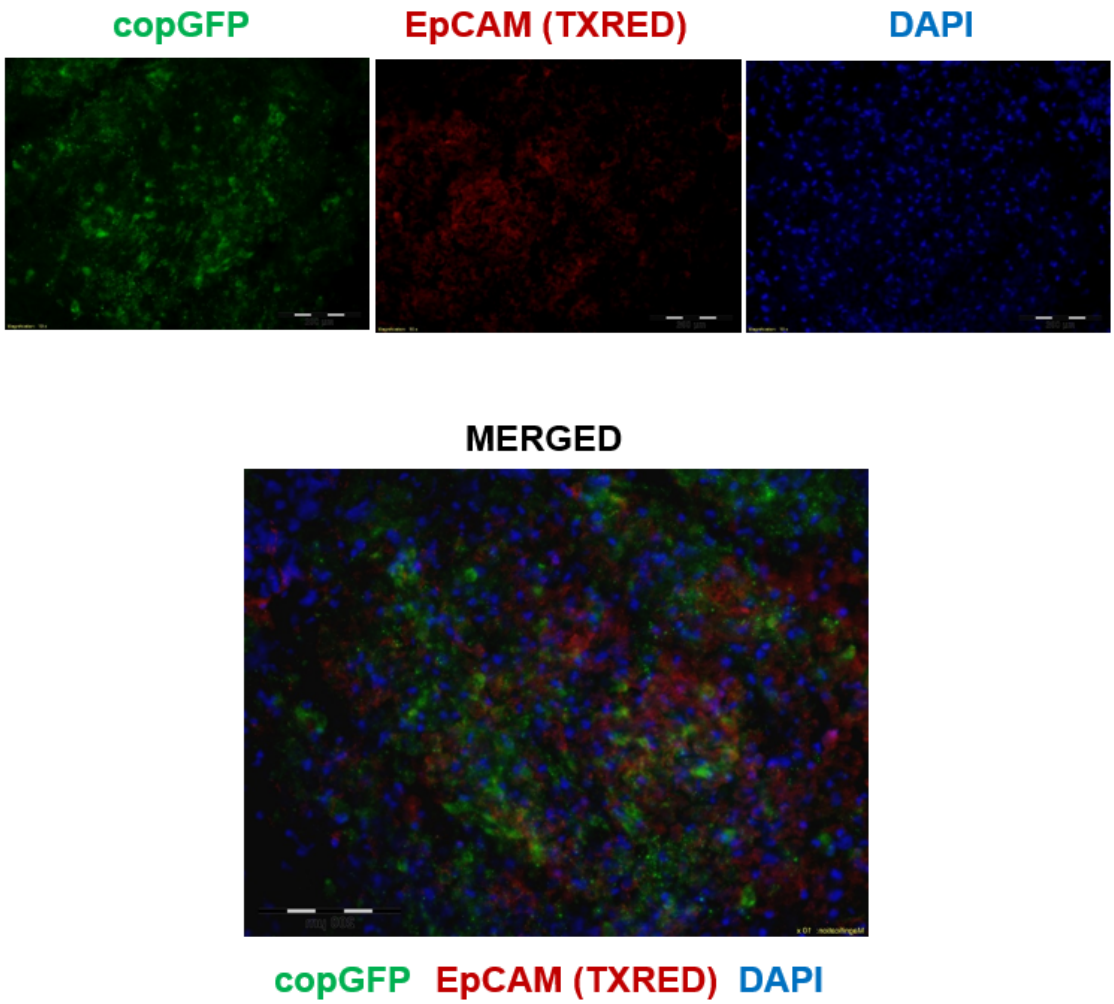

Figure 4.6: IHC-Fz staining of tumor from EpCAM+ CSCs in orthotopic NASH mouse model: ICC confirmed that tumor arising from copGFP expressing EpCAM+ CSCs in NASH animals. Green fluorescence was natural fluorescence from copGFP. EpCAM was detected by Rabbit-Anti-EpCAM (1:100) followed by secondary signal amplification using Goat-Anti-Rabbit (1:500, Alexafluor – 594). FITC channel was used for detecting copGFP and TXRED channel used for detecting EpCAM. DAPI stain for nuclei was detected by UV channel filter. Upper panel showed individual images and lower panel was merged images confirmed copGFP and EpCAM co-expression.

4.2) EpCAM+ve CSCs (copGFP tagged) are contributing to tumor initiation and not EpCAM-ve (mCherry tagged).

We designed lineage tracking study with the objective to (1) identify the source of tumor initiation in orthotopic immunocompetent NASH microenvironment, and (2) systematically evaluate potential contribution of EpCAM+ and EpCAM- Hepa1-6 cells, and host liver cells in tumorigenesis. For this experiment, in addition to two groups injected with either $2x10^6$ EpCAM+ or EpCAM- Hepa1-6 cells alone (stably expressing copGFP), we introduced a third group defined as "mixed group" with 50/50 ratio of EpCAM+/EpCAM- Hepa1-6 cells (Figure 4.7–A). In the "mixed group" NASH animals, $1x10^6$ EpCAM+ cells stably expressing copGFP and $1x10^6$ EpCAM- Hepa1-6 cells stably expressing mCherry, were mixed and injected into left liver lobes of animals by orthotopic injection procedure established for earlier experiments.

Tumor growth was observed and recorded non-invasively with high-frequency ultrasound imaging. All animals were euthanized on Day 18 post injection. Tumor incidence and tumor burden were found to be dose dependent on the numbers of injected EpCAM+ Hepa1-6 cells (Figure 4.7-B). EpCAM+ group (100% EpCAM+ CSCs) showed significant higher liver weight (6.86±0.42 g, $p=0.002$), followed by mixed group with 50% EpCAM+ CSCs (5.00±0.73 g), and lowest in EpCAM- group with 0% CSCs, (3.13±0.59 g) (Figure 4.7-C, upper box plot). Similarly, tumor weight were significantly higher in EpCAM+ group (4.56±0.42 g, $p<0.001$), followed by mixed group with 50% EpCAM+ CSCs

(2.77±0.69 g), and least in EpCAM- group with 0% CSCs, (0.8±0.50 g) (Figure 4.7-C, lower box plot).

Mixed group's tumors were of the highest interest for us, because these tumors were initiated from 50/50 mixture of copGFP expressing EpCAM+ CSCs and mCherry expressing EpCAM- non-CSCs (Hepa1-6 cells). Therefore, we could track the tumor lineage *in vivo*. As shown in figure 4.8-A, majority of tumor growth was contributed by EpCAM+ cells (high copGFP expression). Two tumors from different animals were analyzed by IHC-Fz analysis. Tumor # 2 showed a faint expression of mCherry, but not significant, thus suggesting EpCAM+ cells (copGFP expression) dominated growth within tumor microenvironment over EpCAM- cells (mCherry). We confirmed the copGFP expression by IHC-P analysis, as shown in figure 4.8-B. Left "control" slide was performed to rule out non-specific antibody interaction (only secondary polymer incubated followed by DAB color development). Finally, we confirmed the expression with Western Blot analysis (Figure 4.8-C). We only observed copGFP expression in the mixed group and EpCAM+ groups, but not in the EpCAM- group. Similarly, no expression was detected for mCherry in the mixed group.

Taken together, we have demonstrated that EpCAM+ Hepa1-6 CSCs possess tumor initiating property in immunocompetent NASH microenvironment.

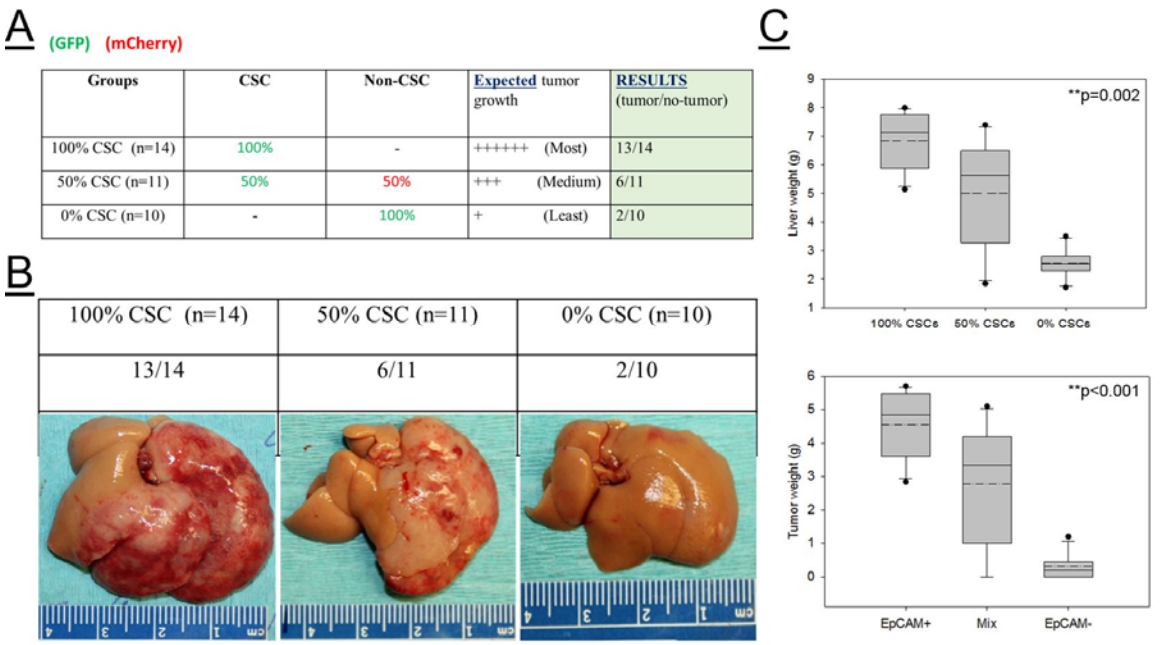

Figure 4.7: Tumor initiation in NASH liver microenvironment is dose dependent on intial EpCAM+ CSCs: NASH group mice were orthotopically injected with 2 million Hepa1-6 cells. **(A)** Table showing experimental scheme of 3 groups, expected and observed results. **(B)** Representative gross liver pictures with tumor burden for each of the 3 group of NASH mice. **(C)** Box plot showing whole liver weight, **(D)** Box plot showing tumor weight, for each experimental group. EpCAM+ group (100% EpCAM+ CSCs) showed significant higher liver weight (6.86±0.42 g, p=0.002) and tumor weight (4.56±0.42 g, p<0.001), followed by mix group with 50% EpCAM+ CSCs (Liver: 5.00±0.73 g, and tumor: 2.77±0.69 g), and lowest in EpCAM- group with 0% CSCs, (Liver: 3.13±0.59 g, and tumor: 0.8±0.50 g). Solid line in box plot represent median and dotted line represent arithmetic mean of each groups. Significance was calculated by one way ANOVA, and p value showed on upper right corner of each box plots.

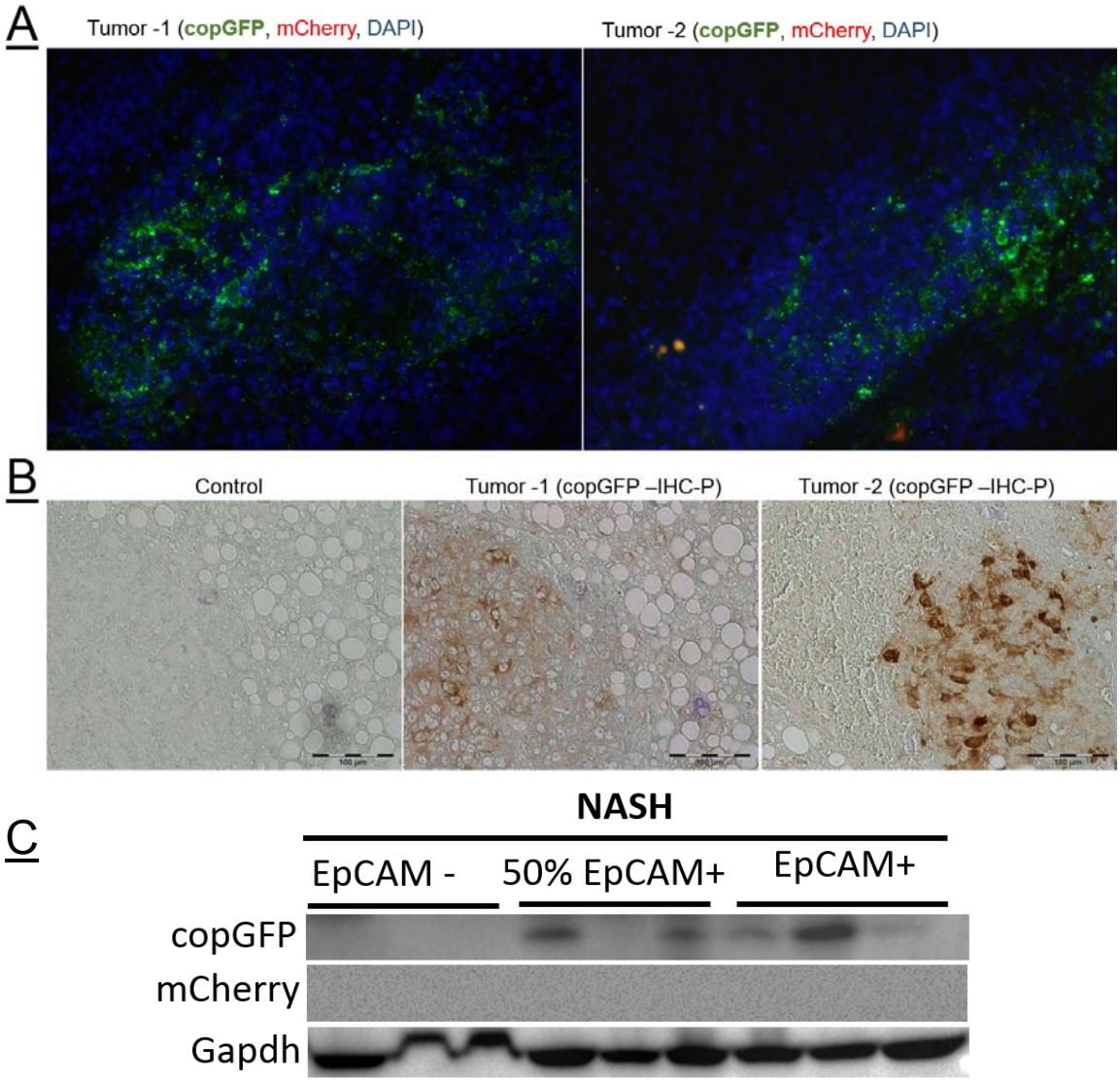

Figure 4.8: Lineage tracking confirmed EpCAM+ CSCs (copGFP) contribute to tumor initiation in NASH immunocompetent microenvironment. (A) IHC-Fz staining and analysis of two different tumors from the mixed group (50:50 , EpCAM+:EpCAM-) in orthotopic NASH mouse model. Majority of tumors showed with green fluorescence (copGFP tagged EpCAM+ CSCs), while only very minute fraction of tumor showed red fluorescence in tumor # 2 (mCherry tagged EpCAM- non-CSCs). **(B)** IHC-P staining confirmed copGFP expression using anti-copGFP antibody staining with secondary DAB color development with HRP-polymer. **(C)** Western Blot analysis confirmed copGFP expression from tumors of the mixed group and EpCAM+ group while no mCherry expression detected in mixed group tumors.

4.3) EpCAM-High Hep3B cells showed tumor initiation property and aggressive tumor growth in liver microenvironment of Nu/J nude mice.

Hep3B is EpCAM+ human cell line with hepatitis B virus integrated into its genome but not infective or actively propagating [81]. Hep3B is a well studied HCC cell line for orthotopic liver microenvironment which show characteristics of human HCC with detectable plasma levels of AFP in BALB/C nude mice [113]. However, none of the previous studies tested property of Hep3B cells with different degree of EpCAM expression using orthotopic nude mice model. Therefore, we systematically studied the ability of EpCAM-Low and EpCAM-High CSCs in orthotopic liver microenvironment of Nu/J athymic mice.

Stable copGFP expressing Hep3B cell line was established with lentivirus transduction for the purpose of potential *in vivo* lineage tracking. 2 million EpCAM-Low or EpCAM-High Hep3B cells were sorted by FACS and injected into left liver lobes of 10 week old athymic Nu/J nude mice by survival surgery as explained earlier (n=4 mice/group, two groups = EpCAM-Low and EpCAM-High). Tumor growth was monitored using non-invasive ultrasound imaging, and first tumor was detected on Day 35 in EpCAM-High group (data not shown). Mice were followed for 70 days and euthanized (none of the mice died in either group).

At the end of 70 days from the Hep3B injection, 4/4 EpCAM-High group confirmed very high tumor growth while only 1/4 EpCAM-low group confirmed tumor (significantly lower in tumor size and volume compared with EpCAM-High group tumors). As shown in figure 4.9–A, gross liver observation and H&E staining confirmed presence of tumor in EpCAM-High group of animals. EpCAM-High

group of animals showed significantly higher tumor volume (2451.25±443.34 g, p=0.013, n=4 mice/group) and significantly higher liver weight (4.375±0.7 g, p=0.023, n=4 mice/group) compared to EpCAM-Low group of animals (tumor volume: 282.22±282 g, liver weight:1.7±0.1 g) (Figure 4.9-B). We further analyzed expression of β-catenin, EpCAM, and copGFP. As shown in figure 4.9-C, EpCAM-High group tumors confirmed copGFP expression suggesting tumors were initiated from the injected EpCAM cells. Increased levels of EpCAM and β-catenin in EpCAM-High group suggest that EpCAM-high Hep3B cells preserved their expression and properties *in vivo* within liver microenvironment and were responsible for tumor initiation. Absence of tumor and copGFP/EpCAM expression in EpCAM-low group suggest that Hep3B cells with lower EpCAM expression inherently possess lower tumor initiation capability *in vivo*.

Taken together, our Hep3B – Nu/J mouse model data suggest, for the very first time, that tumor initiation observed by Hep3B were primarily contributed by EpCAM expressing CSCs, especially EpCAM-high CSCs. Also, these EpCAM-High and EpCAM-low Hep3B cells did not change/alter their EpCAM expression profile and/or tumor initiating property in *vivo* post injection. For the first time, we have demonstrated that, without genetic alteration, spectrum of EpCAM expression on Hep3B cells possess distinct tumor initiating capability, and thus possibly contribute distinctly to tumorigenesis.

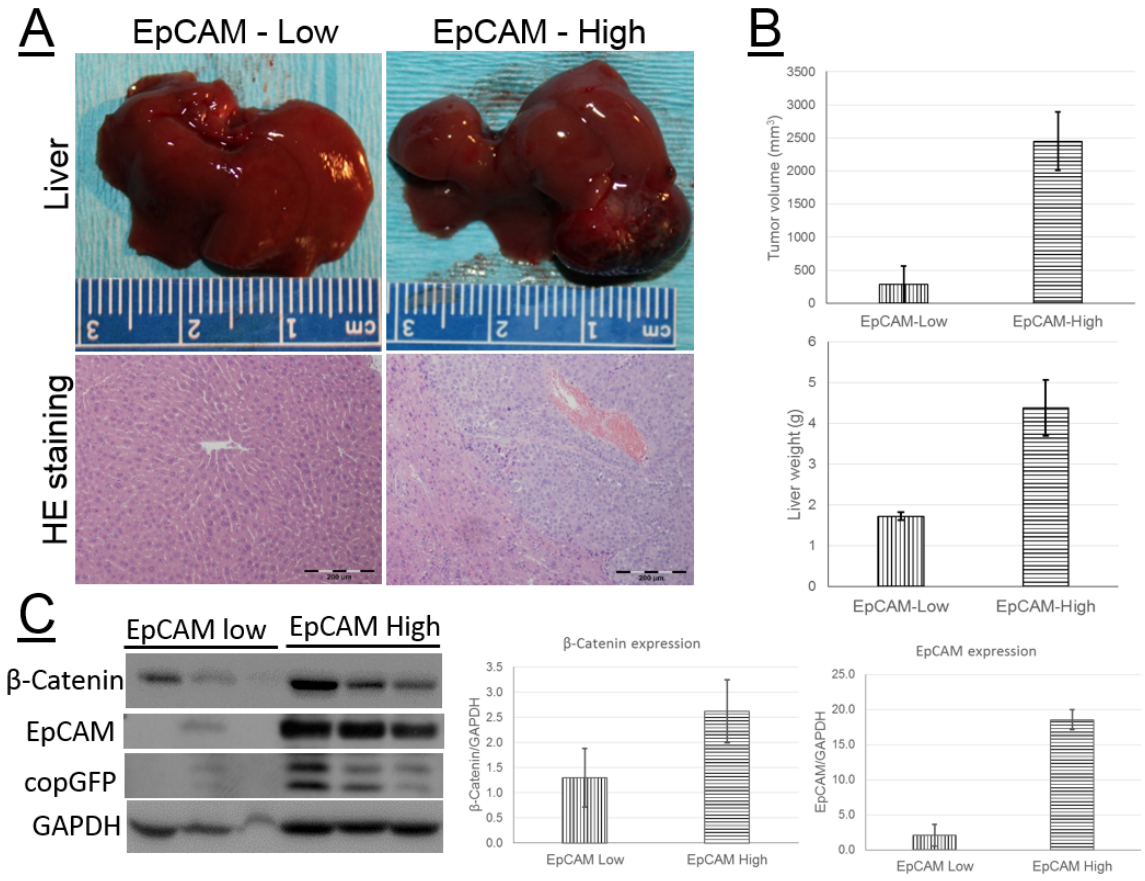

Figure 4.9: EpCAM-High Hep3B subset possess tumorigenic potential in orthotopic Nu/J mouse model: 2 million sorted EpCAM-low or EpCAM-high Hep3B cells with constitutive copGFP expression were injected into left liver lobe of athymic Nu/J nude mice with survival surgery, and tumor growth was monitored for 70 Days. **(A)** Gross liver and HE stain of EpCAM-low and EpCAM-High animals. All 4/4 animals in EpCAM-high group confirmed tumor by HE staining, while only 1/4 animals in EpCAM-low group showed minor tumor in injection lob. **(B)** EpCAM-high group showed significant higher tumor volume and liver weight compared with EpCAM-low groups. **(C)**Western blot analysis showed that EpCAM-high group animals/tumors show significant higher β-catenin and concomitant EpCAM expression, with copGFP co-expression. Bar graphs show densitometric analysis of β-catenin (*p<0.05) and EpCAM (**p<0.001). GAPDH is used as internal control to normalize expression.

4.4) Liver microenvironment promotes HepG2 mediated tumorigenesis in orthotopic athymic nude mice (Nu/J).

HepG2 is another EpCAM+ human cell line with characteristics of human HCC [81]. ATCC have showed that HepG2 is non-tumorigenic cell line, while a few studies have found that HepG2 can initiate tumor in nude and SCID mice [50]. HepG2 is unique HCC cell line, correlated with high Wnt/β-catenin HCC subtype in clinic due to somatic mutation leading to a truncated β-catenin which is constitutively active [114, 115]. As EpCAM expression is regulated by Wnt/β-catenin pathway, fate of HepG2 cell line in orthotopic liver microenvironment could be very distinct from that of Hepa1-6 and Hep3B cell lines.

We established stable copGFP expressing HepG2 cell line, and sorted these cells for EpCAM-Low and EpCAM-High subgroups, similar to Hep3B study. FACS sorted 2 million cells were then injected into orthotopic Nu/J mice left liver lobes and established two groups (n=4 mice/group, EpCAM High and EpCAM Low). Animals were observed for tumor development by non-invasive ultrasound.

We found the detectable tumors on day 30, in both EpCAM high and EpCAM low group animals. We followed tumor growth for 70 days, and animals were euthanized. As showed in figure 4.10-A, all mice in both EpCAM-High and EpCAM-Low group confirmed presence of tumors by observing gross liver and HE histology analysis. No significant differences were observed in liver weight and tumor volume between these two groups (Figure 4.10–B). Orthotopic tumors were observed with high necrotic regions and soft fluid filled regions. As explained earlier, HepG2 cell line possess mutant β-catenin which is constitutively active,

therefore tumorigenesis in EpCAM-Low group could explain the outcome with a rationale of higher β-catenin tumorigenic downstream activity.

Interestingly, metastatic HCC occurred in 2/4 EpCAM-High animals (Figure 4.11), and we confirmed presence of tumors by H&E histology analysis. In one mouse, tumor was observed near to bladder (overlapping with bladder tissue and connecting tissues), and in the second mouse, we found two distinct metastatic tumors in right kidney and pancreas respectively (Figure 4.11). These results were surprising to us because HepG2 cells have not been reported as a metastatic cell line.

Taken together, we have shown that tumor initiation capability of HepG2 cells were not significantly affected by EpCAM expression *in vivo* in orthotopic liver microenvironment. However, EpCAM-High HepG2 cells acquired metastatic abilities, suggesting EpCAM's unique role in tumorigenesis despite constitutively active Wnt/β-catenin signaling due to predominant mutant β-catenin in HepG2 cells.

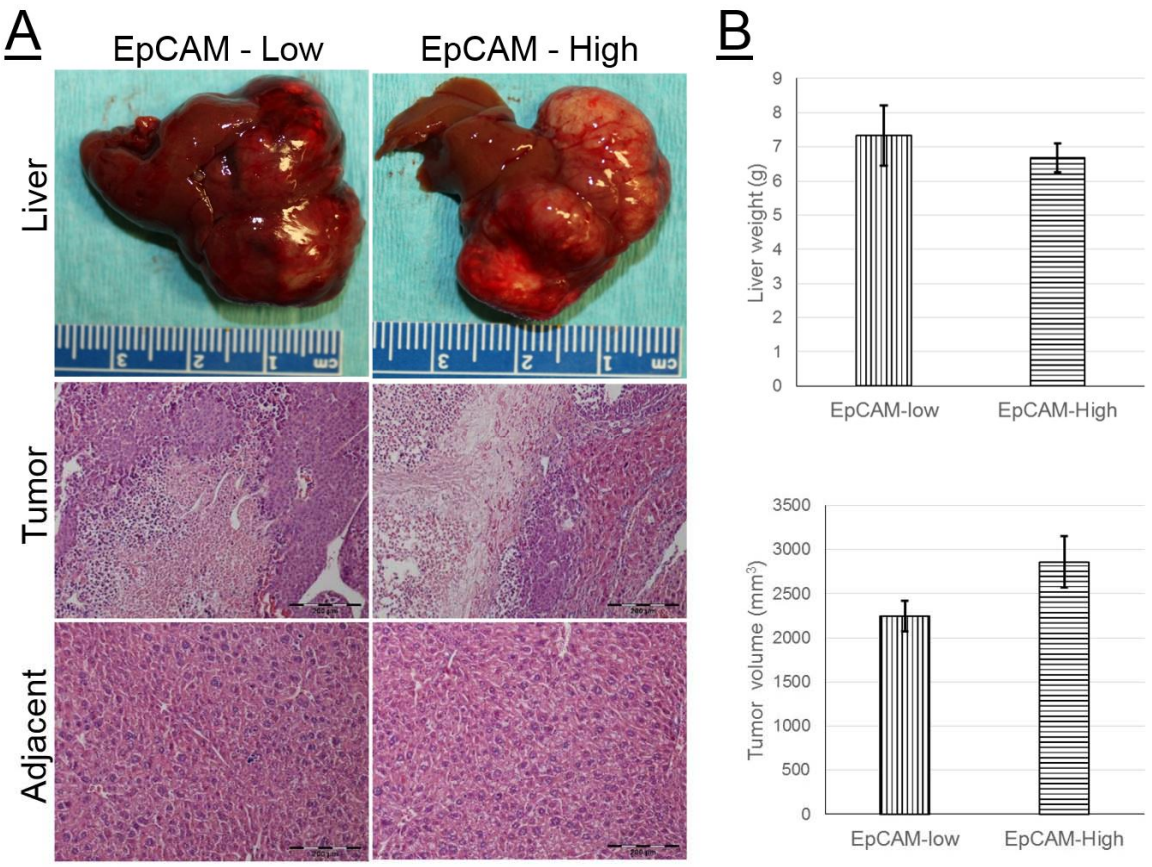

Figure 4.10: HepG2 EpCAM-Low and EpCAM-High HepG2 cell's fate in orthotopic Nu/J mouse model of HCC: 2 million sorted EpCAM-low or EpCAM-high HepG2 cells with constitutive copGFP expression were injected into left liver lobe of athymic Nu/J nude mice with survival surgery, and tumor growth was monitored for 70 Days. **(A)** Gross liver and HE staining of EpCAM-Low and EpCAM-High animals. All 4/4 animals in EpCAM-Low and EpCAM-High group confirmed tumor by H&E staining. **(B)** There was no significant difference observed in liver weight and/or tumor volume between both groups. Total n=4 mice/group, p=NS.

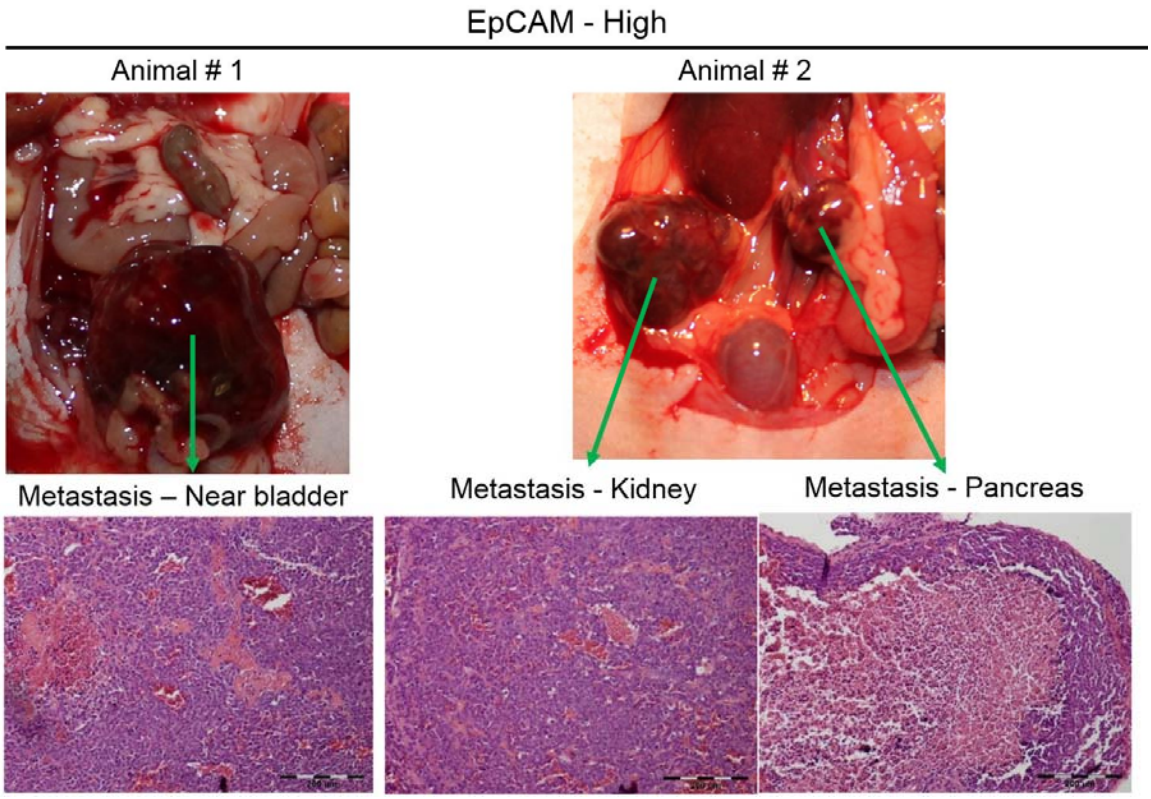

Figure 4.11: EpCAM-High HepG2 cells metastasize in orthotopic athymic Nu/J mouse model: Two of the four animals showed metastasis of HepG2. In the first animal, metastasis was observed near bladder, and second animal showed metastasis in Kidney and Pancreas. Lower panel shown H&E staining of metastatic tissues, confirming tumors.

Summary

We established different mouse models representing 3 distinct diet induced liver microenvironments i.e. healthy (control), steatosis (HFD), and inflammatory steatohepatitis (NASH). Then, we systematically studied tumorigenic abilities of EpCAM+ CSCs and EpCAM- Hepa1-6 cells in livers of animals, injected orthotopically. Tumor growth was accurately monitored by non-invasive high-frequency ultrasound imaging. Control and HFD group of animals failed to initiate tumor following 2 million Hepa1-6 EpCAM+ cells, suggesting healthy liver and mild steatosis liver microenvironment rejected EpCAM+ CSCs. In NASH microenvironment, EpCAM+ CSCs showed aggressive tumor growth while EpCAM- Hepa1-6 cells demonstrated incidental tumor initiation (2/10 mice with tumors, much smaller in size and volume compared to EpCAM+ tumor). We next performed lineage tracking studies to identify source of tumor initiation in NASH microenvironment. For this objective, we established constitutive copGFP expressing EpCAM+ CSCs and mCherry expressing EpCAM- cells. Our findings in lineage tracking studies showed that HCC initiation in C57L/J NASH mice was predominantly from EpCAM+ CSCs and not from EpCAM- Hepa1-6 cells.

Next, we evaluated two human EpCAM+ cell lines (Hep3B and HepG2). We sorted EpCAM-Low and EpCAM-High Hep3B cells and injected them into liver lobes of Nu/J mice orthotopically. EpCAM-High group confirmed all 4/4 mice with aggressive tumor growth, while EpCAM-Low group showed only 1/4 mouse with successful tumor initiation (tumor in EpCAM-Low group is significantly smaller compared to EpCAM-High group). Western Blot analysis confirmed that

expression of β-catenin was significantly high in Hep3B tumors derived from EpCAM-High group compared to EpCAM-Low liver/tumor tissues. Our results demonstrate that EpCAM expression of Hep3B dictated tumor initiation capability in liver microenvironment.

Similarly, we tested HepG2 tumorigenic property in orthotopic Nu/J mouse model. We sorted EpCAM-Low and EpCAM-High HepG2 subsets, and injected them into liver lobes of Nu/J mice orthotopically. HepG2 experiments demonstrated successful tumor initiation in livers of both EpCAM-High and EpCAM-Low group of animals. No significant differences were observed in tumor volume or liver weight between EpCAM-High and EpCAM-Low groups. HepG2 cells have a constitutively active mutant β-catenin (~75 KD) which may explain failure to see differences in tumorigenesis in these experiments. However, 2/4 EpCAM-High animals confirmed metastasis to kidney and pancreas. Our results demonstrate that EpCAM expression of HepG2 cells did not affect its tumorigenic abilities, but potentially facilitate metastasis in liver microenvironment.

Overall, our extensive and comprehensive *in vivo* study confirmed that higher tumorigenic capabilities were characteristic of EpCAM expressing CSCs in immunocompetent and immunocompromised liver microenvironment. As EpCAM is a proposed target of Wnt/β-catenin, we next studied the role of Wnt/β-catenin pathway in hepatocellular carcinoma CSC activation.

CHAPTER 5

ROLE OF CANONICAL WNT/BETA-CATENIN COMPONENTS IN HCC CSCS ACTIVATION

Introduction:

Canonical Wnt/β-catenin pathway is well implicated in HCC [64]. Indeed, analysis of NIH-NCI's cancer genome atlas identified CTNNB1 (β-catenin) as the 3rd most mutated gene after TP53 in the HCC patients. In Chapter 3, we found that β-catenin was upregulated in Hepa1-6 and HepG2 CSC spheroids. Our findings suggest that β-catenin could be playing a critical role in the activation of CSCs or enrichment of CSCs in spheroids. Our systematic study in orthotopic animal models (Chapter 4) suggest that EpCAM+ CSCs inherent tumorigenic property in liver microenvironment. Extensive studies by Yamashita et.al. established EpCAM as CSC marker in HCC and also found that EpCAM is the target of Wnt/ β-catenin pathway in HCC CSCs and liver cancer [38, 95]. In colon cancer cell lines, β-catenin contribute to form colonospheres *in vitro*, an important characteristic of CSCs [87]. However, how β-catenin contributes to HCC CSCs activation is not yet known. Hence, here we evaluated canonical Wnt/β-catenin pathway to identify CSC activation event contributing to enrichment of CSCs spheroids and CSC activation.

Results:

5.1) Analysis of human specimens found significant higher EpCAM expressions in HCC tissues:

Total protein was extracted from 8 pairs of malignant tissues and adjacent benign tissues. Western Blot analysis was performed to analyze the EpCAM and β-catenin expression in these tissues (Figure 5.1-A & B). In 4 paired tissues, EpCAM expression was higher in malignant tissues compared to the benign adjacent tissues (samples 1, 2, 5, and 6). In 3 paired tissues, EpCAM expression was only slightly increased in malignant tissues compared to the benign adjacent tissues (samples 3, 4, and 8). However, in one pair (sample 7), EpCAM expression remained unchanged. β-catenin expression levels were found to be high in 5 paired samples (samples 1, 2, 4, 5, and 6). However, in pair 3, pair 7 and pair 8, β-catenin expression levels were found to be lower in malignant tissues compared to benign adjacent tissues.

We have also examined 24 pairs of HCC tissues and adjacent benign control by IHC (Figure 5.1-C). Our data showed a significantly higher expression of EpCAM in specimens with HCC (483.75 ± 119.92, $p<0.0001$) when compared with the normal liver tissue within the resected specimens (38.44 ± 7.31).

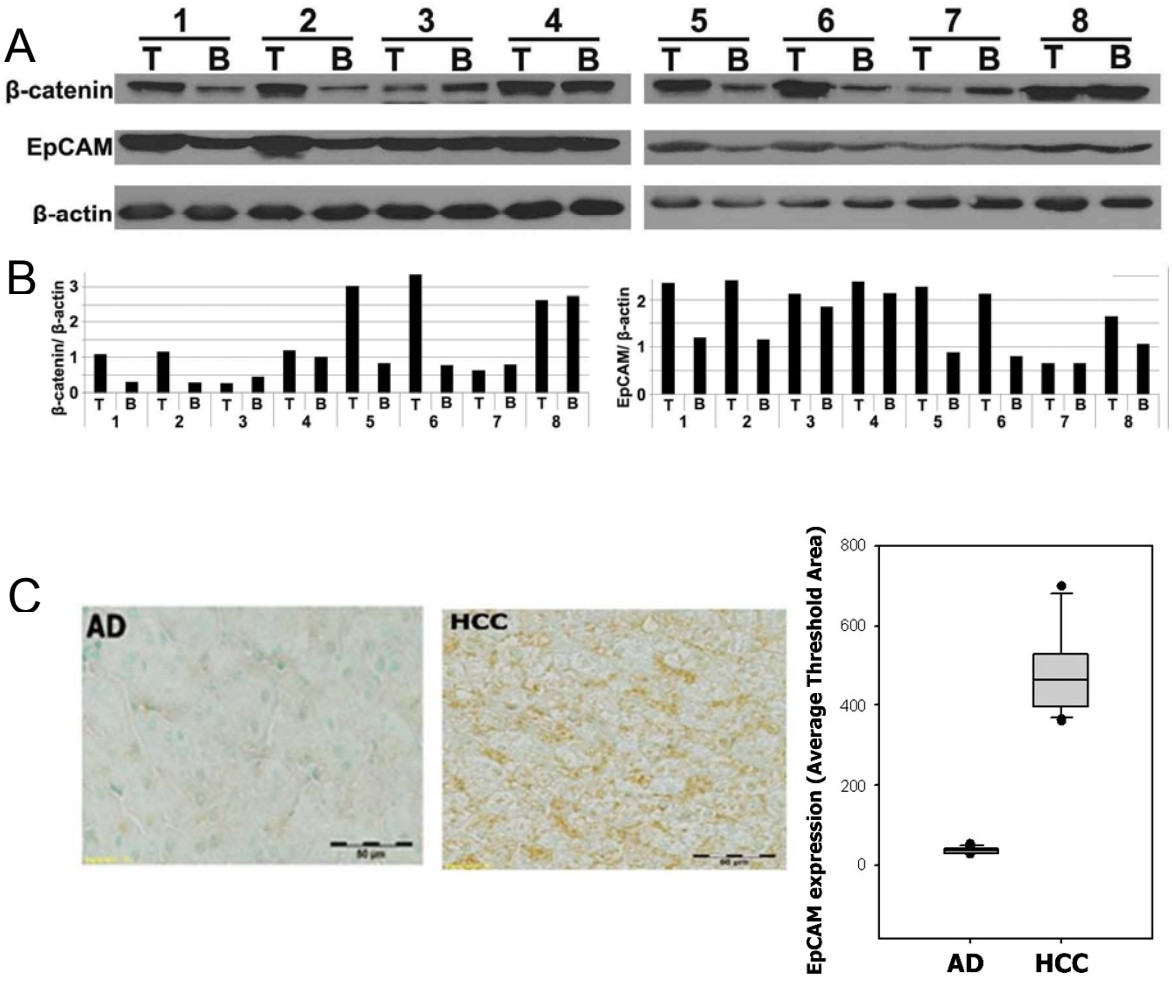

Figure 5.1: Analysis of human HCC specimens. Total proteins were extracted from 8 pairs of human HCC specimens (tumor tissue and adjacent benign tissue) and analyzed SDS-PAGE followed by Western Blot for EpCAM and β-catenin expression. **(A)** Western blot; **(B)** densitometry image analysis of EpCAM (left) and β-catenin (right) expression in malignant tumor tissue and adjacent benign tissue (n=8). **T**: tumor tissue; **B**: benign adjacent tissue. Total 24 pairs of HCC specimens were analyzed by IHC staining. **(C)** Left: Representative images of IHC EpCAM staining of human tissue specimens. Right: Quantified EpCAM expression (n=24, paired benign AD and HCC specimens). 40X magnification (Bar = 50 μm) **AD**: adjacent normal liver; **HCC**: hepatocellular carcinoma.

5.2) Gene expression analysis revealed Wnt/β-catenin upregulation induce potential dedifferentiation in Hepa1-6 CSCs

Concomitant expression of EpCAM and β-catenin in HCC patients (Figure 5.1) suggested β-catenin dependent tumorigenesis process during HCC development. Role of β-catenin in HCC development and EpCAM+ CSC activation is well established [62, 95]. Hence, we were intrigued to identify the source of EpCAM+ CSCs in Hepa1-6 spheroids. We hypothesized that EpCAM+ CSCs were enriching via Wnt/β-catenin dependent dedifferentiation of Hepa1-6 HCC cells.

In order to test our hypothesis, Hepa1-6 control and spheroids were grown and harvested on Days1, 3, 5, and 7 to extract total RNA. Gene expression for β-catenin, canonical Wnt pathway components (Wnt3a, Notum, Lrp5, Lrp6, GSK3β), HCC prognostic markers (EpCAM, AFP), Wnt independent stem cell activation markers (Lin28B, Sox2, Oct4) and EMT markers (E-Cadherin and Vimentin) were performed by qRT-PCR. All the results were analyzed by Pearson correlation analysis to identify linkage group genes regulated together.

Figure 5.2 show heat-map gene analysis with correlation linkage of all the targets (left) and experimental groups (bottom). EpCAM and AFP expression were tightly regulated, as well as showed positive correlation with CD44 and CycD1 (Wnt targets), vimentin, Notum (Wnt feedback inhibitor), β-catenin, Lrp5 and Lrp6 (wnt co-receptors), and Lin28B (Wnt independent stem-cell marker). These data confirm previous findings in human HCC specimens (Figure 5.1) and are consistent with *in vitro* data for Hepa1-6 CSCs enrichment in spheroids, where we found upregulation of EpCAM. In addition to EpCAM, CSCs spheroids also showed

Lin28B upregulation in association with β-catenin and EpCAM. Lin28B is independent of β-catenin mediated regulation and a key protein in stem cell pathway, but also plays a role in tumorigenesis.

Taken together, gene analysis data and Pearson correlation analysis suggested that CSC spheroids were enriched by potential dedifferentiation mechanisms by activating canonical Wnt/β-catenin pathway.

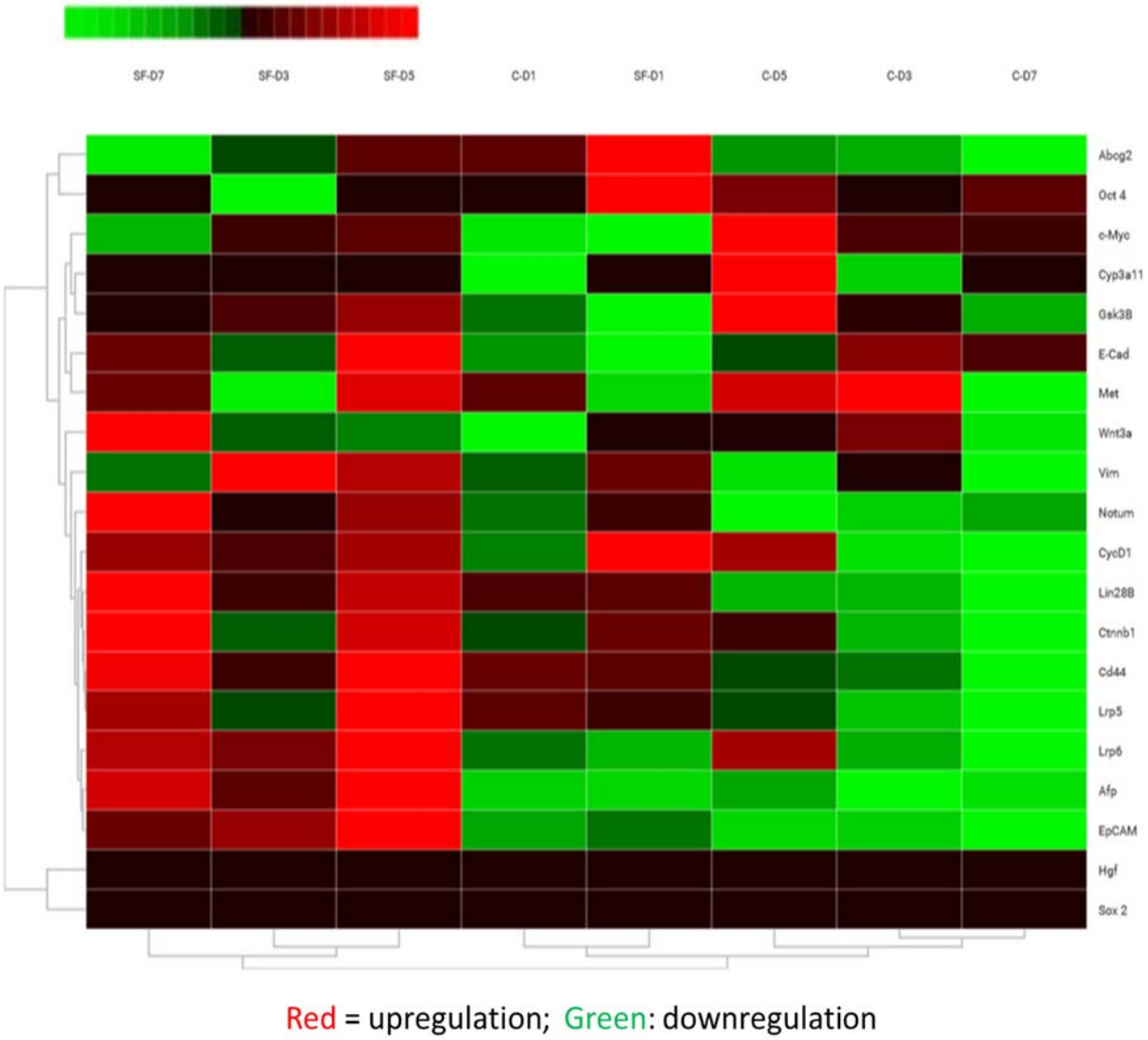

Figure 5.2: Wnt/β-catenin upregulation induce potential dedifferentiation in Hepa1-6 CSCs: Hepa1-6 control and spheroids were grown and harvested on D1, D3, D5, and D7 to extract total RNA. Gene expression for canonical Wnt pathway and dedifferentiation were analyzed by qRT-PCR. **Heat-map** showing gene analysis of all the experiments to identify genes which are related using Pearson correlation analysis.

5.3) Silencing β-catenin reversed CSCs properties

Silencing β-catenin reverses spheroid phenotype of CSCs in EpCAM positive HCC cell lines.

Upregulation of β-catenin led us to investigate the role of β-catenin in spontaneous generation of HCC CSC spheroids. Therefore, to further study implication of loss of function of β-catenin in spontaneous spheroid formation, we knocked down Ctnnb1 (β-catenin gene) using siRNA.

Knockdown validation of Ctnnb1 (mouse) and CTNNB1 (human) were confirmed by Western Blot (Figure 5.2-A). We achieved >70% knockdown efficiency by siRNA mediated transfection. After 48-72 hours of Ctnnb1 knockdown (n=3 independent experiments), Hepa1-6 cells lost the spheroid phenotype and shifted to the differentiated phenotype, similar to their parent cells growing in the medium with serum (Figure-5.2-B). This shifted phenotype of HCC spheroid was further confirmed in HepG2, a human EpCAM positive cell line. Upon CTNNB1 knockdown by siRNA, HepG2 spheroids showed close to 98% reversal to differentiated phenotype in serum-free media (Figure 5.2-C). Loss of spheroid phenotype was more effective in HepG2 compared to Hepa1-6 upon the siRNA-mediated knockdown of β-catenin.

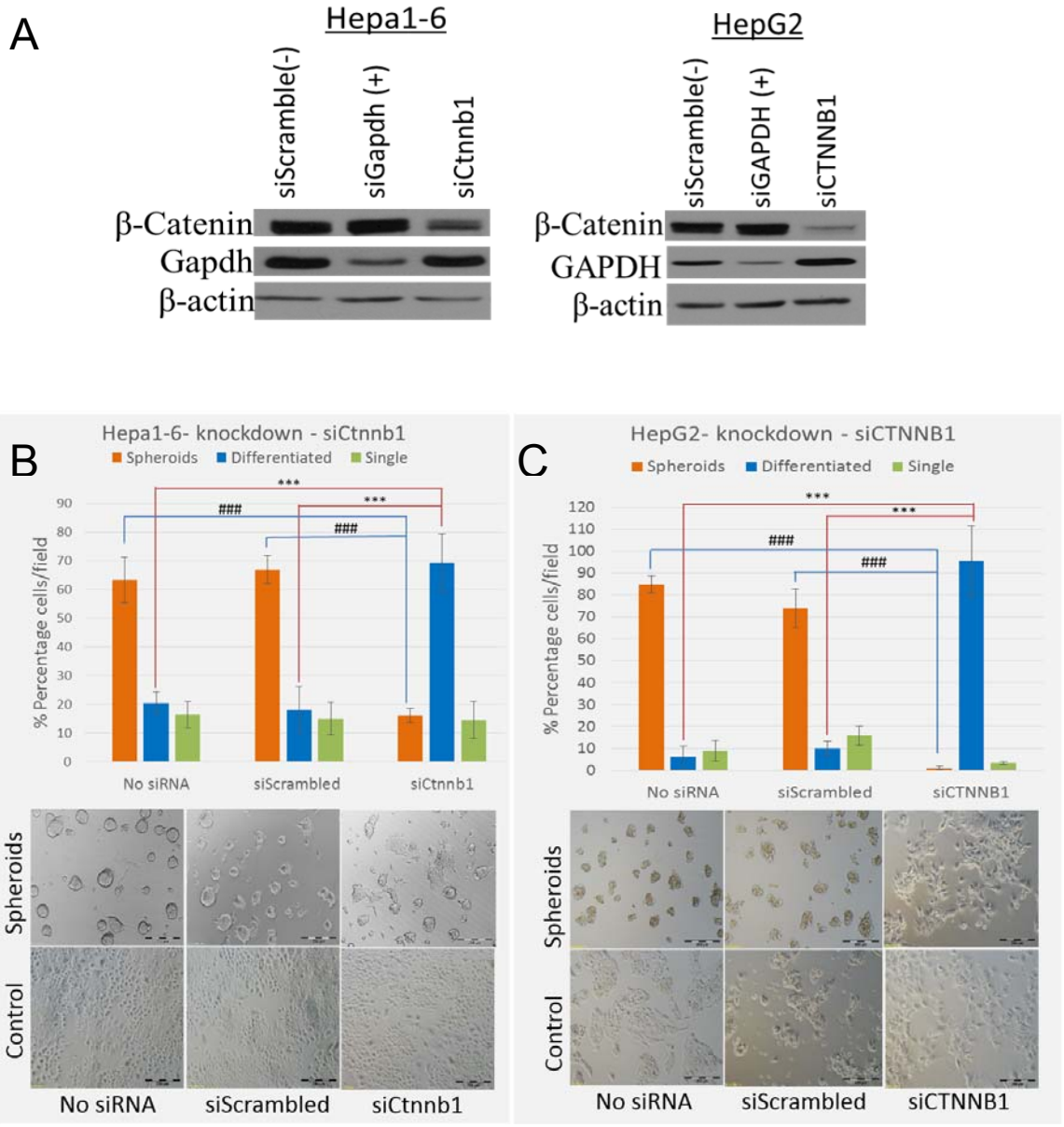

Figure 5.3: Silencing β-catenin expression reversed CSC spheroids phenotype. Hepa1-6 and HepG2 cells were grown in control or spheroid media for 4 days, transient transfection with scrambled siRNA control or siCTNNB1, followed by 48 to 72 hours incubation. **(A)** Western blot confirming ≥70% efficient knockdown. GAPDH used as positive control for transfection (n=3 independent experiments). **(B)** Hepa1-6; **(C)** HepG2 cells. Upper panels show average quantification (n=5 random fields/group) of spheroids (orange), adherent (blue), and single cells (green). Error bar is representing S.D. n=3 independent experiments, *** ($p \leq 0.005$, control), ### ($p \leq 0.005$, spheroids). Lower panel show visual representative images of corresponding experimental group.

Silencing β-catenin abolish drug resistance property of HCC CSCs

Acquired resistance to chemotherapy contribute to minimal residual disease (MRD) after primary tumor treatment, and thus responsible for tumor recurrence. We investigated and confirmed in Chapter 1 that spheroid enrichment of CSCs in all 3 HCC cell lines acquired resistance to doxorubicin, a first line chemotherapeutic drug in HCC treatment. Transient knockdown of β-catenin by siRNA exhibited reversal of spheroid formation, a key CSC property as explained earlier in Chapter 5.3. Therefore, we sought to investigate if β-catenin knockdown also abolish HCC CSC's drug resistance property.

Hep3B and HepG2 cells were grown in control or spheroid media for 3 days. On day 3, we performed transient transfection with scrambled siRNA control or siCTNNB1 with optimized conditions as established and validated for spheroid reversibility experiment (Figure 5.3-A). After 24 hours post transfection, (on day 4) , we treated cells with 0.5 μM doxorubicin and incubated for additional 48 to 72 hours, harvested and analyzed for viability by XTT assay. Hep3B spheroids with siCTNNB1 significantly lose doxorubicin resistance partially after 72 hours compared to siScrambled and doxorubicin alone (siCTNNB1+Dox: 0.38±0.032 , siScrambled+Dox: 0.51±0.48, Dox only:0.53±0.01, $p<0.05$, n=3 independent experiments). Loss of doxorubicin resistance was also analyzed in HepG2 cells and found to be more apparent and drastic compared to Hep3B spheroids. In HepG2 spheroids, siCTNNB1 caused significant loss of doxorubicin resistance after 48 hours compared to siScrambled and doxorubicin alone (siCTNNB1+Dox:

0.35±0.01, siScrambled+Dox: 0.55±0.06, Dox only:0.51±0.025, $p<0.005$, n=3 independent experiments).

Additionally, in HepG2 cells, viability of siCTNNB1+Dox group was comparable to Control group after 48 hours (spheroids: siCTNNB1+Dox: 0.35±0.01, Control: siCTNNB1+Dox: 0.33±0.01). Thus suggesting that silencing β-catenin led to complete loss of acquired doxorubicin property of HepG2 CSCs. Notably, these findings in HepG2 cell line were consistent with complete reversibility observed after β-catenin knockdown (Figure 5.3-C).

HepG2 is a unique HCC cell line, correlated with high Wnt/β-catenin HCC subtype in clinic due to a somatic mutation resulting in a constitutively active truncated β-catenin form (~75 KD) [114, 115]. Silencing β-catenin by siRNA decreased levels of full-length β-catenin (~92 KD), and truncated β-catenin in HepG2. Also, HepG2 cell lines may have a higher turn-over of β-catenin.

Overall, our data suggest that β-catenin serves as crucial player in activation and enrichment of HCC CSCs, and its silencing led to loss of CSC properties. Importantly, we provided first direct phenotypic evidence of spheroid reversibility with loss of function association with β-catenin.

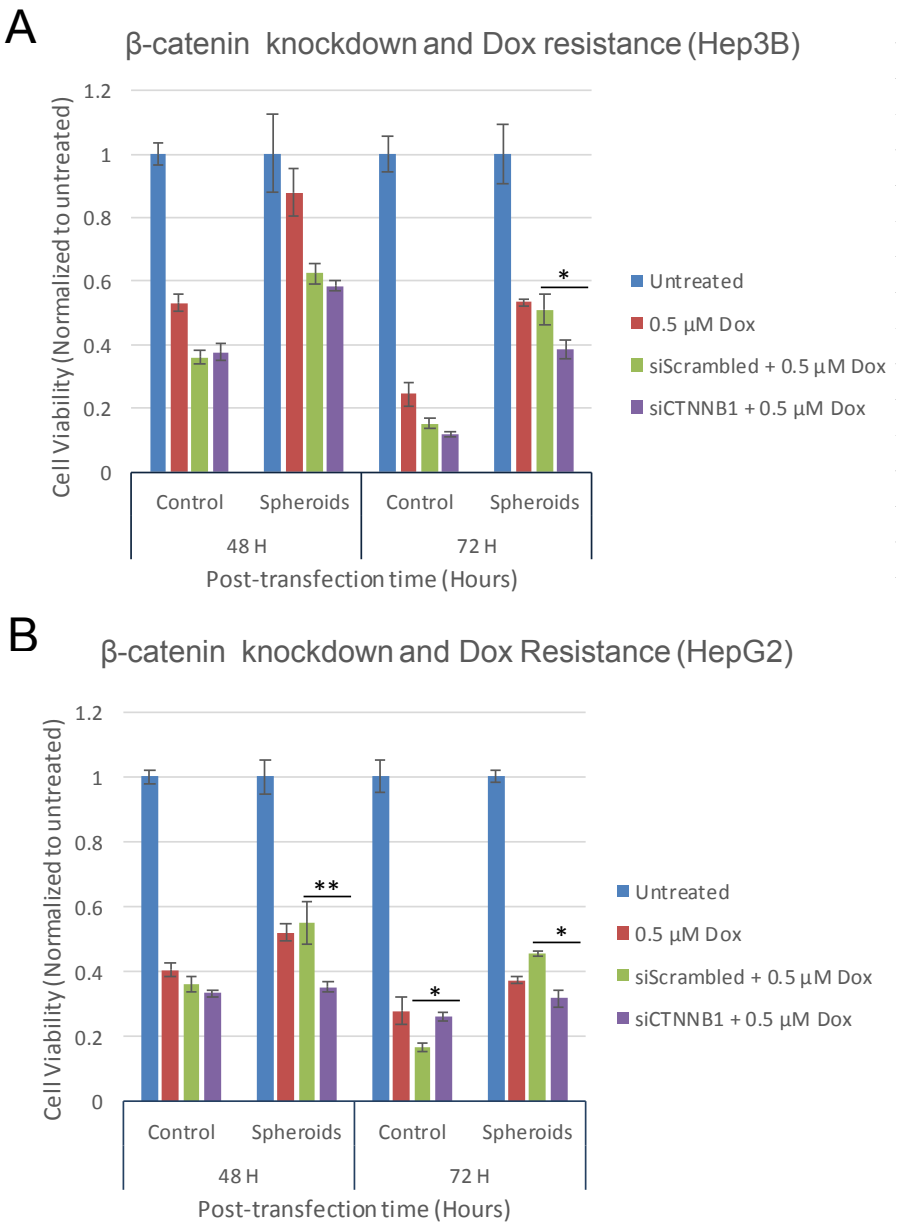

Figure 5.4: Silencing of β-catenin abolished resistance to doxorubicin in HCC CSCs. Hep3B and HepG2 cells were grown in control or spheroid media for 3 days, transient transfection with scrambled siRNA control or siCTNNB1 on day 3, and treated for 0.5 µM Doxorubicin from day 4 to be followed by 48 to 72 hours incubation. **(A)** Hep3B spheroids showed significant loss of doxorubicin resistance after 72 hours compared with scrambled control (n=3 independent experiments, 2 different siRNAs targeting CTNNB1). **(B)** HepG2 spheroids showed significant loss of doxorubicin resistance after 42 hours compared with scrambled control. Untreated (blue), Doxorubicin alone (red), Scrambled siRNA (green), and siCTNNB1 (purple). Error bar is representing S.D. n=3 independent experiments, ** $p \leqslant 0.005$), * $p \leqslant 0.05$.

5.4) Regulation of HCC CSCs activation resides at nuclear level – study of Wnt/β-catenin pathway components by pharmacological inhibitors.

Our results from Chapter 1 (Figure 1.12) identified increased levels of inactive GSK-3β phosphorylated at Ser9, suggested possible regulation at destruction level complex in the cytoplasm. In order to decipher exact point-of-action for CSC activation mechanism we have systematically analyzed the Wnt/β-catenin pathway with different chemical inhibitors (each targeting one step at a time). We selected 4 chemical inhibitors (LiCl, MG132, XAV939, and FH5355) for this objective after preliminary experiments (Figure 5.4). We determined optimal effective concentrations for each of the 3 HCC cell lines i.e. Hepa1-6, HepG2, and Hep3B after extensive preliminary experiments (data not shown). We used these optimum concentrations for further studies i.e. LiCl =10 mM , XAV939 = 10 μM, and FH535 = 10 μM. MG132 was not used because of high apoptosis induction possibly because of non-specific accumulation of other cellular proteins. LiCl activates Wnt/ β-catenin signaling by inhibiting Ser9 phosphorylation of GSK-3β and thus stabilizing cytoplasmic pool of β-catenin. XAV939 and FH535 inhibit Wnt/β-catenin pathway at cytoplasmic (destruction complex level) and nuclear transcriptional levels, respectively.

Figure 5.4-B showed confirmation of functional effects by inhibitor treatment on Hepa1-6 cell line experiments. LiCl significantly increased β-catenin and EpCAM expression, while XAV939 induced degradation of β-catenin and decreased EpCAM expression.

We expected treatment with XAV939 and FH535 to produce similar results of spheroid reversibility as observed in Figure 5.3 after siRNA mediated β-catenin knockdown.

As seen in Figure 5.6, CSC spheroid culture of all 3 HCC cell lines respond only to FH535 but not XAV939. These results suggest that destruction complex inhibition by XAV939 did not exhibit functional consequences on spheroid formation of CSCs, and thus CSC activation and/or spheroid activation regulation must be occurring downstream of GSK-3β dependent destruction complex regulation. CSCs spheroids in all 3 cell lines responded to FH535 treatment and inhibition of spheroid formation were observed. Because we activated Wnt pathway with LiCl treatment simultaneously, plenty of stabilized β-catenin should be available for nuclear translocation and downstream gene activation at transcription levels. However, FH535 inhibits transcriptional level activity of β-catenin in HCC CSCs, suggesting that regulation of CSC activation takes place at the nuclear level.

Overall, we have identified the regulation switch of HCC CSC activation and spheroid formation, and it occurs at the nuclear level and not at the destruction complex level in cytoplasm.

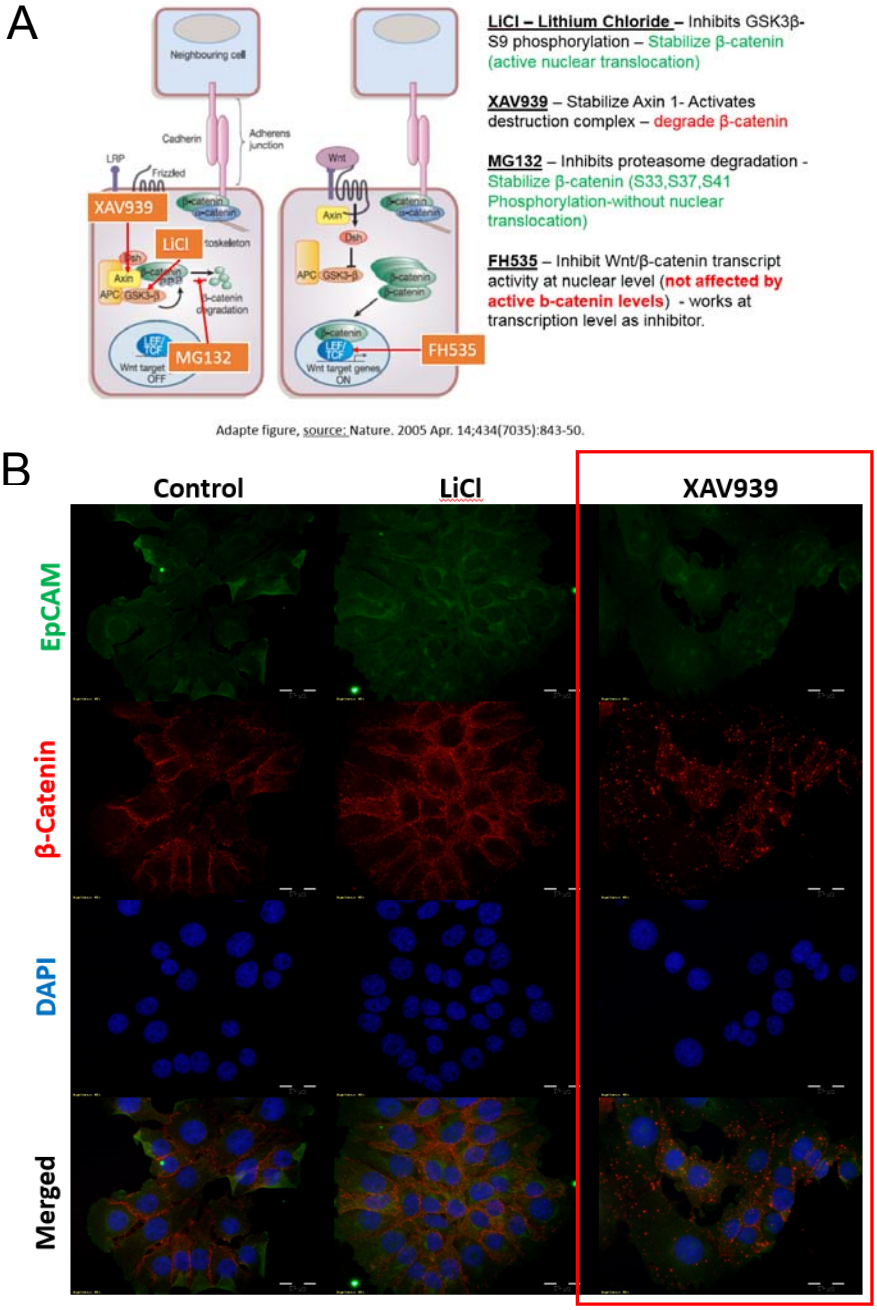

Figure 5.5: Inhibitor study to identify control point of Wnt/β-catenin pathway during CSC activation. (A) Cartoon figure showing mechanism of action of chemical inhibitors used, with brief explanation of their mechanism of actions on right side. **(B)** ICC staining of Hepa1-6 cells: untreated control, treated with 10 mM LiCl and 10 μM XAV939. EpCAM (Green, Alexafluor-488)), β-catenin (Red, Alexafluor-594), DAPI – nuclear (Blue), Control = untreated cells. LiCl increased EpCAM-ICD and β-catenin expression while XAV939 decreased EpCAM-ICD expression and direct β-catenin for ubiquitin mediated degradation following S33/37/41 phosphorylation priming (red dots). 40x magnification, bar=50 μm.

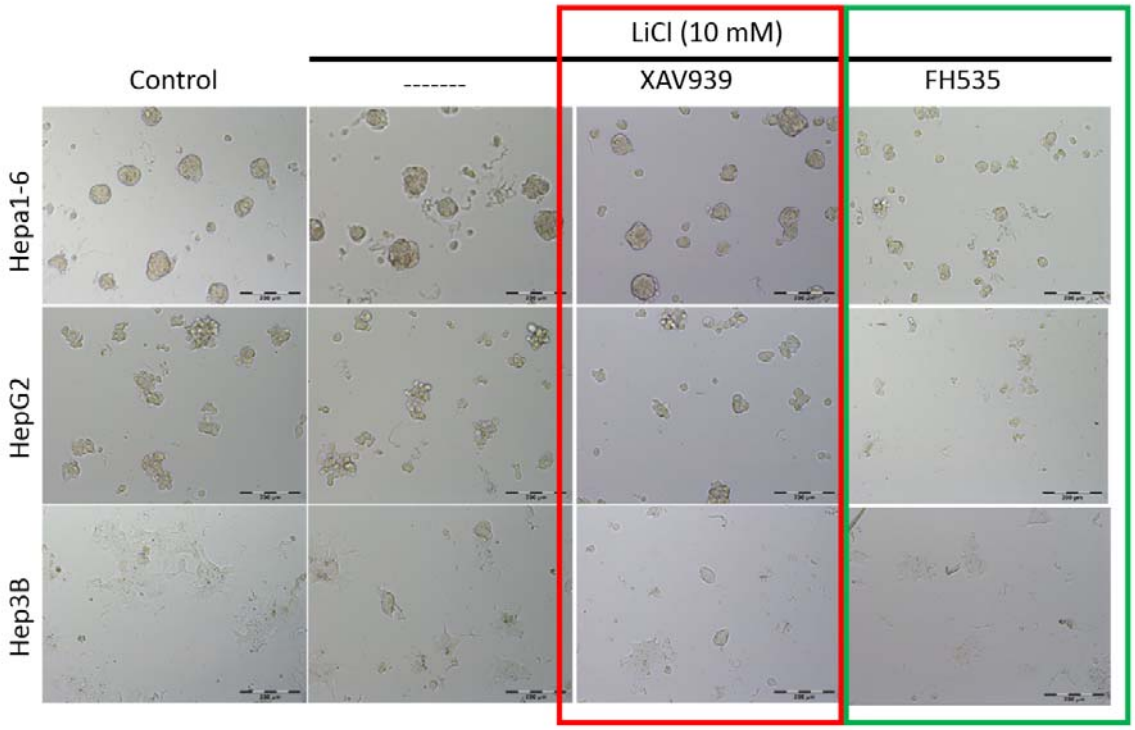

Figure 5.6: HCC CSC activation and spheroid formation is β-catenin dependent and regulated at the nuclear level. All 3 HCC cell lines were cultured in serum free media for 7 days to generate CSCs spheroids. On day 8, cells were treated with LiCl alone, LiCl + XAV939, and LiCl + FH535 for 48 hours. After 48 hours, cells were observed by microscope and bright field images were captures. As showed in figure red box, XAV939 treatment was ineffective to revere or destroy spheroid formation. However, FH535 treatment was effective in all 3 cell lines to inhibit or reverse spheroid formation. 10x magnification, bar = 200 μm.

5.5) NOTUM inhibition feedback in Wnt/β-catenin pathway turned non-responsive in EpCAM+ tumors of NASH mouse model and human HCC.

Recently, Wnt/β-catenin feedback inhibitor NOTUM was deciphered [116]. NOTUM is target of Wnt/β-catenin signaling which deacylates Wnt to turn off the signaling. This feedback inhibition check point prevents accidental activation of Wnt signaling.

We analyzed 5 human HCC tumors and adjacent tissues. 4/5 HCC specimens showed higher NOTUM expression compared to adjacent control (Figure 5.7-A). Similarly, IHC-P staining of tumors developed in EpCAM+ CSCs NASH group mice from Chapter 4, showed higher expression of both Wnt3a and NOTUM (Figure 5.7-B). Increased NOTUM expression in human and mouse tumors suggest that Wnt/β-catenin driven tumors failed to respond to NOTUM feedback inhibition. This makes sense because, as shown in Chapter 5-3, Wnt/β-catenin signaling in HCC CSCs is not regulated at cytoplasmic destruction complex level but at the nuclear level.

Taken together, NOTUM mediated feedback is ineffective to switch off upregulated Wnt/β-catenin signaling in HCC tumors. Nuclear level regulation of β-catenin allows constitutive activation of downstream oncogenic targets, and as a result, one of the downstream targets, NOTUM, showed upregulation. However, since NOTUM mediated feedback inhibition required cytoplasmic signaling regulation, which is lacking in HCC CSCs, increase in NOTUM expression does not help to slow-down these β-catenin driven tumors.

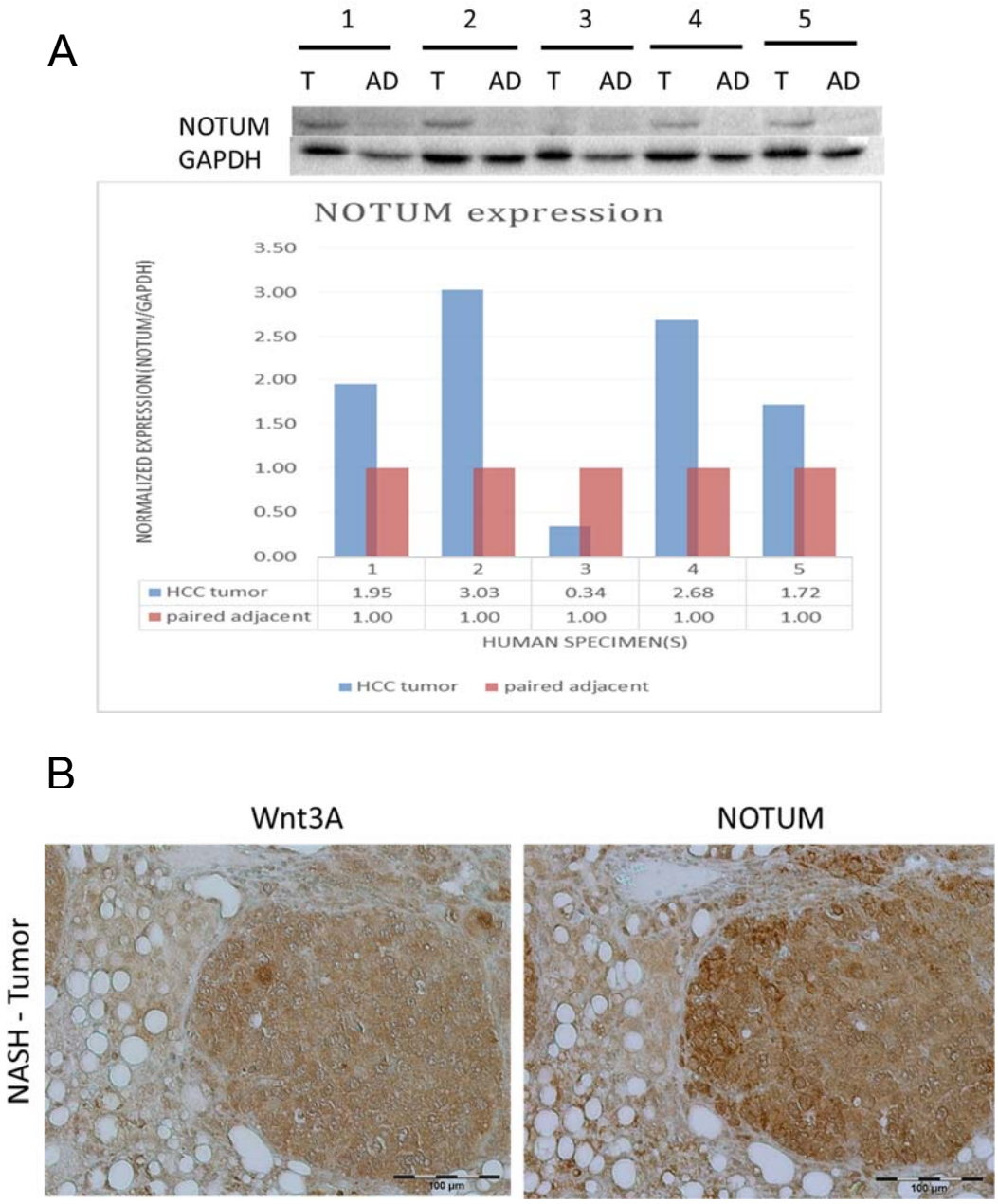

Figure 5.7: Aberrant NOTUM inhibition feedback in HCC patients and EpCAM+ CSCs NASH mice tumors. (A) 4/5 human HCC specimens showed increase NOTUM levels in tumor compared with adjacent. **(B)** Representative EpCAM+ CSC tumor from orthotopic NASH animal showing increased Wnt3a and NOTUM expressions.

Summary

We demonstrated that EpCAM and β-catenin are concomitantly increased or decreased in human HCC specimens compared to adjacent healthy controls. CSC spheroid enrichment gene analysis in Hepa1-6 revealed possible dedifferentiation events occurring during spheroid formation. Importantly, HCC and Wnt pathway genes are upregulated with spheroid enrichment, and Pearson correlation analysis linked them to stem cell activation genes (Lin28B, β-catenin). Loss of function study of β-catenin showed that properties of CSCs are lost upon transiently silencing β-catenin, (1) Hepa1-6 and HepG2 reversed CSC spheroids to adherent phenotype, (2) HepG2 and Hep3B EpCAM positive cell lines lost acquired doxorubicin resistance. Meticulous chemical inhibition of Wnt/β-catenin pathway components identified regulation of HCC CSCs activation resides at the nuclear level. And lastly, recently identified canonical Wnt/β-catenin feedback inhibitor, NOTUM, showed increased expression in human and mouse NASH tumors. These findings suggest an important role of β-catenin in CSC mediated tumorigenesis. Importantly, our findings suggest that aberrant Wnt/β-catenin pathway activation in CSCs via nuclear level changes, made β-catenin driven HCC tumors non-responsive to NOTUM feedback inhibitions.

CHAPTER 6

DISCUSSION

The existence of cancer stem cells (CSCs) is no longer a debatable topic since they have been definitively identified by three independent lineage tracking studies [41-43]. However, the origin of CSCs has not been elucidated and is still an active area of investigation [101, 117]. Primarily two arguments exist:(1) CSCs originate by dedifferentiation from either cancer cells or normal cells, and (2) CSCs originate by mutations and biochemical changes in tissue-specific pools of normal progenitor or stem-cell compartments [118-122]. A study by Yamanaka et.al. showed that terminally differentiated fibroblast cells possess reprogramming capabilities to go back to the pluripotent stem cell niche [123]. Considering unpredictable tumor cell fate and the poorly understood tumor microenvironment, the origin of CSCs from differentiated cancer cells seems a likely possibility [32, 124].

Our results suggest that β-catenin plays a strategic role in switching from a differentiated cancer cell phenotype to a dedifferentiated CSC phenotype in HCC cell lines. Results from Chapter 3 demonstrated that both cytoplasmic and nuclear levels of β-catenin in HCC CSCs were significantly increased compared to adherent control, and these increased levels of β-catenin display functional effects on downstream targets i.e. increase in TCF1, LEF1, CycD1 expression. We also

found that increased levels of β-catenin and downstream dedifferentiation effects were regulated at destruction complex level, at least partially, which was confirmed by increase in inactive GSK3β levels (Ser9-phosphorylation). Our findings in HCC spheroids are consistent with a study in colonosphere which showed aberrantly increased levels of β-catenin in spheroids compared to adherent cell lines [87]. Surprisingly experiments in Chapter 5 where we systematically studied canonical Wnt/β-catenin by means of chemical inhibitors, revealed that inhibiting GSK3β by XAV939 failed to reverse HCC CSC spheroids. However, these CSC spheroids responded to nuclear level β-catenin transcription inhibition by FH535 and led to arrest in their growth. Taken together, these findings suggested that nuclear regulation of β-catenin plays a fundamental role in CSC activation compared to cytoplasmic canonical Wnt/β-catenin regulation.

Loss of β-catenin by siRNA confirmed and complemented results of the inhibitor, FH535, where upon β-catenin silencing HCC CSCs spheroids reversed to adherent phenotype and lost doxorubicin resistance. Indeed, siRNA experiments confirmed central role of β-catenin in regulation of CSC activation and ruled out possibility of β-catenin independent (non-canonical) Wnt signaling. Loss of cytoplasmic regulation at destruction complex level (GSK3β level) suggested that stabilizing and translocating cytoplasmic β-catenin no longer serve as a rate limiting step for canonical Wnt pathway mediated HCC CSCs activation [125]. Mokkapati et al. showed that β-catenin activation alone in liver progenitor cells is sufficient to cause tumorigenesis in HCC [102]. This is further supported by studies in breast cancer and colon cancer [84, 87]. In breast cancer, targeting Wnt/β-

catenin pathway has shown to chemosensitize CSCs [59, 60]. In head and neck cancers, Wnt antagonist was shown to chemosensitize CSCs [61]. Study by Hashimoto et.al. showed that dedifferentiated spheroid cells confer chemoresistance in HCC as shown in our preliminary studies [58]. Our results in Chapter 5 (β-catenin silencing by siRNA) also observed loss of acquired doxorubicin resistance upon β-catenin silencing, and consistent with current literature. Involvement of β-catenin strongly implies that the heterogeneous cancer cells in a tumor mass could be an important pool of cancer-cell progenitors or CSCs. These CSCs are enriched via β-catenin mediated transcription activation, and contributing to HCC recurrence via chemotherapy resistance and minimal residual disease.

EpCAM correlates with poor HCC prognosis and downstream target of Wnt/β-catenin signaling [53, 95]. We further investigated specific EpCAM+ CSCs using orthotopic immunocompetent mouse model in 3 distinct liver microenvironments (Control, HFD, NASH). Hepa1-6 cell line was reported as a non-immunogenic murine cell line with an ability to form tumors in normal immunocompetent C57L/J mice, both orthotopically and subcutaneously [78-80], thus provide more clinically relevant mouse model to study tumorigenesis in presence of all immune system components, unlike athymic nude or SCID mouse models which lack an immune system.

In this dissertation project, we demonstrated that Wnt/β-catenin signaling plays a central regulatory role in HCC CSCs activation and enrichment *in vitro*.

We systematically studied *in vivo* fate of EpCAM+ CSCs of three different HCC cell lines in orthotropic models.

The major findings of this dissertation

Current and previous clinical trials targeting CSC activation pathway face challenges due to a lack of complete understanding of stemness plasticity [126]. Clinical trials rely on data obtained from pre-clinical rodent models, and majority of current CSCs knowledge was developed from athymic or SCID mice with hind limb xenografts [106]. There remains an unmet need to test and claim CSC properties in clinically relevant orthotopic rodent models.

In this study, we tested CSCs derived from HCC cell lines in orthotopic liver mouse models. Hepa1-6 is a murine HCC cell line closely representing poorly differentiated HCC growth in C57BL/6J and C57L/J mouse models [127, 128]. As explained in chapter 4, we have tested EpCAM+ Hepa1-6 CSCs in three different liver microenvironments i.e healthy controls, steatosis, and NASH. It has already been established that fatty liver progression exacerbate HCC carcinogenic events within liver microenvironment [109]. We have demonstrated that the NASH liver is favorable to EpCAM+ CSCs mediated tumorigenesis in immunocompetent microenvironment, while control and steatosis are not. Importantly, our findings suggested that EpCAM+ CSCs could successfully evade host immune surveillance in the NASH liver microenvironment. Therefore, the NASH mouse model can be vital tool to study immune checkpoint therapies and immune surveillance in tumor immunology.

Hep3B cell line is p53 null with mesenchymal phenotype, slow growing, and demonstrate well differentiated HCC tumors in mouse model [81] [113]. Orthotopic evaluation of EpCAM-High and EpCAM-low subsets of Hep3B demonstrated that the degree of EpCAM expression, not merely its presence or absence, positively correlates with severity of tumorigenesis. Hep3B/Nu-J experiments provide glimpse into nature of EpCAM expressing CSCs that hierarchal EpCAM expression bears different tumor initiating capability.

HepG2 cell line express a constitutively active form of β-catenin (truncated β-catenin, ~75 KD), but is considered as non-neoplastic hepatoma cell line [114, 115]. However, only a few studies have been successful in tumor initiation in animal models [50, 129]. Therefore, we tested HepG2 EpCAM-High and EpCAM—low subsets in orthotopic animal models, and found no significant differences in tumorigenesis potential. Considering constitutively active β-catenin status in HepG2 as explained above, distinct outcomes of HepG2/Nu-J experiments are not surprising. However, this study is first to report that the EpCAM-High HepG2 subset possess metastatic ability. Interestingly, HepG2/Nu-J experiments demonstrated that despite a constitutively active β-catenin, higher degree of EpCAM expression can steer these cells towards metastasis.

In chapter 5, data demonstrated central role of β-catenin in spheroid enrichment and doxorubicin resistance. Using XAV939 and FH535 chemical inhibitors, we also deciphered that β-catenin mediated CSC activation is regulated at the nuclear level. Subsequent analysis in human and animal tissues showed

that NOTUM feedback regulation is disturbed, which could be a potential mechanism for uninhibited β-catenin driven tumors *in vivo*.

Limitations of this dissertation

This dissertation was focused on EpCAM expressing CSCs, regulated by Wnt/β-catenin signaling. All 3 HCC cell lines we chose are expressing EpCAM. To be specific, Hepa1-6 is heterogeneous cell line in terms of EpCAM expression, while both HepG2 and Hep3B are EpCAM positive cell lines. Other Wnt/β-catenin signaling mediated CSC targets such as CD44 and ABCG2 were not studied as extensively as EpCAM in this dissertation, therefore, interpretation of current work should not be applied for CD44+ CSCs and ABCG2+ CSCs.

Future directions

Experimental work in this dissertation identified critical role of β-catenin in CSC enrichment, and demonstrated that aberrant activation of β-catenin in CSCs is regulated at the nuclear level, at least partially. This aberrant activation of β-catenin subsequently abolish NOTUM mediated feedback inhibition loop of the Wnt/β-catenin pathway. Deciphering this puzzle of nuclear β-catenin transcription activation in CSCs in HCC should be pursued next.

A few studies have shown direct nuclear activation of β-catenin mediated transcriptions. Study by Zhao et.al. identified YY1AP1 in EpCAM+AFP+ HCC, and proposed that both YY1PA1 and β-catenin contribute to EpCAM expression, which

however depends on p53 signaling status [50]. In another study, LEF1 protein, one of the nuclear interactive partners of β-catenin, is regulated by hepatocyte growth factor (HGF, paracrine) in breast and liver cancer cell lines [130]. A study by Li et.al. reported that TBL1-TBLR1 and β-catenin recruit each other to Wnt target-gene promoter and activate transcription [131]. Dimitrova et.al. identified that novel direct ubiquitination of β-catenin by Siah-1 and TBL1 protected β-catenin from degradation by competitive binding on the armadillo repeat domain of β-catenin [132]. Additionally, Choi et.al. suggested that SUMOylation of TBL1-TBLR1 regulates β-catenin expression and activity.

Orthotopic animal models that we developed could serve as more clinically relevant tools to study tumor immunology in HCC. Despite success of checkpoint inhibitors in other cancers, there isn't a significant progress in HCC. Our immunocompetent mouse model of NASH liver microenvironment (C57L/J) bearing EpCAM+ Hepa1-6 cells injected orthotopically in the left lobe, could serve as a system to understand how EpCAM+ cells evade host immune-surveillance in NASH (but failed to evade in healthy control and mild steatosis livers). Overall, our data with EpCAM expressing CSCs suggest that CSCs with other markers like CD90, CD44, and CD133 can also be systematically studied in similar immunocompetent models with orthotopic injections of CSCs instead of flank-implant xenografts, which lack the liver microenvironment.

Concluding remarks

This dissertation identified role of Wnt/β-catenin in activation of cancer stem cells in Hepatocellular carcinoma. These CSC spheroids acquired Doxorubicin resistance, and upon silencing β-catenin, there was not only a loss the spheroid phenotype, but also reversal to the adherent phenotype, and subsequent loss of resistance to doxorubicin. HCC spheroids showed significantly higher tumorigenic abilities in orthotopic immunocompetent mouse models. We further tested fate of EpCAM+ CSCs in 3 different HCC cell lines, in more clinically relevant orthotropic mouse models. In immunocompetent mice, we demonstrated that EpCAM+ CSCs need NASH microenvironment to initiate HCC. Immunocompromised mice with Hep3B and HepG2 cells offered insights into effect of EpCAM expression on tumorigenesis. Gene analysis studies suggested that CSCs are capable of dedifferentiation mediated by the Wnt/β-catenin pathway. We also demonstrated that activation of CSCs resides at the nuclear level as a result of gene transcription stimulated by β-catenin. Lastly, dysregulation of the canonical Wnt pathway in the cytoplasm leads to dysregulation of its NOTUM feedback inhibition loop.

REFERENCES

1. Altekruse, S.F., K.A. McGlynn, and M.E. Reichman, *Hepatocellular carcinoma incidence, mortality, and survival trends in the United States from 1975 to 2005.* J Clin Oncol, 2009. **27**(9): p. 1485-91.

2. Parkin, D.M., et al., *Global cancer statistics, 2002.* CA Cancer J Clin, 2005. **55**(2): p. 74-108.

3. El-Serag, H.B., *Hepatocellular Carcinoma.* New England Journal of Medicine, 2011. **365**(12): p. 1118-1127.

4. U.S. Cancer Statistics Working Group, *United States Cancer Statistics: 1999–2010 Incidence and Mortality Web-based Report*, in www.cdc.gov/uscs. 2013.

5. NCI, *Surveillance, Epidemiology, and End Results (SEER) Program* Last accessed April 2016, Natinal Cancer Institute: www.seer.cancer.gov.

6. Regimbeau, J.M., et al., *Obesity and diabetes as a risk factor for hepatocellular carcinoma.* Liver Transpl, 2004. **10**(2 Suppl 1): p. S69-73.

7. Dyson, J., et al., *Hepatocellular cancer: the impact of obesity, type 2 diabetes and a multidisciplinary team.* J Hepatol, 2014. **60**(1): p. 110-7.

8. El-Serag, H.B. and K.L. Rudolph, *Hepatocellular carcinoma: epidemiology and molecular carcinogenesis.* Gastroenterology, 2007. **132**(7): p. 2557-76.

9. Fattovich, G., et al., *Hepatocellular carcinoma in cirrhosis: incidence and risk factors.* Gastroenterology, 2004. **127**(5 Suppl 1): p. S35-50.

10. Goldberg, D., et al., *Changes in the Prevalence of Hepatitis C Virus Infection, Nonalcoholic Steatohepatitis, and Alcoholic Liver Disease Among Patients With Cirrhosis or Liver Failure on the Waitlist for Liver Transplantation.* Gastroenterology, 2017. **152**(5): p. 1090-1099.e1.

11. Flemming, J.A., et al., *Reduction in liver transplant wait-listing in the era of direct-acting antiviral therapy.* Hepatology, 2017. **65**(3): p. 804-812.

12. Welzel, T.M., et al., *Metabolic syndrome increases the risk of primary liver cancer in the United States: a study in the SEER-Medicare database.* Hepatology, 2011. **54**(2): p. 463-71.

13. Ligibel, J.A., et al., *American Society of Clinical Oncology position statement on obesity and cancer.* J Clin Oncol, 2014. **32**(31): p. 3568-74.

14. Flegal, K.M., et al., *Prevalence of obesity and trends in the distribution of body mass index among US adults, 1999-2010.* Jama, 2012. **307**(5): p. 491-7.

15. Ogden, C.L., et al., *Prevalence of high body mass index in US children and adolescents, 2007-2008.* Jama, 2010. **303**(3): p. 242-9.

16. Calle, E.E., et al., *Overweight, obesity, and mortality from cancer in a prospectively studied cohort of U.S. adults.* N Engl J Med, 2003. **348**(17): p. 1625-38.

17. Davila, J.A., et al., *Diabetes increases the risk of hepatocellular carcinoma in the United States: a population based case control study.* Gut, 2005. **54**(4): p. 533-539.

18. Kasmari, A.J., et al., *Independent of Cirrhosis, Hepatocellular Carcinoma Risk Is Increased with Diabetes and Metabolic Syndrome.* Am J Med, 2017. **130**(6): p. 746.e1-746.e7.

19. Lazo, M., et al., *Prevalence of nonalcoholic fatty liver disease in the United States: the Third National Health and Nutrition Examination Survey, 1988-1994.* Am J Epidemiol, 2013. **178**(1): p. 38-45.

20. McCullough, A.J., *Epidemiology of the metabolic syndrome in the USA.* Journal of Digestive Diseases, 2010. **12**(5): p. 333-340.

21. Calzadilla Bertot, L. and L.A. Adams, *The Natural Course of Non-Alcoholic Fatty Liver Disease.* International Journal of Molecular Sciences, 2016. **17**(5): p. 774.

22. Ekstedt, M., et al., *Long-term follow-up of patients with NAFLD and elevated liver enzymes.* Hepatology, 2006. **44**(4): p. 865-73.

23. Leung, C., et al., *Characteristics of hepatocellular carcinoma in cirrhotic and non-cirrhotic non-alcoholic fatty liver disease.* World J Gastroenterol, 2015. **21**(4): p. 1189-96.

24. Yopp, A.C. and M.A. Choti, *Non-Alcoholic Steatohepatitis-Related Hepatocellular Carcinoma: A Growing Epidemic?* Digestive Diseases, 2015. **33**(5): p. 642-647.

25. Michelotti, G.A., M.V. Machado, and A.M. Diehl, *NAFLD, NASH and liver cancer.* Nat Rev Gastroenterol Hepatol, 2013. **10**(11): p. 656-65.

26. European Association for the Study of the Liver. Electronic address, e.e.e. and L. European Association for the Study of the, *EASL Clinical Practice Guidelines: Management of hepatocellular carcinoma.* J Hepatol, 2018. **69**(1): p. 182-236.

27. Forner, A., et al., *Current strategy for staging and treatment: the BCLC update and future prospects.* Semin Liver Dis, 2010. **30**(1): p. 61-74.

28. Bruix, J. and J.M. Llovet, *Major achievements in hepatocellular carcinoma.* The Lancet. **373**(9664): p. 614-616.

29. Ghiaur, G., J. Gerber, and R.J. Jones, *Concise review: Cancer stem cells and minimal residual disease.* Stem Cells, 2012. **30**(1): p. 89-93.

30. Lobo, N.A., et al., *The biology of cancer stem cells.* Annu Rev Cell Dev Biol, 2007. **23**: p. 675-99.

31. Magee, J.A., E. Piskounova, and S.J. Morrison, *Cancer stem cells: impact, heterogeneity, and uncertainty.* Cancer Cell, 2012. **21**(3): p. 283-96.

32. Hanahan, D. and Robert A. Weinberg, *Hallmarks of Cancer: The Next Generation.* Cell, 2011. **144**(5): p. 646-674.

33. Dalerba, P., R.W. Cho, and M.F. Clarke, *Cancer stem cells: models and concepts.* Annu Rev Med, 2007. **58**: p. 267-84.

34. Lapidot, T., et al., *A cell initiating human acute myeloid leukaemia after transplantation into SCID mice.* Nature, 1994. **367**(6464): p. 645-8.

35. Al-Hajj, M., et al., *Prospective identification of tumorigenic breast cancer cells.* Proc Natl Acad Sci U S A, 2003. **100**(7): p. 3983-8.

36. Dalerba, P., et al., *Phenotypic characterization of human colorectal cancer stem cells.* Proc Natl Acad Sci U S A, 2007. **104**(24): p. 10158-63.

37. Hermann, P.C., et al., *Distinct populations of cancer stem cells determine tumor growth and metastatic activity in human pancreatic cancer.* Cell Stem Cell, 2007. **1**(3): p. 313-23.

38. Yamashita, T., et al., *EpCAM-positive hepatocellular carcinoma cells are tumor-initiating cells with stem/progenitor cell features.* Gastroenterology, 2009. **136**(3): p. 1012-24.

39. Yang, Z.F., et al., *Significance of CD90+ cancer stem cells in human liver cancer.* Cancer Cell, 2008. **13**(2): p. 153-66.

40. Yang, Z.F., et al., *Identification of local and circulating cancer stem cells in human liver cancer.* Hepatology, 2008. **47**(3): p. 919-28.

41. Barker, N., et al., *Identification of stem cells in small intestine and colon by marker gene Lgr5.* Nature, 2007. **449**(7165): p. 1003-7.

42. Driessens, G., et al., *Defining the mode of tumour growth by clonal analysis.* Nature, 2012. **488**(7412): p. 527-30.

43. Schepers, A.G., et al., *Lineage tracing reveals Lgr5+ stem cell activity in mouse intestinal adenomas.* Science, 2012. **337**(6095): p. 730-5.

44. Ji, J. and X.W. Wang, *Clinical implications of cancer stem cell biology in hepatocellular carcinoma.* Semin Oncol, 2012. **39**(4): p. 461-72.

45. Yoon, S.K., *The biology of cancer stem cells and its clinical implication in hepatocellular carcinoma.* Gut Liver, 2012. **6**(1): p. 29-40.

46. Ma, S., et al., *Identification and characterization of tumorigenic liver cancer stem/progenitor cells.* Gastroenterology, 2007. **132**(7): p. 2542-56.

47. Chiba, T., et al., *Cancer stem cells in hepatocellular carcinoma: Recent progress and perspective.* Cancer Lett, 2009. **286**(2): p. 145-53.

48. Haraguchi, N., et al., *Characterization of a side population of cancer cells from human gastrointestinal system.* Stem Cells, 2006. **24**(3): p. 506-13.

49. Ma, S., *Biology and clinical implications of CD133(+) liver cancer stem cells.* Exp Cell Res, 2013. **319**(2): p. 126-32.

50. Zhao, X., et al., *Integrative genomics identifies YY1AP1 as an oncogenic driver in EpCAM(+) AFP(+) hepatocellular carcinoma.* Oncogene, 2015. **34**(39): p. 5095-104.

51. Liu, L.L., et al., *The power and the promise of liver cancer stem cell markers.* Stem Cells Dev, 2011. **20**(12): p. 2023-30.

52. Terris, B., C. Cavard, and C. Perret, *EpCAM, a new marker for cancer stem cells in hepatocellular carcinoma.* J Hepatol, 2010. **52**(2): p. 280-1.

53. Yamashita, T., et al., *EpCAM and alpha-fetoprotein expression defines novel prognostic subtypes of hepatocellular carcinoma.* Cancer Res, 2008. **68**(5): p. 1451-61.

54. Yamashita, T., et al., *Discrete nature of EpCAM+ and CD90+ cancer stem cells in human hepatocellular carcinoma.* Hepatology, 2013. **57**(4): p. 1484-97.

55. Abdullah, L.N. and E.K. Chow, *Mechanisms of chemoresistance in cancer stem cells.* Clin Transl Med, 2013. **2**(1): p. 3.

56. Yamashita, T. and X.W. Wang, *Cancer stem cells in the development of liver cancer.* J Clin Invest, 2013. **123**(5): p. 1911-8.

57. Di, C. and Y. Zhao, *Multiple drug resistance due to resistance to stem cells and stem cell treatment progress in cancer (Review).* Experimental and Therapeutic Medicine, 2014.

58. Hashimoto, N., et al., *Cancer stem-like sphere cells induced from de-differentiated hepatocellular carcinoma-derived cell lines possess the resistance to anti-cancer drugs.* BMC Cancer, 2014. **14**: p. 722.

59. Wang, N., et al., *Dietary compound isoliquiritigenin targets GRP78 to chemosensitize breast cancer stem cells via beta-catenin/ABCG2 signaling.* Carcinogenesis, 2014. **35**(11): p. 2544-54.

60. Wang, Z., et al., *Caveolin-1 mediates chemoresistance in breast cancer stem cells via beta-catenin/ABCG2 signaling pathway.* Carcinogenesis, 2014. **35**(10): p. 2346-56.

61. Warrier, S., et al., *Cancer stem-like cells from head and neck cancers are chemosensitized by the Wnt antagonist, sFRP4, by inducing apoptosis, decreasing stemness, drug resistance and epithelial to mesenchymal transition.* Cancer Gene Ther, 2014. **21**(9): p. 381-8.

62. Nejak-Bowen, K.N. and S.P. Monga, *Beta-catenin signaling, liver regeneration and hepatocellular cancer: sorting the good from the bad.* Semin Cancer Biol, 2011. **21**(1): p. 44-58.

63. Gangavarapu, K.J., et al., *Aldehyde dehydrogenase and ATP binding cassette transporter G2 (ABCG2) functional assays isolate different populations of prostate stem cells where ABCG2 function selects for cells with increased stem cell activity.* Stem Cell Res Ther, 2013. **4**(5): p. 132.

64. Takigawa, Y. and A.M. Brown, *Wnt signaling in liver cancer.* Curr Drug Targets, 2008. **9**(11): p. 1013-24.

65. Chau, W.K., et al., *c-Kit mediates chemoresistance and tumor-initiating capacity of ovarian cancer cells through activation of Wnt/beta-catenin-ATP-binding cassette G2 signaling.* Oncogene, 2013. **32**(22): p. 2767-81.

66. Miller, A.B., et al., *Reporting results of cancer treatment.* Cancer, 1981. **47**(1): p. 207-14.

67. Therasse, P., et al., *New guidelines to evaluate the response to treatment in solid tumors. European Organization for Research and Treatment of Cancer, National Cancer Institute of the United States, National Cancer Institute of Canada.* J Natl Cancer Inst, 2000. **92**(3): p. 205-16.

68. European Association For The Study Of The, L., R. European Organisation For, and C. Treatment Of, *EASL-EORTC clinical practice guidelines: management of hepatocellular carcinoma.* J Hepatol, 2012. **56**(4): p. 908-43.

69. Lencioni, R. and J.M. Llovet, *Modified RECIST (mRECIST) assessment for hepatocellular carcinoma.* Semin Liver Dis, 2010. **30**(1): p. 52-60.

70. Wong, C.Y., et al., *Evaluating 90Y-glass microsphere treatment response of unresectable colorectal liver metastases by [18F]FDG PET: a comparison with CT or MRI.* Eur J Nucl Med Mol Imaging, 2002. **29**(6): p. 815-20.

71. Singh, P. and G. Anil, *Yttrium-90 radioembolization of liver tumors: what do the images tell us?* Cancer Imaging, 2014. **13**(4): p. 645-57.

72. Llovet, J.M., et al., *Design and endpoints of clinical trials in hepatocellular carcinoma.* J Natl Cancer Inst, 2008. **100**(10): p. 698-711.

73. Bruix, J., et al., *Clinical management of hepatocellular carcinoma. Conclusions of the Barcelona-2000 EASL conference. European Association for the Study of the Liver.* J Hepatol, 2001. **35**(3): p. 421-30.

74. Keppke, A.L., et al., *Imaging of hepatocellular carcinoma after treatment with yttrium-90 microspheres.* AJR Am J Roentgenol, 2007. **188**(3): p. 768-75.

75. Sato, K., et al., *Treatment of unresectable primary and metastatic liver cancer with yttrium-90 microspheres (TheraSphere): assessment of hepatic arterial embolization.* Cardiovasc Intervent Radiol, 2006. **29**(4): p. 522-9.

76. Kitisin, K., et al., *Liver stem cells and molecular signaling pathways in hepatocellular carcinoma.* Gastrointest Cancer Res, 2007. **1**(4 Suppl 2): p. S13-21.

77. Ma, S., et al., *CD133+ HCC cancer stem cells confer chemoresistance by preferential expression of the Akt/PKB survival pathway.* Oncogene, 2008. **27**(12): p. 1749-58.

78. Kroger, A., et al., *Growth suppression of the hepatocellular carcinoma cell line Hepa1-6 by an activatable interferon regulatory factor-1 in mice.* Cancer Res, 2001. **61**(6): p. 2609-17.

79. Dan, Q., et al., *Non-immunogenic murine hepatocellular carcinoma Hepa1-6 cells expressing the membrane form of macrophage colony stimulating factor are rejected in vivo and lead to CD8+ T-cell immunity against the parental tumor.* Mol Ther, 2001. **4**(5): p. 427-37.

80. Li, Y., et al., *Hepatic protection and anticancer activity of curcuma: a potential chemopreventive strategy against hepatocellular carcinoma.* Int J Oncol, 2014. **44**(2): p. 505-13.

81. Knowles, B.B., C.C. Howe, and D.P. Aden, *Human hepatocellular carcinoma cell lines secrete the major plasma proteins and hepatitis B surface antigen.* Science, 1980. **209**(4455): p. 497-9.

82. Liang, W., et al., *Establishment of a general NAFLD scoring system for rodent models and comparison to human liver pathology.* PLoS One, 2014. **9**(12): p. e115922.

83. Kleiner, D.E., et al., *Design and validation of a histological scoring system for nonalcoholic fatty liver disease.* Hepatology, 2005. **41**(6): p. 1313-21.

84. Dontu, G., et al., *In vitro propagation and transcriptional profiling of human mammary stem/progenitor cells.* Genes Dev, 2003. **17**(10): p. 1253-70.

85. Kunjithapatham, R., et al., *Reversal of anchorage-independent multicellular spheroid into a monolayer mimics a metastatic model.* Sci Rep, 2014. **4**: p. 6816.

86. Chen, Q., et al., *Selective proliferation of rat hepatocyte progenitor cells in serum-free culture.* Nat Protoc, 2007. **2**(5): p. 1197-205.

87. Kanwar, S.S., et al., *The Wnt/beta-catenin pathway regulates growth and maintenance of colonospheres.* Mol Cancer, 2010. **9**: p. 212.

88. Ponti, D., et al., *Isolation and in vitro propagation of tumorigenic breast cancer cells with stem/progenitor cell properties.* Cancer Res, 2005. **65**(13): p. 5506-11.

89. Lee, J., et al., *Tumor stem cells derived from glioblastomas cultured in bFGF and EGF more closely mirror the phenotype and genotype of primary tumors than do serum-cultured cell lines.* Cancer Cell, 2006. **9**(5): p. 391-403.

90. Kondo, T., *Stem cell-like cancer cells in cancer cell lines.* Cancer Biomark, 2007. **3**(4-5): p. 245-50.

91. Weiswald, L.B., D. Bellet, and V. Dangles-Marie, *Spherical cancer models in tumor biology.* Neoplasia, 2015. **17**(1): p. 1-15.

92. Calvet, C.Y., F.M. Andre, and L.M. Mir, *The culture of cancer cell lines as tumorspheres does not systematically result in cancer stem cell enrichment.* PLoS One, 2014. **9**(2): p. e89644.

93. Scheel, C. and R.A. Weinberg, *Cancer stem cells and epithelial-mesenchymal transition: concepts and molecular links.* Semin Cancer Biol, 2012. **22**(5-6): p. 396-403.

94. Wielenga, V.J., et al., *Expression of CD44 in Apc and Tcf mutant mice implies regulation by the WNT pathway.* Am J Pathol, 1999. **154**(2): p. 515-23.

95. Yamashita, T., et al., *Activation of hepatic stem cell marker EpCAM by Wnt-beta-catenin signaling in hepatocellular carcinoma.* Cancer Res, 2007. **67**(22): p. 10831-9.

96. Maric, D., et al., *Self-renewing and differentiating properties of cortical neural stem cells are selectively regulated by basic fibroblast growth factor (FGF) signaling via specific FGF receptors.* J Neurosci, 2007. **27**(8): p. 1836-52.

97. Greene, R.F., et al., *Plasma pharmacokinetics of adriamycin and adriamycinol: implications for the design of in vitro experiments and treatment protocols.* Cancer Res, 1983. **43**(7): p. 3417-21.

98. Oliva, J., et al., *The identification of stem cells in human liver diseases and hepatocellular carcinoma.* Exp Mol Pathol, 2010. **88**(3): p. 331-40.

99. Kamohara, Y., et al., *The search for cancer stem cells in hepatocellular carcinoma.* Surgery, 2008. **144**(2): p. 119-24.

100. Ma, S., et al., *Aldehyde dehydrogenase discriminates the CD133 liver cancer stem cell populations.* Mol Cancer Res, 2008. **6**(7): p. 1146-53.

101. Pattabiraman, D.R. and R.A. Weinberg, *Tackling the cancer stem cells [mdash] what challenges do they pose?* Nat Rev Drug Discov, 2014. **13**(7): p. 497-512.

102. Mokkapati, S., et al., *beta-catenin activation in a novel liver progenitor cell type is sufficient to cause hepatocellular carcinoma and hepatoblastoma.* Cancer Res, 2014. **74**(16): p. 4515-25.

103. Srivastava, S., et al., *Expression of proteins associated with hypoxia and Wnt pathway activation is of prognostic significance in hepatocellular carcinoma.* Virchows Arch, 2015.

104. Chen, Daniel S. and I. Mellman, *Oncology Meets Immunology: The Cancer-Immunity Cycle.* Immunity, 2013. **39**(1): p. 1-10.

105. Lee, Y., et al., *CD44+ Cells in Head and Neck Squamous Cell Carcinoma Suppress T-Cell–Mediated Immunity by Selective Constitutive and Inducible Expression of PD-L1.* Clinical Cancer Research, 2016.

106. Bruttel, V.S. and J. Wischhusen, *Cancer Stem Cell Immunology: Key to Understanding Tumorigenesis and Tumor Immune Escape?* Frontiers in Immunology, 2014. **5**: p. 360.

107. Maccalli, C., et al., *Immunology of cancer stem cells in solid tumours. A review.* Eur J Cancer, 2014. **50**(3): p. 649-55.

108. Sharma, P. and J.P. Allison, *The future of immune checkpoint therapy.* Science, 2015. **348**(6230): p. 56-61.

109. Starley, B.Q., C.J. Calcagno, and S.A. Harrison, *Nonalcoholic fatty liver disease and hepatocellular carcinoma: a weighty connection.* Hepatology, 2010. **51**(5): p. 1820-32.

110. Tong, C.M., S. Ma, and X.Y. Guan, *Biology of hepatic cancer stem cells.* J Gastroenterol Hepatol, 2011. **26**(8): p. 1229-37.

111. Ferraioli, G. and M.F. Meloni, *Contrast-enhanced ultrasonography of the liver using SonoVue.* 2018. **37**(1): p. 25-35.

112. Cocciolillo, S., G. Parruti, and L. Marzio, *CEUS and Fibroscan in non-alcoholic fatty liver disease and non-alcoholic steatohepatitis.* World Journal of Hepatology, 2014. **6**(7): p. 496-503.

113. Yao, X., et al., *A Novel Orthotopic Tumor Model to Study Growth Factors and Oncogenes in Hepatocarcinogenesis.* Clinical Cancer Research, 2003. **9**(7): p. 2719-2726.

114. Carruba, G., et al., *Truncated form of beta-catenin and reduced expression of wild-type catenins feature HepG2 human liver cancer cells.* Ann N Y Acad Sci, 1999. **886**: p. 212-6.

115. de La Coste, A., et al., *Somatic mutations of the beta-catenin gene are frequent in mouse and human hepatocellular carcinomas.* Proc Natl Acad Sci U S A, 1998. **95**(15): p. 8847-51.

116. Kakugawa, S., et al., *Notum deacylates Wnt proteins to suppress signalling activity.* Nature, 2015. **519**(7542): p. 187-192.

117. Marjanovic, N.D., R.A. Weinberg, and C.L. Chaffer, *Cell plasticity and heterogeneity in cancer.* Clin Chem, 2013. **59**(1): p. 168-79.

118. Chen, Y., et al., *Mature hepatocytes exhibit unexpected plasticity by direct dedifferentiation into liver progenitor cells in culture.* Hepatology, 2012. **55**(2): p. 563-74.

119. Herreros-Villanueva, M., et al., *SOX2 promotes dedifferentiation and imparts stem cell-like features to pancreatic cancer cells.* Oncogenesis, 2013. **2**: p. e61.

120. Jabari, S., et al., *Cellular plasticity of trans- and dedifferentiation markers in human hepatoma cells in vitro and in vivo.* Int J Oncol, 2009. **35**(1): p. 69-80.

121. Jopling, C., S. Boue, and J.C. Izpisua Belmonte, *Dedifferentiation, transdifferentiation and reprogramming: three routes to regeneration.* Nat Rev Mol Cell Biol, 2011. **12**(2): p. 79-89.

122. Kumar, S.M., et al., *Acquired cancer stem cell phenotypes through Oct4-mediated dedifferentiation.* Oncogene, 2012. **31**(47): p. 4898-911.

123. Takahashi, K. and S. Yamanaka, *Induction of pluripotent stem cells from mouse embryonic and adult fibroblast cultures by defined factors.* Cell, 2006. **126**(4): p. 663-76.

124. Fessler, E., et al., *Cancer stem cell dynamics in tumor progression and metastasis: is the microenvironment to blame?* Cancer Lett, 2013. **341**(1): p. 97-104.

125. Moon, R.T., et al., *WNT and beta-catenin signalling: diseases and therapies.* Nat Rev Genet, 2004. **5**(9): p. 691-701.

126. Ramos, E.K., et al., *New Opportunities and Challenges to Defeat Cancer Stem Cells.* Trends Cancer, 2017. **3**(11): p. 780-796.

127. Lee, W.C., et al., *Effective treatment of small murine hepatocellular carcinoma by dendritic cells.* Hepatology, 2001. **34**(5): p. 896-905.

128. Wang, Q., et al., *Non-invasive in vivo imaging for liver tumour progression using an orthotopic hepatocellular carcinoma model in immunocompetent mice.* Liver Int, 2011. **31**(8): p. 1200-8.

129. Lachenmayer, A., et al., *Wnt-pathway activation in two molecular classes of hepatocellular carcinoma and experimental modulation by sorafenib.* Clin Cancer Res, 2012. **18**(18): p. 4997-5007.

130. Huang, F.I., et al., *Hepatocyte growth factor activates Wnt pathway by transcriptional activation of LEF1 to facilitate tumor invasion.* Carcinogenesis, 2012. **33**(6): p. 1142-8.

131. Li, J. and C.Y. Wang, *TBL1-TBLR1 and beta-catenin recruit each other to Wnt target-gene promoter for transcription activation and oncogenesis.* Nat Cell Biol, 2008. **10**(2): p. 160-9.

132. Dimitrova, Y.N., et al., *Direct ubiquitination of beta-catenin by Siah-1 and regulation by the exchange factor TBL1.* J Biol Chem, 2010. **285**(18): p. 13507-16.

Footnote:

I have acknowledged and cited all sources used in the reference section. This Ph.D. dissertation is an extension of Master's thesis work. Master's thesis work provided the first set of results and established the foundation for this dissertation study and research direction (Pandit H, Pharmacology & Toxicology, 2015). Therefore, methods and results from the master's work were used and discussed in this dissertation, with an aim to provide comprehensive understanding of the study. I hereby declare that this dissertation (and master's thesis) is my original work.

CURRICULUM VITAE

Harshul Pandit, MS.

107 Fenley Ave Apt Y1

Louisville, KY 40207

+1- (502) 657-8783

harshul.pandit@louisville.edu

harshul.pandit@gmail.com

EDUCATION

2013-2018	Ph.D. in Pharmacology & Toxicology, University of Louisville, Louisville, KY, U.S.A.
2013-2015	MS in Pharmacology & Toxicology (Thesis), University of Louisville, Louisville, KY, U.S.A.
2005-2007	M.Sc. in Biochemistry (Thesis), M.S.University of Baroda, Baroda, India
2004-2005	PG. Diploma in Applied Biochemistry, M.S.University of Baroda, Baroda, India
2001-2004	B.Sc. in Biotechnology, Sardar Patel University, Vallabh Vidhyanagar, India

Ph.D. mentor:

Dr. Robert C.G. Martin II, MD, Ph.D., FACS

Professor of Surgery, and Pharmacology and Toxicology,

Director, Division of Surgical Oncology,

Hiram C. Polk Jr. M.D. Department of Surgery,

University of Louisville School of Medicine

robert.martin@louisville.edu Phone: 502-629-3355 Fax: 502-629-3030

ACADEMIC APPOINTMENTS

2013-Present Graduate Research Assistant, Division of Surgical Oncology, Department of Surgery, University of Louisville, Louisville, KY

2012-2012 Graduate Teaching Assistant, Department of Biochemistry, University of Louisville, Louisville, KY

2010-2011 Instructor (Mathematics), PT Education Center, Bhuj, India

OTHER POSITIONS AND EMPLOYMENT

2014-2017 Graduate Student Representative (Elected) for the School of Medicine Faculty Forum, School of Medicine, University of Louisville, KY

2013-Present Laboratory procurement management, Surgical Oncology Lab, Department of Surgery, Louisville, KY

2009-2010 Research Associate E-I, R&D Division, Protein purification - Down Stream Process Lab, Intas Biopharmaceuticals Ltd, Ahmedabad, India

2008-2009 Trainee Research Associate E-II, R&D Division, Protein purification - Down Stream Process Lab, Intas Biopharmaceuticals Ltd, Ahmedabad, India

2004-2007 Laboratory and Chemical In-charge, Department of Biochemistry, M.S.University of Baroda, Baroda, India

HONORS AND AWARDS

2017 Conference travel award, Graduate Student Council - SIGS, University of Louisville, KY, U.S.A

2016 Conference travel award, Graduate Student Council - SIGS, University of Louisville, KY, U.S.A

2015 2nd place in poster presentation, Research Louisville 2015, University of Louisville, KY, U.S.A

2015 Conference travel award, Graduate Student Council - SIGS, University of Louisville, KY, U.S.A

2014 Conference travel award, HSC research office, University of Louisville, Louisville, KY, U.S.A.

2014	Conference travel award, Graduate Student Council - SIGS, University of Louisville, KY, U.S.A
2011-2013	Interdisciplinary Program in Biomedical Sciences (IPIBS) fellowship, University of Louisville, Louisville, KY, U.S.A.
2009	Selected for 35th Mahabaleshwar Seminar at national level, organized by Tata Institute of Fundamental Research (TIFR) Mumbai, India.
2006-2007	Selected for 3rd Bangalore Benny Shilo course in Developmental Biology at International level, organized by Weizmann Institute, Israel & National Center for Biological Sciences (NCBS), Bangalore, India
2003	Charutar Vidhya Mandal (CVM) award - "Scholar student in the college", N.V.Patel College of Pure and Applied Sciences, Vallabh Vidhyanagar, India

PROFESSIONAL MEMBERSHIP AND ACTIVITIES

2016-Present	Student member, Society of Toxicology (SOT) – OVSOT reginal chapter.
2016-Present	Student member, American Society for Pharmacology and Experimental Therapeutics (ASPET)
2015-Present	Associate member, American Association for Cancer Research (AACR)
2014-Present	Student member, American Society of Clinical Oncology (ASCO)
2014-present	Student member, American College of Surgeons (ACS) – KY regional chapter

PUBLICATIONS

1. **Pandit H**, Zhang W, Li Y, Agle S, Li X, Li S, Li Y, Martin R,. Manganese Superoxide Dismutase (MnSOD) expression is negatively associated with microRNA-301a levels in human Pancreatic Ductal Adenocarcinoma (PDAC). Cancer Gene Ther. 2015 Oct;22(10):481-6. **PMID:** 26384137

2. **Pandit H,** Li Y, Li X, Zhang W, Li SP, Martin RCG. Enrichment of cancer stem cells via β-catenin contributing to the tumorigenesis of hepatocellular carcinoma**.** BMC Cancer. 2018 Aug 3; 18(1);783. **PMID:** 30075764

3. **Pandit H**.,Tinney J. , Li Y., Cui G., Li SP., Keller B., Martin RCG. Utilizing contrast-enhanced ultrasound imaging for evaluating fatty liver disease progression in pre-clinical mouse models**,** Ultrasound in Medicine and Biology (Official Journal of World Federation of Ultrasound) – **In communication.**

4. **Pandit H,** Li Y, Cui G, Li SP, Martin RCG. *Fate of EpCAM+ Cancer Stem Cells in Orthotopic Liver Microenvironments – A Lineage Tracking Study of HCC Initiation in Immunocompetent and Immunocompromised Mouse Models* - **Under preparation**

5. **Harshul Pandit**, Young Hong, Yan Li, Jack Rostas III, Zachary Pulliam, SuPing Li, Robert C.G. Martin II, *Evaluating Immunomodulation Effect of Irreversible Electroporation in Pancreatic Adenocarcinoma*. **Under preparation**

6. **Pandit H**, Cui G, Rostas J, Zheng Q, Li SP, Martin RCG, Li Y. *High fat diet increases the incidence of hepatocellular carcinoma in mice with p53 Germline Variant (rs78378222[C])* - **Under preparation**

7. Li Y, Zhang W, Doughtie A, Cui G, Li X, **Pandit H**, Li S, Martin R,. Up-regulation of Fibroblast Growth Factor 19 in Fatty Liver and Hepatocellular Carcinoma. Oncotarget. Vol. 7, No. 32, 2016 Jul 21. doi: 10.18632/oncotarget.10750. **PMID:** 27447573, http://www.impactjournals.com/oncotarget/index.php?journal=oncotarget

8. Guozhen Cui, Robert C. Martin, Hang Jin, Xingkai Liu, **Harshul Pandit**, Hengjun Zhao, Lu Cai, Ping Zhang, Wei Li, Yan Li. Up-regulation of FGF15/19 signaling promotes hepatocellular carcinoma in the background of fatty liver. BMC - Journal of Experimental and Clinical Cancer Research - 2018 Jul 4;37(1):136. https://doi.org/10.1186/s13046-018-0781-8

9. Yan Li, Guozhen Cui, Russell Farmer, Kevin Jacob, **Harshul Pandit**, Xuanyi Li, Robert CG. Martin Exposure to bile acids alters the intracellular location and function of MnSOD in Barrett's esophagus. Journal of Surgical Research 229, 156-163. https://doi.org/10.1016/j.jss.2018.03.055

10. Guozhen Cui, Robert Martin, Xingkai Liu, **Harshul Pandit**, Suping Li, Ping Zhang, Wei Li, and Yan Li. Characteristics of ultrasound and serological markers for steatohepatitis and liver cancer in mice. **In Communication**

11. Li Y, Li S, Li X, Cui G, **Pandit H,** Martin RCG,. Chemotherapy Induced Expression of EpCAM in Esophageal Adenocarcinoma: A Method of Chemoresistance? **In Communication**

ABSTRACTS AND PRESENTATIONS

Oral Presentations

1. Harshul Pandit, Wnt/β-catenin Mediated Cancer Stem Cells (CSCs) Enrichment in Hepatocellular Carcinoma (HCC) - Downward Spiral for Acquired Chemotherapy Resistance and Tumor Recurrence? Price Institute of Surgical Research, Dr. Hiram C. Polk Jr. Department of Surgery, University of Louisville. – **March 2018**

2. **Harshul Pandit**, Young Hong, Yan Li, Jack Rostas III, Zachary Pulliam, SuPing Li, Robert C.G. Martin II, Evaluating Immunomodulation Effect of Irreversible Electroporation in Pancreatic Adenocarcinoma. **Oral presentation – HPB parallel session**, Society of Surgical Oncology, SSO Annual meeting, Chicago – **March 23rd 2018**.

3. Identifying Cancer Stem Cells (CSCs) in Hepatocellular Carcinoma – Culprit to Blame for Chemotherapy Resistance and Tumor Relapse? Price Institute of Surgical Research, Dr. Hiram C. Polk Jr. Department of Surgery, University of Louisville. – **Sep 2015**

4. New insights in miRNA processing – what is happening prior to Drosha and Dicer? Department of Biochemistry & Molecular Biology, University of Louisville. - **Dec 2012**

Research Posters/Abstracts

1. **Harshul Pandit**, Yan Li, Gouzhen Cui, Qianqian Zheng, Suping Li, Robert Martin. *Wnt/β-catenin mediated enrichment of EpCAM positive cancer stem cells promote drug resistance in hepatocellular carcinoma.* [Abstract #1120]. Chicago : AACR 2018 annual meeting; **Apr -2018**

2. Qianqian Zheng, **Harshul Pandit**, Xingkai Liu, Youxi Yu, Suping Li, Shelby Turner, Xin Meng, Robert Martin, Yan Li. *Lack of FGF21 accelerates the Th17-IL-17 axis-mediated transition from nonalcoholic steatohepatitis to hepatocellular carcinoma.* [Abstract #4393]. Chicago : AACR 2018 annual meeting; **Apr -2018**

3. Neal Bhutiani, **Harshul Pandit**, Qianqian Zheng, Suping Li, Yan Li, Robert C. G. Martin, II. *Electrochemotherapy with irreversible electroporation and FOLFIRINOX improves survival in murine pancreatic adenocarcinoma by*

increasing apoptosis and decreasing tumor cell proliferation [Abstract #7394]. Chicago : AACR 2018 annual meeting; **Apr -2018**

4. **Harshul Pandit**, Young K Hong, Yan Li, Jack Rostas III, Zachary Pullium, Suping Li, Robert C.G. Martin. Evaluating Regulatory Immunomodulation Effect of Irreversible Electroporation in Pancreatic Adenocarcinoma. SSO annual meeting, March 2018, Chicago **– Oral Presentation**

5. Young K Hong, **Harshul Pandit**, Zachary Pulliam, Norman Galbraith, Su Ping Li, Yan Li, Robert CG Martin. Epigenetic Modulation Enhances Immunotherapy for Hepatocellular Carcinoma. American College of Surgeons (ACS) Clinical Congress – Oct 2017, https://doi.org/10.1016/j.jamcollsurg.2017.07.435

6. Young K. Hong, **Harshul Pandit**, Neil Bhutiani, Suping Li, Yan Li, Robert C.Martin. Enhancing Immunotherapy by Epigenetic Silencing of Histone and DNA Methylation in Pancreatic Cancer. –DDW/SSAT, May 2017, Chicago https://doi.org/10.1016/S0016-5085(17)34077-5

7. Young K. Hong, **Harshul Pandit**, Neil Bhutiani, Suping Li, Yan Li, Robert C. Martin. Induction of PD-L1 expression in hepatocellular tumor microenvironment by IFN: Rationale for PD-L1 therapy combination. 58th Annual Meeting – SSAT, May 2017, Chicago. http://meetings.ssat.com/abstracts/2017/810.cgi

8. **Pandit H**, Li Y, Cui G, Li SP, Li X, Martin RCG., Non-alcoholic steatohepatitis promotes EpCAM positive cancer stem cells mediated tumorigenesis in immunocompetent mouse model of hepatocellular carcinoma [abstract]. In: Proceedings of the American Association for Cancer Research Annual Meeting 2017; 2017 Apr 1-5; Washington, DC. Philadelphia (PA): AACR; Cancer Res 2017;77(13 Suppl):Abstract nr 1909. **APRIL 2017** http://dx.doi.org/10.1158/1538-7445.AM2017-1909

9. **Pandit H**, Li Y, Cui G, Li X, Li SP, Yang Y, Rosta J, Martin RCG., EpCAM Positive Cancer Stem Cells Acquired Chemoresistance in Hepatocellular Carcinoma. [abstract]. In: Proceedings of the 107th Annual Meeting of the American Association for Cancer Research; 2016 Apr 16-20; New Orleans, LA. Philadelphia (PA): AACR; Cancer Res 2016;76(14 Suppl):Abstract nr 2535. **Apr -2016** http://dx.doi.org/10.1158/1538-7445.AM2016-2535

10. Cui G, Liu X, **Pandit H**, Yang Y, Li SP, Cai L, Martin RCG, Zhao H, Li W, Li Y., Metabolic hormones FGF19/15 promote hepatocellular carcinoma through activation of CSCs in fatty liver. [abstract]. In: Proceedings of the 107th Annual Meeting of the American Association for Cancer Research; 2016 Apr 16-20; New Orleans, LA. Philadelphia (PA): AACR; Cancer Res 2016;76(14 Suppl):Abstract nr 1039. **Apr -2016** http://dx.doi.org/10.1158/1538-7445.AM2016-1039

11. **Pandit H**, Li Y, Zhang W, Li SP, Li X, Cui G, Yang Y, Martin RCG., Acquired Doxorubicin Resistance in Hepatocellular Carcinoma Cells with Cancer Stem Cell Like Properties. Research Louisville 2015, Louisville, KY, USA (**Awarded 2nd place in poster presentation - doctoral student category) Oct -2015**

12. **Pandit H**, Li Y, Zhang W, Li SP, Li X, Cui G, Yang Y, Martin RCG., Acquired Doxorubicin Resistance in Hepatocellular Carcinoma Cells with Cancer Stem Cell Like Properties. Clinical Congress 2015, American College of Surgeons, Chicago, IL, USA. **Oct 2015**

13. Yan Li, **Harshul Pandit**, Xuanyi Li, Suping Li, Jingwen Zhang, Guozhen Cui, Robert C. Martin. Abolish cancer progenitor cells in a mouse model of diabetes associated hepatocellular carcinoma. [abstract]. In: Proceedings of the 106th Annual Meeting of the American Association for Cancer Research; 2015 Apr 18-22; Philadelphia, PA. Philadelphia (PA): AACR; Cancer Res 2015;75(15 Suppl):Abstract nr 4069. **Apr - 2015** http://dx.doi.org/10.1158/1538-7445.AM2015-4069

14. **Pandit H**, Li Y, Li S, Li X, Zhang W, Martin R., Identifying Cancer Stem Cell (CSC) like characters in Hepatocellular Carcinoma (HCC) cells and their role in HCC recurrence., Clinical Congress 2014, American College of Surgeons, San Francisco, CA, USA, **Oct - 2014**
http://dx.doi.org/10.1016/j.jamcollsurg.2014.07.855

15. **Pandit H**, Li Y, Li S, Li X, Zhang W, Martin R., Identifying Cancer Stem Cell (CSC) like characters in Hepatocellular Carcinoma (HCC) cells, and their role in chemotherapy resistance., Research Louisville 2014, Louisville, KY, **Aug-2014.**

16. **Pandit H**, Hadpe S, Patel C., Multivariate Data Analysis (MVDA) of Biopharmaceutical downstream process. Annual conference, Intas Biopharmaceuticals, Ahmedabad, India. **Nov - 2010.**

17. Hadpe S**, Pandit H**, Patel C., Implementation of Quality by Design (QbD) approach in biopharmaceutical operations. Annual conference, Intas Biopharmaceuticals, Ahmedabad, India. **Nov -2010.**

REFERENCES

Available on request.